Studies on the Reactivity of a Bis–Mesityl Imidazolyl Carbene Intermediate toward
Carbon Dioxide and Stability of the Resulting Carboxylate

By

Seon Young Ka

Submitted in Partial Fulfillment of the Requirements

For the Degree of

Master of Science

In the

Chemistry

Program

YOUNGSTOWN STATE UNIVERSITY

August, 2019

Studies on the Reactivity of a Bis–Mesityl Imidazolyl Carbene Intermediate with Carbon Dioxide and the Stability Characterization after Carbon Dioxide Adduction

Seon Young Ka

I hereby release this thesis to the public. I understand that this thesis will be made available from the OhioLINK ETD Center and the Maag Library Circulation Desk for public access. I also authorize the University or other individuals to make copies of this thesis as needed for scholarly research.

Signature:

_____

Seon Young Ka, Student   Date

Approvals:

_____

Clovis A. Linkous, Thesis Advisor   Date

_____

John A. Jackson, Committee Member   Date

_____

Michael A. Serra, Committee Member   Date

_____

Dr. Salvatore A. Sanders, Dean of Graduate Studies   Date

ABSTRACT

1,3–bis(2,4,6–trimethylphenyl)imidazolium carboxylate, an adduct between CO_2 and the N–heterocyclic carbene (NHC), 1,3–bis(2,4,6–trimethylphenyl)–1,3–dihydro–2H–imidazol–2–ylidene, was synthesized to study the reactivity of CO_2 after binding to the carbene intermediate. Nuclear magnetic resonance (NMR) spectroscopy, infrared (IR) spectroscopy, X–ray powder diffraction (XRD), gas chromatography (GC) and thermal gravimetric analysis (TGA) were employed to characterize the final imidazolium carboxylate. GC was specifically used to study the dissociation of the CO_2 adduct. The structure of the synthesized zwitterion was confirmed via ^1H and ^{13}C NMR, where adduct formation generated a new peak in the ^{13}C NMR spectrum. IR spectroscopic data showed a significant characteristic peak for C=O stretch at around 1670 cm^{-1}. TGA spectra showed that the zwitterion's weight loss of 13% at 155 °C which is the percent weight of CO_2. The GC study of CO_2, which was released after treating the imidazolium carboxylate with 5% H_2O in CH_3CN, enabled the possibility of the reversibility of CO_2–NHC adduct formation. The stability and air sensitivity of the imidazolium carboxylate were tested in polar, nonpolar, acidic, basic, and mixed solvents via simple effervescence tests and GC. The hydrolytic stability of the imidazolium carboxylate was examined. The bis-mesityl carboxylate showed reasonable stability in water, in contrast to carboxylates with smaller alkyl substituents, but admixture with organic solvent would cause it to break down into the corresponding imidazolium bicarbonate. After exposure to H_2 (g) and heat, there was evidence for the reductive conversion of the carboxylate into imidazolium formate. This suggests the application of the mesityl imidazolyl carbene as an organic catalyst for CO_2 reduction.

ACKNOWLEDGEMENTS

For Rudy,

My joy, my heart, my baby

TABLE OF CONTENTS

LIST OF FIGURES

LIST OF TABLES

LIST OF EQUATIONS

LIST OF ABBREVIATIONS

Abbreviations	Full name
I^iPrCO_2	1,3-bis(2,6-diisopropylphenyl)imidazole-2-carboxylate
IMes carbene	Contaminated 1,3–bis(2,4,6–trimethylphenyl)–1,3–dihydro–2H–imidazole–2–ylidene (**1**)
IMes	1,3–bis(2,4,6–trimethylphenyl)–1,3–dihydro–2H–imidazole–2–ylidene (**2**)
SIMes	1,3-bis(2,4,6-trimethylphenyl)imidazolin-2-ylidene
$IMesCO_2$	1,3-bis(2,4,6-trimethylphenyl)imidazolium-2-carboxylate (**3**)
$IMeCO_2$	1,3-dimethylimidazolium-2-carboxylate
CCS	Carbon Capture and Sequestration
COSY	Correlation Spectroscopy
CV	Cyclic Voltammogram
D	Debye
DPV	Differential Pulse Voltammogram
GC	Gas Chromatography
IR	Infrared
NHC	N–Heterocyclic Carbene
NMR	Nuclear Magnetic Resonance
NOESY	Nuclear Overhauser Effect Spectroscopy
ppm	Parts Per Million
PXRD	Powder X–Ray Diffraction
TGA	Thermogravimetric Analysis
XRD	X–Ray Diffraction

CHAPTER 1: INTRODUCTION

Background

Environmental concerns, such as pollution of water, air, and soil, have been at the forefront since the development of new technology. Mining, deforestation, littering, and industrial development have caused degradation of the earth's surface. These developments involving habitat destruction cause the loss of biodiversity. Natural disasters happen more frequently than ever before.[1]

Natural disasters often cause CO_2 emission into the atmosphere. Climate change and global warming, which is caused by CO_2 emission, can decrease the glacial coverage which then changes the geological structure. One example is a volcano eruption. Typically, a volcanic eruption emits, on average, about 250 million metric tons. Coal–fired power generation in the US emits about 1.02 metric tons of CO_2 per megawatt–hour. Scientists compared the volcanic records with the glacial coverage and discovered that the greater the glacial coverage the less the volcanic activity due to the pressure that the ice is putting on Earth's surface.[2] A geological professor, Ben Edwards,[3] commented that there is more to look into regarding the relationship between climate change and volcanic activity.

Excess emission from the development of technologies and poor management of harmful gases have caused rising sea levels, longer and more destructive wildfire seasons, more frequent and more intense heat waves, health issues, and heavier rainfalls, which are complicated by temperature escalation.[4] An average atmospheric temperature has increased since 1800 and has been climbing significantly since 1997. The United States of America set a record in 2012 for the hottest year on record. In particular, the State of

Ohio experienced numerous broken records: fifty–five heat records, ten snow records, ten precipitation records, and one wildfire in 2012.[1,5,6]

Furthermore, air pollution in the form of smog and increased airborne pollen cause respiratory illness in the form of asthma and cardiac or pulmonary diseases. Water and other food supplies are threatened. An increase in the number of droughts has caused decreases in crop harvests and fish populations, impacting local food supplies and increasing the risk of foodborne illnesses. The lack of available water is predicted to introduce more stress for some 3.77 billion people in 2050, since the available water will have remained the same as the year 1990, according to Hayashi, A. et al.[7] In addition, the change in temperature increases the rapid development of virulent pathogens and mosquitos, which transmit diseases such as dengue fever and West Nile virus.[1,2,6]

Climate change causes floods, storms, heat waves, air pollution, airborne allergen production, vector–borne and water–borne infections, water/food supply shortages, a rise in sea–level, and storm surges. The consequences of these climate change effects could result in infectious disease outbreaks, mental health impacts on affected communities, increase in allergic illnesses, spread of infectious diseases, more frequent drought, increase in world food insecurity, increase in the risks of foodborne illnesses, contamination of drinking water supplies, even increases in the concentration of ground–level ozone smog and fine particulate matter.[1,8]

Stronger–impact disasters have been occurring in every year and everywhere due to these climate changes. One of the recognized climate change consequences is El Niño (La Niña) Southern Oscillation (ENSO). It is the effect of a band of sea surface temperatures becoming warmer (El Niño) or colder (La Niña) for long periods of time,

which in the end causes climate fluctuation across the tropics and subtropics.[9] The worst

aspect is that the surface temperature of the earth already will have another 1.0 °F

increase for the next five more years due to global warming, regardless of whether

preventive measure are taken or not.[1,6]

Simple searches about "global warming" on *SciFinder* gave 19,662 references in

2015 and 23,875 in 2018. It may not mean that every reference mainly deals with global

warming, but it does imply that societies do have an awareness of the seriousness of

global warming. The level of awareness has noticeably increased in these years. Global

warming starts when greenhouse gases such as ozone, carbon dioxide, methane, nitrous

oxide, fluorinated gases, or even excess water vapor are held or trapped in the

atmosphere.

The term "greenhouse gases" (GHG) refers to gases which absorb infrared

radiation and generate heat to maintain the temperature of the planet.[10] About 70% of the

energy content of solar radiation reaching the earth is converted to some other form and

remains there. The heat resulting from ultraviolet and visible radiation absorption turns

into infrared radiation that is absorbed by GHGs in the atmosphere to keep the earth

warm. Water vapor is condensed into clouds to eventually produce rain, but it also acts as

a reservoir for heat, so we feel muggy even when it rains with no sun out.[11,12] The

website by Mr. Kukreja[12] well–illustrates how greenhouse gases, including water vapor,

come into the planet, are trapped and emitted.

U.S. GHG emissions in 2013 showed that the most emitted gas by weight was

carbon dioxide (82%) followed by methane (10%), nitrous oxide (5%), and fluorinated

gases (3%). The most common sources of carbon dioxide gas are from the combustion of

fossil fuels, the decay of solid waste, trees, and certain chemical reactions. Most anthropogenic gas emission is from electricity generation (37%) followed by transportation (31%); non–fossil fuel combustion is 6% of the total emissions. In 2016, the GHG emission showed that the total carbon dioxide emissions in the U.S. were about 6,500 million metric tons; the emissions have decreased by about 2.8 % since 2015.[1,13]

Most of the CO_2 gas is recycled via photosynthesis in the biological carbon cycle. In photosynthesis, CO_2 combines with water, generating glucose and oxygen. Nevertheless, the concentration of carbon dioxide on earth is too high, so that the biological carbon cycle does not relieve the unbalanced ecosystem. In 2011, China was the largest single emitter of energy-related CO_2 at 27% of the total, followed by the United States of America at 17%. There were 18 more countries, each of which emitted 1% or more, and together comprised 36% of CO_2 emission. To accurately predict the imbalance, one must also include CO_2 emission from the biological carbon cycle. Additionally, CO_2 emission per capita data show that Australia and the U.S.A. have the most gas emissions at 18.6% and 18%, respectively.[1,14]

Carbon dioxide is a colorless and odorless gas that is a product of the respiratory cycle for animals; it is utilized in photosynthesis to produce glucose for plants. CO_2 has alternate names, depending on the application: in terms of acid–base chemistry, it can be called carbonic anhydride; in the solid state, it is commonly known as dry ice. The critical temperature and pressure are 304.13 K and 7.375 MPa, respectively, so that it can be conveniently made into a non–aqueous solvent with unique solvating properties. Its IR absorption is in the 1630 cm^{-1} to 1740 cm^{-1} range. The Globally Harmonized System of Classification and Labeling of Chemicals (GHS), which is a United Nations classification

system to categorize hazardous chemicals and to enlighten users, has a "warning" sign for CO_2 (g). Inhalation at elevated levels can result in dizziness, headache, elevated blood pressure, increased pulse rate, asphyxiation, unconsciousness, and even death. Nevertheless, the gas is noncombustible. Oddly, inhalation of CO_2 gas has been used during anesthetic surgery as apneic oxygen insufflation during lung surgery and open cardiac surgery.[15]

As early as the 1990s, climate change due to the greenhouse effect was recognized as a political issue for societies, and scientists have been trying to figure out how to slow down the rate of heating of the earth. The *Union of Concerned Scientists* mentioned that CO_2 gas is the major man–induced climate driver followed by methane. Several strategies designed to assist photosynthesis have been developed to reduce the concentration of CO_2, such as enhanced oil recovery, alkaline scrubbing, underground storage in caverns and sandstone formations, deep oceanic injection, carbonate mineral formation, and syn–gas processes.[16]

Even before talking about reducing the CO_2 concentration in the atmosphere, simple steps could reduce the rate of CO_2 released into the atmosphere such as planting more trees, reducing the use of fossil fuels, and increasing the use of clean energy. Since the cost of clean energy is generally higher, governments must help subsidize the price for the clean energy. For example, residential buildings should adopt codes to promote consumer energy savings. Governments could provide incentives to those who install clean energy fixtures or energy–efficient lights.[1]

Another method that scientists have studied is physical sequestration of CO_2. Several methods are terrestrial sequestration, ocean storage, or even a direct chemical

conversion to fuel. One of the methods is underground storage into a geological formation. Takeshita and Yamaju[17] determined that geological storage could be cost–effective when coupled with coal gasification conversion. If both cost and leakage issues are solved, coal gasification is a promising subject for future implementation. One major disadvantage of the method is that chances of earthquakes increase since injection disturbs the sub–ground levels. Besides, discovering a stable region for gas storage is extremely demanding since the method needs a stable terrestrial level to hold so much pressure and volume. Another issue is that geological formations will have an intrinsic leak rate of 0.01% per year of CO_2 even if there are no seismic events requiring remediation.[18,19]

An additional physical method of reducing the level of CO_2 emitted to the atmosphere is enhanced oil recovery (EOR), where CO_2 is injected through oil pipelines to underground levels to clean up residual petroleum from oil fields. The US is introducing approximately 30 to 50 million metric tons of CO_2 into oil field pipelines each year. CO_2 has also been directly injected to 12 m thick gas fields at approximately 1,100 m depths, where the storage reservoir is about 60 m thick and the cap rock is about 150 m thick. These injections of CO_2 are to store the gas for semi–permanent or permanent storage. Despite several problems, geological storage formations are most encouraging as a prospective sequestration strategy.

The other physical sequestration method is tailoring the ocean environment to sequester CO_2. CO_2 is dissolved into the oceanic water at 1000 meters via pipeline or can be liquefied when it is injected 3000 meters or deeper. These types of storage can hold the gas up to 1000˝s of years. An additional way is to transform the gas into crystals by

forming aqueous solvent cages around the gas, which are called gas clathrates. However, oceanic Carbon Capture and Sequestration (CCS) lowers the pH level of the ocean which affects the life cycle of marine organisms. Chemical means of sequestering the gas are alkaline scrubbing and syn–gas processes.

Chemical means of sequestering the gas are alkaline scrubbing and syn–gas processes. Alkaline scrubbing, which is known as post combustion or "CO_2 scrubbing process," is where NaOH takes up CO_2 to generate Na_2CO_3, but the result is not very cost–effective. Syn–gas describes a variety of fuel conversion processes, where CO_2 can be produced and separated from other species either before (pre–) or after (post–) combustion. Pre–combustion processes seem to be more useful than post combustion–it uses carbonaceous fuel to generate CO_2 and H_2; eventually, release of CO_2 is not permitted and H_2 will be used as fuel. A variety of possible materials such as metal organic frameworks, polyamine adsorbent materials, ionic liquids, and frustrated Lewis pairs, in which the pairs have both a Lewis acid and a Lewis base, for CCS reagents have been studied.

Some researchers have tried to perform carboxylation of organic compounds as a way of recycling CO_2 from the atmosphere. Sarve et al.[20] utilized CO_2 to study stoichiometry, the order of reaction, the rate constant, and rate law of the carboxylation of toluene via both Friedel−Crafts reaction. Mori et al.[21] investigated the percent yield of the carboxylation of several organic compounds. Bigger the organic compounds, the greater the percent yields of their carboxylated acids.

Reducing CO_2 emission is part of "Green Chemistry." The term includes principles of reduction or limiting the generation of harmful and environmentally

unfriendly substances for life on earth. It is designed to prevent pollution by decreasing the emission of greenhouse gases, to reduce or to limit the usage of chemicals that potentially harm the planet, and to eliminate existing hazardous products and processes. For example, volatile organic solvents can be replaced with ionic liquids which have high thermal stability, low volatility, and variation in co–solvent miscibility. It is different from cleaning up or treating waste. Cleaning up pollution requires the separation of hazardous chemicals from other materials and the use of processes to make them safe for disposal. The principles of green chemistry are to prevent wastes, to maximize the final product, to increase energy efficiency, to get accustomed to renewable feedstock or catalysts, and to utilize biodegradable chemicals and products. Also, the purpose is to use less harmful and safer chemical syntheses with safer solvents and reaction conditions, so any potential accidents can be minimized.[9,16]

NHCs and Their Applications and Publications

Numerous research papers have been published over the years about N–heterocyclic carbenes (NHC). Carbene compounds are neutral bivalent carbon intermediates having a single carbon atom with its two remaining valence electrons that are distributed between two non–bonding orbitals. A singlet NMR spectrum forms if the two electrons are spin–paired; a singlet is formed when the carbene possesses ρ–orbitals with two non–bonding spin–paired electrons and empty orthogonal ρ–orbitals. A triplet forms if two electrons are parallel.[22] Whether it is electrophilic or nucleophilic depends on the electron withdrawing or donating groups attached to the carbene. Electron donating groups would render the carbene nucleophilic; however, the divalent carbon is typically singly bound to a heteroatom such as oxygen or nitrogen in which carbon becomes more electrophilic and reactive.[23,24]

Other studies of imidazolium salts or carbenes have shown them to be sensitive precursors to capture carbon dioxide; the resulting zwitterions have been used as a stable CO_2 delivery agent (**Figure 1**).[27-29]
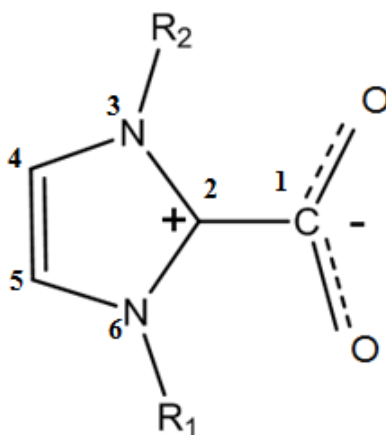
Figure 1: General Structure of Imidazolium Carboxylate[26]

Duong, et al.,[27] took a couple of NHCs and converted them into their corresponding imidazolium carboxylates. They found out that the carboxylate forms are more stable in air and more heat resistant. Conversion of new types of NHCs to the corresponding imidazolium carboxylate could produce new NHC–CO_2 adducts, leaving the reactant imidazolium carboxylate as its ylidene form. It proved that the reversibility of the imidazolium carboxylate was possible.

Ferve[30] reviewed the reactions between the imidazolium carboxylate, the targeted product in the work, and water to generate HCO_3^- proving that NHCs and the imidazolium carbonyl products are efficient pre–catalysts in molecular reactions. A dissertation of Van Ausdall[28] states that an NHC can be rapidly protonated by introducing H_2O to a solution of NHC–CO_2 in CD_2Cl_2, due to the high reactivity of NHC in mixed solvents.

In other applications of NHC complexes, the strength and distances between the C(2)–CO_2 bond was studied and the charge separation between the imidazolium and carboxylate was analyzed. Polar solvents preferred a shorter, stronger C(2)–CO_2 bond and entailed higher charge separation between the imidazolium and carboxylate. In contrast, in the gas phase and nonpolar solvents, the bond became longer and weaker and was accompanied by reduced charge separation.[23]

Also, N–phenyl imidazolium carboxylates were stable in both pure water and pure acetonitrile, but when a small amount of water was added to organic solvents such as 1,4–dioxane, acetonitrile, or methanol, the decarboxylation rate rapidly increased. For example, D. M. Denning[24] studied the decomposition rate of imidazolium carboxylate in

CH$_3$CN/H$_2$O mixtures and found that the decomposition rate exhibited a maximum at 5% (v/v) H$_2$O in CH$_3$CN.

Due to the dielectric and acid–base properties of pure acetonitrile and water, the decomposition rate could proceed via either of two different mechanisms. In a nonpolar solvent medium, a stepwise mechanism was predicted leaving an imidazolium salt as a product without any byproduct of a released carbonyl carbon. However, in a polar solvent medium, a concerted mechanism was predicted with an imidazolium salt and a byproduct of a released carbonyl carbon. The regeneration of CO$_2$ and imidazolyl carbene or salt from imidazolium carboxylate was successful with H$_2$O in polar solvents.[25]

Numerous research papers have been published over the years where N–heterocyclic carbene (NHC) ligands were bound to metal complexes such as copper (I), ruthenium (III), osmium (III), and other transition metals. Scientists studied the redox potentials of certain synthesized compounds that were associated with copper (I) and NHC ligands such as 2,6–bis(3–alkylimidazol–2–ylidene)pyridine, which is abbreviated as I(R)^{CNC} and 2,6–bis(3–alkylimidazol–2–ylidene)methylpyridine, I(R)$^{C^\wedge N^\wedge C}$, where R groups could be Me, Et, or i–Pr using CV and DPV.[31]

Once the compounds were made, D. Domyati et al.[31] compared and observed how the metal complex containing NHC behaved. The solvent–state conductivity data showed that 1:2 electrolyte behavior for I(R)^{CNC} was dominant, while 1:1 electrolyte behavior for I(R)$^{C^\wedge N^\wedge C}$ was dominant. The cyclic voltammetry and differential pulse voltammetry studies showed an irreversible and two quasi–reversible peaks for I(R)^{CNC} complexes. They concluded that redox potentials depended on solvents and their concentration.

Cyclometalated ruthenium (II) NHC complexes synthesis was characterized via NMR, X–ray, and UV Vis, CV, and DFT methods. The compounds of interest were metal complexes with NHC bidentate ligands in which the ligands contain both a carbocation and a carbene moiety.[32] Schleicher et al.[33] synthesized novel osmium (II) complexes–NHC complexes instead of osmium (III). To study the redox and electrochemical activity of enzymes, electrode surfaces, and other applications, many scientists have utilized compounds bearing NHC ligands.

Since the first synthesis of a stable crystalline carbene in 1990 by Arduengo et al.,[34] they have completed studies on many NHCs and metal ions adducts, such as pnictinidene, phosphorus (V), phosphinidene, mercury (II) complexes, diaminocarbene, bis(carbene) adducts of iodine (1+), magnesium, zinc, silver (I), copper (I), alane, and more. The stabilities or the discovery of these carbene intermediates motivated other researchers to synthesize NHCs either as ligands for transition metals or as organic catalysts. Other published articles contain the reactions between NHC and fluoroolefins[30] and cyanocarbons.[35]

NHCs with alkyl or aryl groups attached to the nitrogen atoms were synthesized into the corresponding carboxylates and characterized by Tudose et al.[36] The synthesized compounds were 1,3–dicyclohexylimidazolium–2–carboxylate, 1,3–bis(2,4,6–trimethylphenyl)imidazolium carboxylate, 1,3–bis(2,6–diisopropylphenyl)imidazolium–2–carboxylate, 1,3–bis(2,6–diisopropylphenyl) –4,5–dihydro–1H–imidazol–3–ium–2–carboxylate, and 1,3–dimesitylimidazolidine–2–carboxylate. The studies examined how imidazolium carboxylates acted as NHC precursors in catalytic applications *in situ* to open a cyclooctene. The results of ring–opening metathesis polymerization of

cyclooctene were promising with ruthenium–NHC precursors. The catalytic activities of those imidazolium carboxylates were as high as or even higher than any of the other cyclic compounds studied, especially with $IMesCO_2$ (1,3–bis(2,4,6–trimethylphenyl)–imidazolium carboxylate) which is my targeted product. $IMesCO_2$ has a 78% conversion percentage for opening the ring.

Studies on ionic liquids, such as phosphonium ionic liquids, generated NHCs that catalyze benzoin condensation and the Kumana–Corriu cross–coupling reaction are additional applications of using NHCs as organic catalysts. The reports relate that the reduction of their salt, 1,3–bis(2,6–diisopropylphenyl)imidazolium chloride occurred at a less negative potential (–2.28 V) than its phosphonium salts, especially those possessing longer alkyl chains such as tetradecyl(trihexyl)phosphonium decanoate (–2.82 V) or tetra–n–octylphosphonium bromide (–3.70 V).[37]

Studies were published on chain polymerization reactions with NHCs. Photoelectrochemical reduction of CO_2 to formic acid (CH_2O_2) has been studied on a metal photocathode with reduced nanowire catalysts.[38] Synthesis of a tri–NHC ligand with azolium salts was studied. [39] Kim et al.[40] studied the performance life cycle of rechargeable lithium–sulfur cells that consist of a mixture of lithium and three different imidazolium salt compounds and showed that the charge–discharge cycle characteristics were enhanced by adding the imidazolium salt compounds.

Zargari et al.[41] suggested a method of hydrogenating carbon dioxide with NHC catalysts. They studied the formation rate of formic acid, methanol, and formaldehyde using NHC–amidate Pd (II) complexes, varying the base that was added. They concluded that three equivalents of CO_2 to H_2 gas produced the maximum number of moles of

formic acid in KOH. The highest turnover number occurred after three hours of reaction. Different bases were employed; calcium hydroxide only yielded methanol, while silver trifluoroacetate generated formaldehyde. Potassium carbonate selectively yielded formic acid.

Initial impact studies on electrochemical reduction of an imidazolium salt were reported in 2004. An imidazolium salt compound was electrochemically reduced into an imidazole–2–ylidene; it was dissolved in the ionic liquid tetradecyl–(trihexyl)–phosphonium chloride. The salt, 1,3–bis (2,4,6–trimethylphenyl) imidazolium chloride, was irreversibly reduced at –2.28 V vs. an SCE at 300 mV•s. The 89% yield of white precipitate of carbene was characterized using NMR.[42]

Much of the work in this thesis is based on the dissertation by Van Ausdall.[28] He synthesized imidazolium carboxylates via carbene intermediates and characterized several series. He studied them with single crystal X–ray diffraction, TGA, IR spectroscopy, and NMR spectroscopy. He studied the formation of imidazolium bicarbonate after adding water to deuterated methylene chloride solutions for several N–aryl imidazolium compounds and found a new singlet at 9.10 ppm, which is the hydrogen attached to the C(2) carbon on the imidazolium ring (NCN$^-$).[29]

The IR spectrum of the N–aryl carboxylates showed the stretching vibration of C = O in $-CO_2$ at 1675 cm^{-1}, which was higher than the N–alkyl carboxylates. The bond was less affected by ortho–substituents, methylation, or saturation of the olefin bond. His TGA results showed that the decarboxylation of $IMesCO_2$ occurred at 155 ºC. The decomposition temperature decreased with an increase in the N–substituent size. Also, a

saturation of the olefinic bond caused the loss of the methyl group on the phenyl in the imidazole ring, hence increasing the pKa at C(2).[28,29]

Van Ausdall[28] concluded in his dissertation that the larger the N–substituted imidazolium, the more stable the crystal structure and the greater the ability to decarboxylate. Also, the decarboxylation temperature of bis–mesitylimidazolium carboxylate was around 155 °C while the Lewis acids $MBPh_4$, where M=Na or Li, bound imidazolium carboxylate had it at around 110 °C. The size of the N–substituted imidazolium decides the degradation temperature rate. The torsional angle between the imidazole ring and the N–substituent, as well as the C(2)–CO_2 bond length are proportional to the size of the N–substituents. The bond length of C(2)–CO_2 increases as the N–substituents rotate more towards the carboxylate moiety. The infrared C = O vibrational stretch stayed around 1629 cm^{-1} to 1683 cm^{-1}, and the larger the N–substituted group, the higher the stretching frequency.

Statement of Purpose

Several careful studies and publications on NHCs, especially on zwitterionic CO_2 adducts in Van Ausdall"s[28] dissertation, pointed to the idea of NHC being a carrier for CO_2, as shown in **Figure 2**, a general schematic of the CO_2 adduct. Depending on the N– substituents, both the physical and chemical properties could be different. Due to the ability of NHC to act as a precursor for CO_2 adduct formation–synthesis of the zwitterion, 1,3–bis(2,4,6–trimethylphenyl)–imidazolium carboxylate was carefully studied and characterized using NMR, IR, TGA, effervescence test, GC, and powder XRD. Also, the bis–mesityl imidazolyl carbene NMR and IR spectrum should be taken to compare its relative chemical sensitivity. The synthesized compound shoul be mixed with 5% (v/v) H_2O in acetonitrile to regenerate the imidazolium precursor and CO_2. The reduced carbonyl carbon should be characterized via TGA and GC.

general NHC form zwitterionic CO_2 adduct
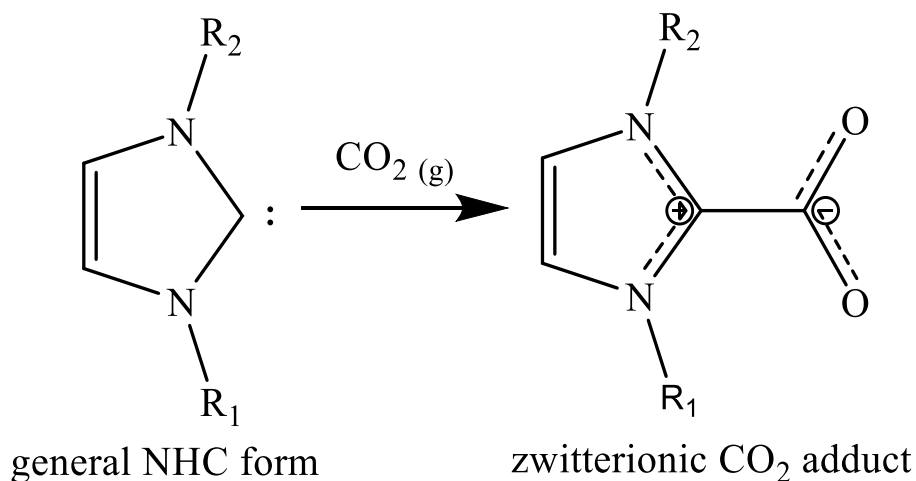
Figure 2: The Schematic of General NHC–CO_2 Production

The analysis of a stable synthesized imidazolium carboxylate, IMesCO$_2$, (**3**) and its characteristics should be compared to the following precursor compound: 1,3– bis(2,4,6–trimethylphenyl)–1,3–dihydro–2H–imidazol–2–ylidene, IMes (**2**) as shown in

Figure 3. To make it easier to refer to, the numbering of the starting material and the final product would be labeled as **1**, **2**, **3a**, and **3b** depending on the time when the measurement took place. Compound **1** would refer to commercial mesityl imidazolyl carbene that was already present in laboratory storage when this work began. A newly purchased mesityl imidazolyl carbene was labeled as **2** and it was used to synthesize mesityl imidazolium carboxylate (**3a**). Compound **3a** would refer to $IMesCO_2$ that was freshly made earlier in the research period. Compound **3b** would indicate $IMesCO_2$ that was after lengthy storage, on order of two years.
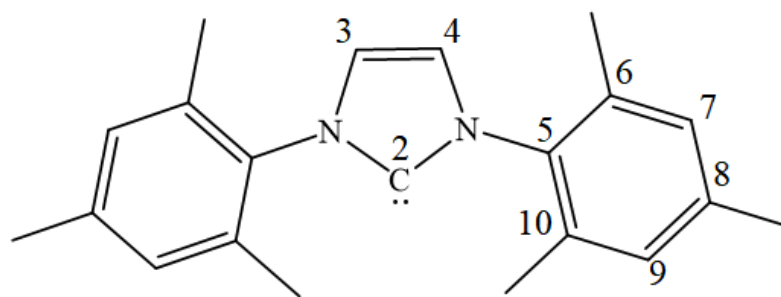
1,3-bis(2,4,6-trimethylphenyl)-1,3-dihydro-2H-imidazole-2-ylidene (**2**)
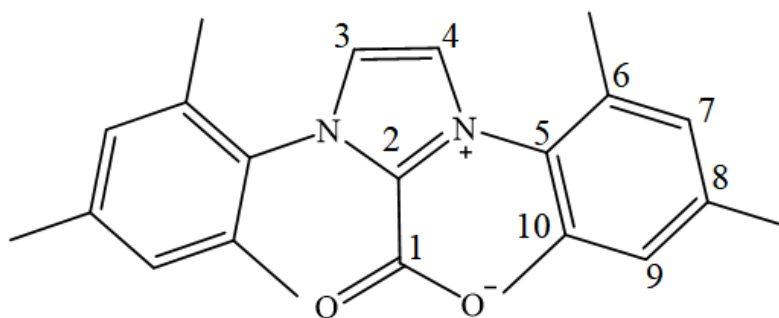
1,3-bis(2,4,6-trimethylphenyl)imidazolium carboxylate (**3**)

Figure 3: Mesityl Imidazolium Compounds of Interest[26]

Only one type of imidazolium carboxylate should be studied: 1,3–bis(2,4,6–trimethylphenyl)imidazolium carboxylate (**3**). A careful selection of solvent, THF, which was initially degassed with N_2, would be used with a CO_2 gas purge to produce the

imidazolium carboxylate. 1,3–bis(2,4,6–trimethylphenyl)–1,3–dihydro–2H–imidazol–2–

ylidene (**2**) shall be selected for the synthesis. A schematic for imidazolium carboxylate

formation is drawn in **Figure 4**.
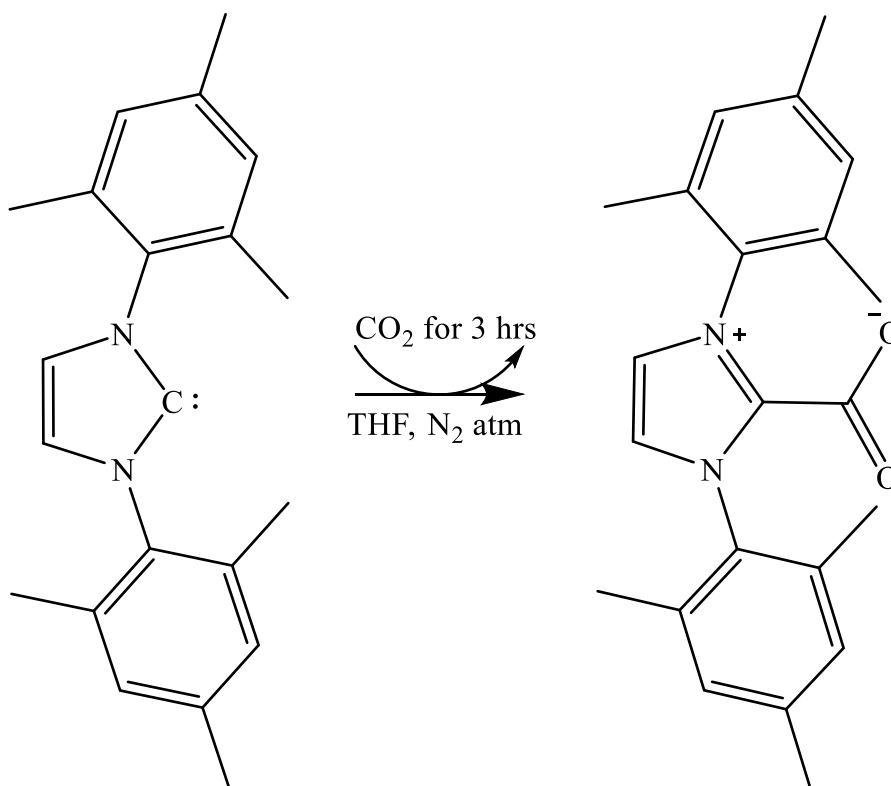
Figure 4: The Schematic of Imidazolium Carboxylate Production[26]

Also, water and several organic solvents would be employed to establish the

reactivity of **3a**. The stabilities of the final product **3b** in water (**4**), **3b** with $H_{2\,(g)}$ (**5**), and

5 with heat treatment (**6**) should be tested along with NMR characterization. Structural

characterization of **3a** and **6** should be performed with powder XRD. In order to

characterize the carbonyl carbon, TGA, GC, powder x–ray, and simple effervescence

tests should be utilized. A mix of non–polar and polar solvents such as hexane, THF,

acetonitrile, toluene, acetone, ether, and water should be used to understand the

differences in solubility and purity of the zwitterion.

CHAPTER 2: MATERIALS AND METHODS

Materials

Deuterated methylene chloride ($CD_2Cl_2 - d_2$) 99.9 D atom%, tetrahydrofuran (THF anhydrous 99.9%), THF–d_8, 1,3–bis(2,4,6–trimethylphenyl)–1,3–dihydro–2H–imidazol–2–ylidene that was characterized before this project (**1**) and imidazolyl carbene that was purchased as this project began (**2**), methylene chloride, dimethyl sulfoxide (C_2D_6OS–d_6), and anhydrous toluene 99.8% were purchased from Sigma–Aldrich. THF was purged with N_2 gas before any usage. Potassium chloride, potassium bromide, and sodium chloride were purchased from Fisher Scientific. Acetone, methanol 99.98% assay, ethanol 99.98% assay, ethyl acetate 99.99% assay, and isopropanol were purchased from Pharmco–Aaper. D_2O (100 atoms %), CD_3Cl 99.8% atom, acetonitrile (CH_3CN 99% assay) and dimethylformamide (DMF 99+% assay) were purchased from Acros Organics. Sodium hydroxide was purchased from VWR. Phenolphthalein indicator (1% (w/v) in 60% (v/v) isopropanol) was purchased from Ricca Chemical Company. Standard pans for TGA study, USP press–QTY 100 part # PS1001, were purchased from Instrument Specialists Inc. Filter paper was from Whatman. Indicating Drierite 8 mesh and molecular sieve 5 Å for gas purifier # 27068 were from W.A. Hammond Drierite Co. The indicator could be regenerated at 425 °F for 1 to 1.5 hours. N_2, He, and CO_2 gas tanks were provided by the Department of Chemistry. Glove bags, inflatable glove chamber model X–37–37 were purchased from Glas–Col Tools for Scientists.

Preparing the Reagents

Several attempts at bis–mesityl imidazolium carboxylate compound synthesis were made using DMF, D_2O, CD_2Cl_2, CD_3Cl, or THF as a solvent. Deuterated solvents were used for NMR spectroscopic analysis. All experiments were performed inside a glove bag with N_2 gas purged. The starting compound **1** was collected for its impurity test before the synthesis of $IMesCO_2$ (**3**). Due to the impurity of **1**, a newly purchased starting compound **2** was collected and dissolved in THF before being purged with CO_2 gas. Detailed procedures are listed in the results and analysis chapter under the synthesis of compound **3a**. Unless it was otherwise stated, every sample was purged with N_2 gas to satisfy the inert atmosphere condition in a glove bag. During the synthesis of **3a**, CO_2 gas was purified and filtered by passing through packed silica columns to remove any excess water.

NMR samples were all 1.0% (w/v) solutions unless otherwise stated. About 10.0 mg of sample was mixed with 1.0 mL of solvent. Detailed descriptions of sample preparations are listed in Results and Analysis. IR samples were prepared as KBr pellets. All amounts are listed in Results and Analysis, but in general, about 10.0 – 50.0 mg of KBr was ground together with 2.0 – 5.0 mg of pre–ground analyte. For TGA experiments, every compound was ground finely and spread evenly on an aluminum pan with a spatula and transferred to the oven plate with a pair of tweezers to reduce any contact with other substances.

Effervescence tests were performed outside of the glove bag and only a few milligrams of **3a** was utilized for 1.0 mL of each solvent. The GC measurements used 14.2 mg of **3a** in a test tube with a cap inside of a N_2 glove bag for compound **3a**. A head

space volume of 2.0 mL was removed from inside of the test tube and discarded before adding a 1.0 mL aliquot of a corresponding solvent. Once **3a** was dissolved, 2.0 mL of head space volume was collected for gas measurement.

Compound **3b** was subjected to different methods in GC measurements. Compound **3b** was collected in an Erlenmeyer flask, which was capped with a N_2 (g) filled balloon before each study. After removing the N_2 (g) filled balloon, 2.0 mL of head space volume was withdrawn and discarded from the flask containing N_2 (g) and **3b** before adding solvents such as 5% (v/v) H_2O in CH_3CN or CH_3CN. As soon as a 1.0 mL aliquot of solvent was added, 1.0 mL of gas was collected for GC measurements.

To determine the stability of **3b** in the presence of different chemicals, 15.6 mg of **3b** was dissolved in a test tube with a 1.0 mL aliquot of H_2O. A test tube was pre–washed with detergent and dried in 120 °C oven for overnight. It was poured onto a watch glass, covered with Parafilm and placed on a laboratory bench overnight. The dried–up powder (**4**) weighed 14.9 mg and was collected in a sanitized vial for further analysis. Also, compound **3b** was first exposed to H_2 (g) for six hours (**5**) and then analyzed via NMR. The stability of **5** to heat was tested by heating the sample at 95 °C for 5 minutes in air. The temperature was selected since the removal of carbonic anhydride happens between 100 °C and 155 °C according to the experimental data.

For single crystal X–ray study, only a few milligrams of **3a**, **3b**, or **5** was added to each solvent for recrystallization. For powder XRD patterns for compound **3a** and **6**, the compound was finely ground and spread onto an open circular recess in an aluminum disc cup and flattened with a clean microscope slide.

Characterization Techniques

Nuclear Magnetic Resonance (NMR) Analysis

NMR spectra data were recorded on a Brucker NMR spectrometer, 400 MHz for ^{1}H NMR, 100 MHz for ^{13}C NMR, COSY (^{1}H–^{1}H), NOESY (^{1}H–^{1}H), and HSQC (^{1}H–^{13}C) using DMSO–d_6, CD_2Cl_2–d_2, THF–d_8, and $CDCl_3$–d_1 as solvents according to sample conditions. The specific solvents are stated in the legend for each spectrum. ^{1}H and ^{13}C NMR charts were calibrated in delta (δ) units in which 1 δ is 1 part per million (ppm). All chemical shifts (ppm) were relative to the chemical shift (ppm) of the internal standard solvents. 2D NOESY NMR was to study the correlations between protons through space; atoms that were less than 5 Å apart were shown in the spectrum. 2D COSY NMR was studied for protons correlations through bonds and it is observed when bonds are 1 – 2 bonds apart.

Infrared (IR) Spectroscopy Analysis

IR spectroscopic analysis was performed using an IR 200 Spectrometer and analyzed by the EZ OMNIC program. After taking an IR spectrum of an air background, KBr pellets with three compounds: **2**, **3a**, and **3b** were analyzed. The experiments were measured in cm^{-1} unless otherwise stated. Signal positions and intensities were carefully assigned according to their properties.[43]

Thermogravimetric Analysis (TGA)

TGA profiles were studied on a Hi–Res TGA 2950 Thermogravimetric Analyzer with Thermal Solutions program. Every profile was analyzed using *TA Universal Analysis*. A sample weight of 1.4750 mg had a starting temperature of 50 °C and was

heated at 1 °C per minute up to 425 °C. A sample of 3.1080 mg had a starting

temperature of 25 °C and was heated at 5 °C per minute up to 200 °C. A sample of

2.2110 mg had a starting temperature of 25 °C and was heated at 5 °C per minute up to

200 °C. A sample weight of 10.5220 mg had a starting temperature of 20 °C and was

heated at 10 °C per minute up to 600 °C. It was set to pyrolyze the rest of the molecule.

Gas Chromatography (GC) Analysis

Carbon dioxide gas that was separated from the bis–mesityl imidazolium

carboxylate was analyzed via a GOW–MAC Instrument Company gas chromatograph,

series 580, equipped with an 8.0 ft long and 0.125 in outer diameters Porapak Q column.

Throughout the experiment, the helium gas pressure was at 60 psi. The temperatures for

column, detector, and injector were at 60 °C, 120 °C, and 120 °C, respectively. The

detector current was at 45 mA. The carrier gas flow rate of the system was 83 mL per

minute. The *DataApex Clarity Lite*^{TM} *advanced chromatography* software for Windows

was used for analysis. The standard graph for CO_2 (g) is in **Figure D1** and **Table D1** for

3a. The standard graphs for CO_2 (g) and and N_2 (g) are in **Figure D3**. **Tables D3** and **D4**

are retention time and response.

Powder X–Ray Diffraction (XRD) Analysis

Powder XRD patterns were collected using a Rigaku Miniflex diffractometer with

Cu–K radiation in reflective mode, with an open aluminum disc cup. The compound was

finely ground before further analysis. The data were analyzed using the *X'Pert HighScore*

software.

Effervescence Test Techniques
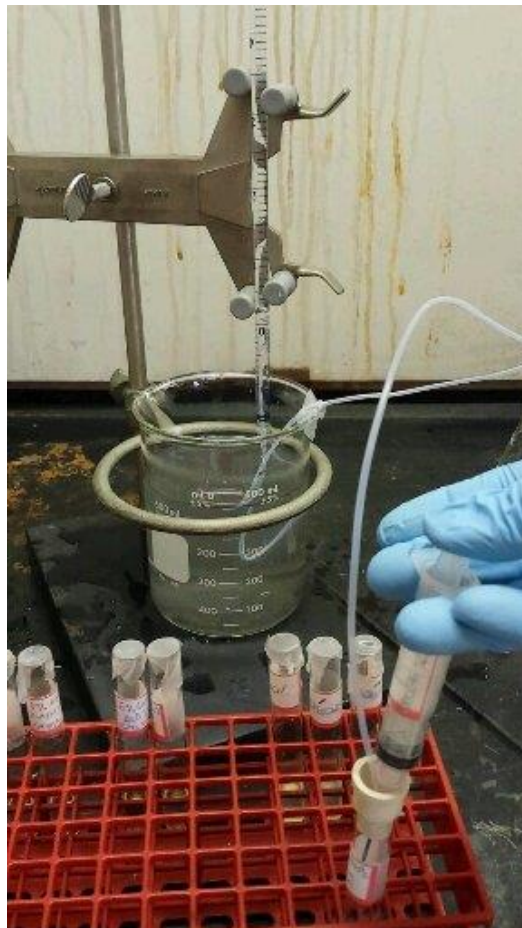
Figure 5: Effervescence Tests Apparatus

The study of measuring gas evolved from **3a**, **3b**, or **5** was performed as shown in **Figure 5**. The tip of a graduated pipette was sealed and filled with water. Once the bottom of the graduated pipette was submerged in water, a pipe was inserted inside the inverted pipette to collect any presence of gas from the experiment. Once compound **3a**, **3b**, or **5** was collected in test tubes, head space volume was removed before any solvents were injected. The gas measurement was taken as the displaced amount of water inside of the sealed graduated pipette.

Solubility Test Techniques

Due to the characteristics of the synthesized compounds **3a**, **3b** and **5**, three types of solvents were studied: polar protic, polar aprotic, and nonpolar. The solubility test was to determine which solvent was the most suitable solvent for crystal growth. Also, several diluted acid and base solvents were tested for **3a** solubility.

Droplets of solvents were mixed until it was determined that the compound was soluble for each solubility study. Several experiments took place where solvents were heated, but not boiled, before adding to the powder.

For the crystal growth trials of **3a**, **3b**, and **5**, a few milligrams of each compound was collected in a sanitized test tube on a laboratory bench. A 1.0 mL aliquot of solvent was added for the study. Once each compound was well mixed with the solvent, it was left on a laboratory bench for crystal growth.

CHAPTER 3: RESULTS AND ANALYSIS

1,3–bis(2,4,6–trimethylphenyl)–1,3–dihydro–2H–imidazole–2–ylidene

NMR Characterization and Analysis

Before the NMR characterization of **2,** the impurity of an existing ylidene (**1**) was performed. The solution consisted of 9.5 mg of **1** dissolved in THF–d_8. Compound **1** was unable to dissolve completely and showed too many signals in the NMR data (**Figures A1** and **A2**). A 1% solution contained 11.2 mg of sample **2**, which was purchased as the project started, and employed CDCl$_3$–d_2 as a solvent. The NMR spectral data are found in Appendix A (**Figures A3–A7**).

^{1}H NMR (400 MHz, CDCl$_3$) δ 2.11 ppm (s, 12H, *ortho*–CH$_3$), 2.27 ppm (s, 6H, *para*–CH^3), 6.99 ppm (s, 4H, *meta*–CH), 7.21 ppm (s, 2H, CHN)

^{13}C NMR (100 MHz, CDCl$_3$) δ 17.65 ppm (s, *ortho*–CH$_3$), 21.11 ppm (s, *para*–CH$_3$), 129.90 ppm (s, C4), 130.28 ppm (s, C5), 130.63 ppm (d, C7 and C9), 137.08 ppm (s, C6 and C10), 141.22 ppm (s, C8), and 142.56 ppm (s, C2)

Figure 6 is the COSY 2D NMR spectrum of IMes (**2**). No correlations between the protons on the imidazolium ring and the protons on the phenyl rings were found. Since the protons on the olefin are far from the phenyl ring, their signals are uncorrelated. Only the *meta*–H correlated with the o- and p-methyl groups, all on the mesityl ring.
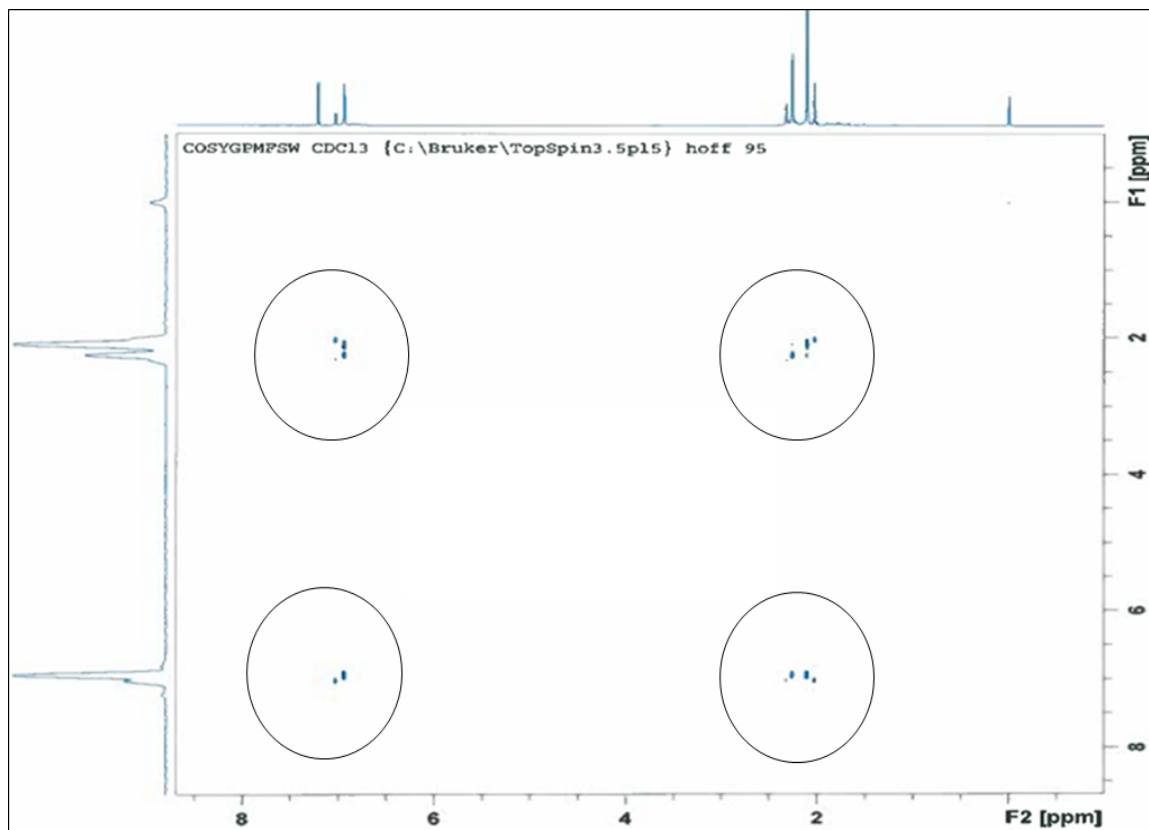
Figure 6: 2D COSY NMR Spectrum of Compound **2**

The 2D NOESY NMR spectrum of **2** shown in **Figure 7** also shows that there are correlations between the *meta*–H's and the three methyl groups on the phenyl rings. However, no correlations between the protons on the imidazolium ring and the protons on the phenyl rings were found. The through space correlation NMR spectrum picked up the presence of protons. See Appendix A for an enlarged **Figure 7**.
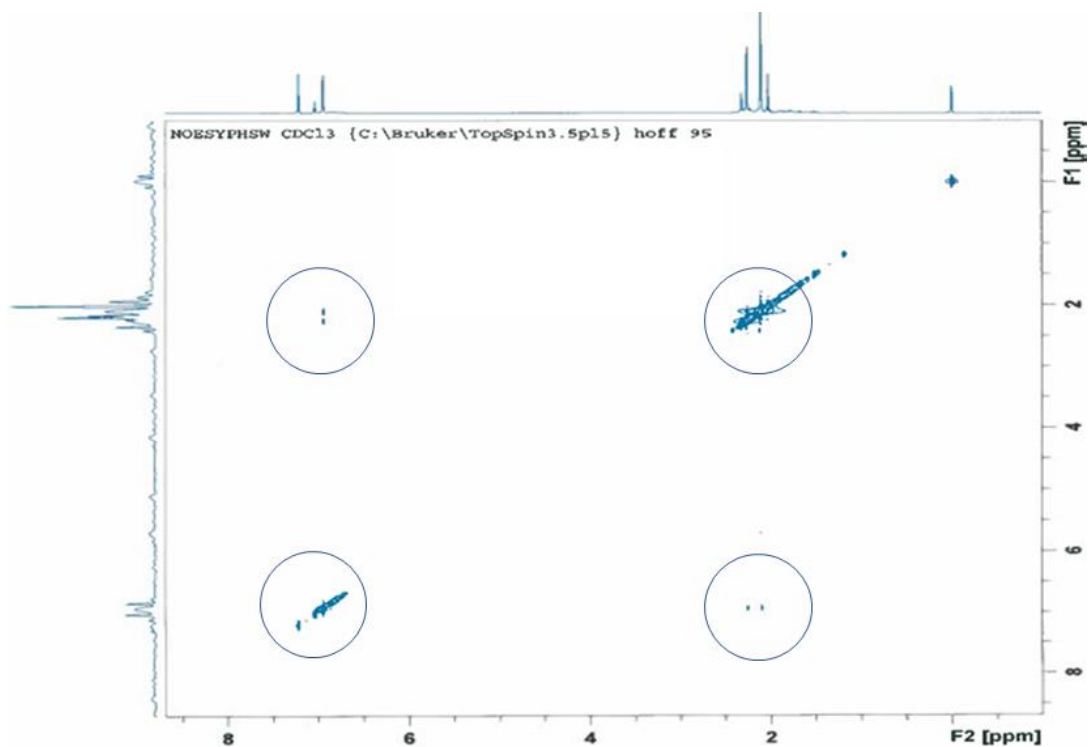
Figure 7: 2D NOESY NMR Spectrum of Compound **2**

The correlations between protons and carbons can be assigned as follows according to the 2D HSQC NMR spectrum data in **Table 1** and a full spectrum is found in **Figure A7**.

Table 1: 2D HSQC NMR Correlations for Compound **2**

Assignments	^{1}H NMR (ppm)	^{13}C NMR (ppm)
ortho–CH$_3$	2.11	17.65
para–CH$_3$	2.272	21.11
meta–CH	6.988	130.63

According to the NMR characterization, no correlations between *meta* protons on the phenyl ring and protons on the imidazole ring were found. Thus, the compound could be planar in solution.

IR Analysis

Sample pellets prepared for IR characterization had a mixture of 57.3 mg KBr and 8.0 mg compound **2**. A full IR spectrum is shown in **Figure B1** and the assignments are as follows: 3158.05 cm^{-1} (C_{phenyl}=CH), 2949.77 cm^{-1} (sp^3 C–H), 1539.20 cm^{-1} (C=C), 1481.05 cm^{-1} (C–CH$_3$), 1379.61 cm^{-1}(N–C), 1230.97 cm^{-1} (C_{phenyl}–C_{phenyl}), and 931.06 cm^{-1} – 675.73 cm^{-1} (C_{phenyl}–H)

Figure 8 shows the presence of peaks at 3639.67 cm^{-1} and 3311.97 cm^{-1} which could be O–H or amine vibrational stretches. The presence of moisture is evident while preparing the KBr pellets or taking the measurements.
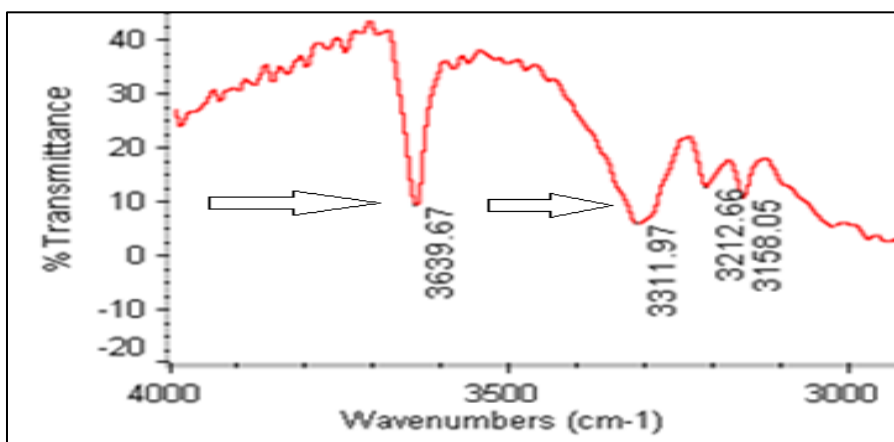
Figure 8: A Partial IR Spectrum of **2** Between 3000 cm^{-1} – 4000 cm^{-1}

Synthesis of 1,3–bis(2,4,6–trimethylphenyl)imidazol–2–carboxylate (3)

The synthesis performed with carbene (**1**) that had already been stored in the laboratory bench for at least one year showed yellow– and dark–colored precipitates after the reaction was finished (**Figure 9**). It was evident that the starting material was impure and would not facilitate an easy work-up. It was decided to reattempt the synthesis with a fresher preparation of the carbene.
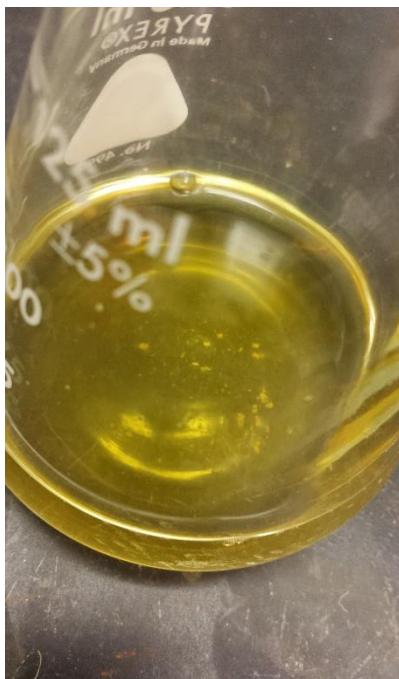
Figure 9: IMes Carbene (**1**) in THF

To synthesize **3a**, a glove bag was filled with N_2 gas. Reactant, IMes, (**2**) was introduced in an Erlenmeyer flask. Enough THF was added so that all IMes (**2**) was well dissolved. While stirring the solution, it was continuously purged with CO_2 gas for at least 3 hours.

Degassed THF was collected in an Erlenmeyer flask (**Figure 10A**). Once compound **2** was added, the color immediately changed to yellow (**Figure 10B**). Upon

addition of CO_2, the solution immediately became hazy, and after one minute, a pale

yellow substance began to precipitate out, as shown in **Figure 10C**.

A) Degassed THF   **B) THF with IMes (2)**   **C) One minute after CO_2 addition**
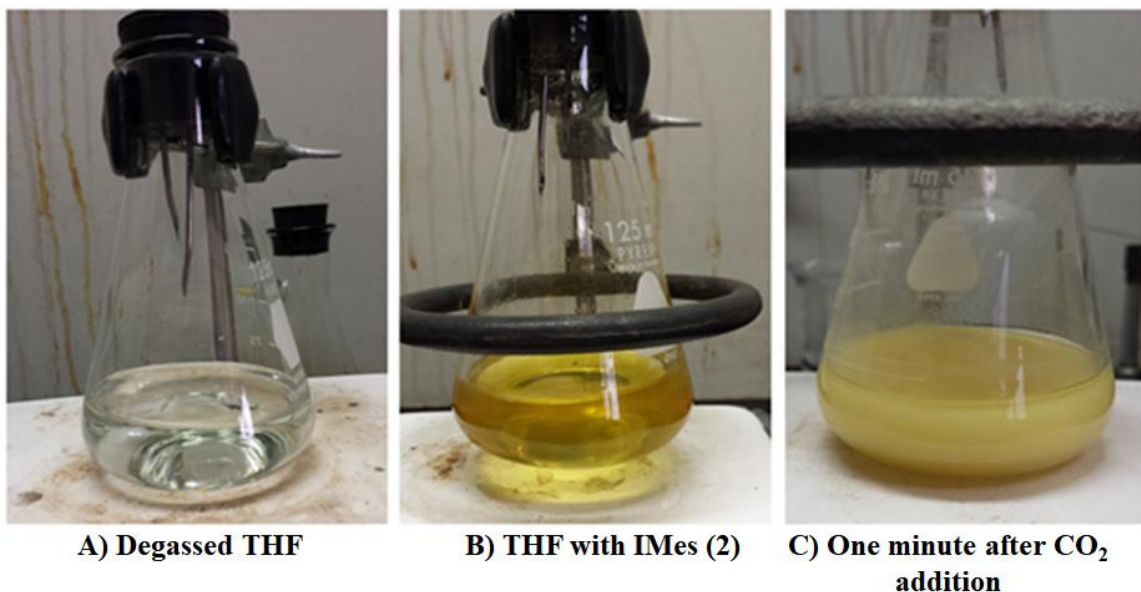
Figure 10: Stages in the Synthesis of IMesCO$_2$ (**3a**)

The mixture was taken out from the glove bag after 3 hours of CO_2 (g) addition,

and vacuum filtered. Any powder that was left was washed with THF. The final product

from each trial was saved in a separate vial and kept inside a desiccator. An average of

363.5 mg (71.1% yield) of the final powder, 1,3-bis(2,4,6-trimethylphenyl)imidazol-2-

carboxylate (**3a**) was formed from several trials as shown in **Table 2** below.

Table 2: IMesCO$_2$ (**3a**) Synthesis

Amount of **2** used (mg)	Yield of **3a** (mg)	Percent Yield (%)
1076.76	950.3	88.26
12.10	9.40	77.7
540.40	482.9	89.36
38.66	11.28	29.19
Average	363.5	71.1

Characterization of 1,3-bis(2,4,6-trimethylphenyl)imidazolium-2-carboxylate (3a)

NMR Characterization and Analysis

For NMR Characterization of **3a**, 10.1 mg of sample was used to make a 1%

CD_2Cl_2–d_2 solution. A full NMR spectroscopic data can be found in **Figures A8–A12**.

^{1}H NMR (400 MHz, CH_2Cl_2–d_2) δ 2.05 ppm (s, 12H, *ortho*–CH_3), 2.27 ppm (s, 6H,

para–CH_3), 6.99 ppm (s, 4H, *meta*–CH), 7.48 ppm (s, 2H, CHN)

^{13}C NMR (100 MHz, CH_2Cl_2–d_2) δ 17.51 ppm (s, *ortho*–CH_3), 21.24 ppm (s, *para*–CH_3),

121.70 ppm (s, C8), 124.72 ppm (s, C4), 129.58 ppm and 130.05 ppm (s, C7 and C9),

131.29 ppm (s, C5), 134.71 ppm and 135.13 ppm (s, C6 and C10), 141.70 ppm (s, C2),

158.47 ppm (s, CO_2^-)

All the hydrogen atoms on the phenyl rings for **3a** show distinct peaks when

compared to IMes (**2**) compound shown in **Table 3**. It is due to the CO_2 adduct

stabilizing the whole compound. The olefin proton of **3a** chemical shift is farther

downfield, from 7.21 ppm to 7.48 ppm. As the carbonyl carbon was added to **2**, protons

at the *meta*, *ortho*, and *para* position were shifted upfield. It indicates that the closer the

protons are to the oxygen with higher electronegativity, a higher electronegative

difference between atoms, in which the difference lowers the chemical shifts.

Table 3: Comparison ^{1}H NMR Chemical Shifts of **2** and **3a**

Assignments	^{1}H NMR of IMes (**2**) (ppm)	^{1}H NMR of IMesCO$_2$ (**3a**) (ppm)
12 H ortho - CH$_3$	2.11	2.05
6 H para - CH$_3$	2.32	2.27
4 H meta - CH	7.03	6.99
2 H - CHN	7.21	7.48

Further, **Figure 11** comparing **3a** and **2** NMR spectra illustrates 4 major peaks: two types of hydrogen atoms on the methyl groups on the phenyl ring, one hydrogen on the *meta* position on the phenyl ring, and the hydrogen atoms on the imidazolium ring. However, the hydrogen peaks on the IMes (**2**) are slightly closer than the hydrogen peaks on the IMesCO$_2$ (**3a**). Also, the proton peaks on **3b** are easier to characterize with less noise than on **2**, due to CO$_2$ adduct on the C(2) carbon. All of these may be due to the instability of **2** by itself and in solution.
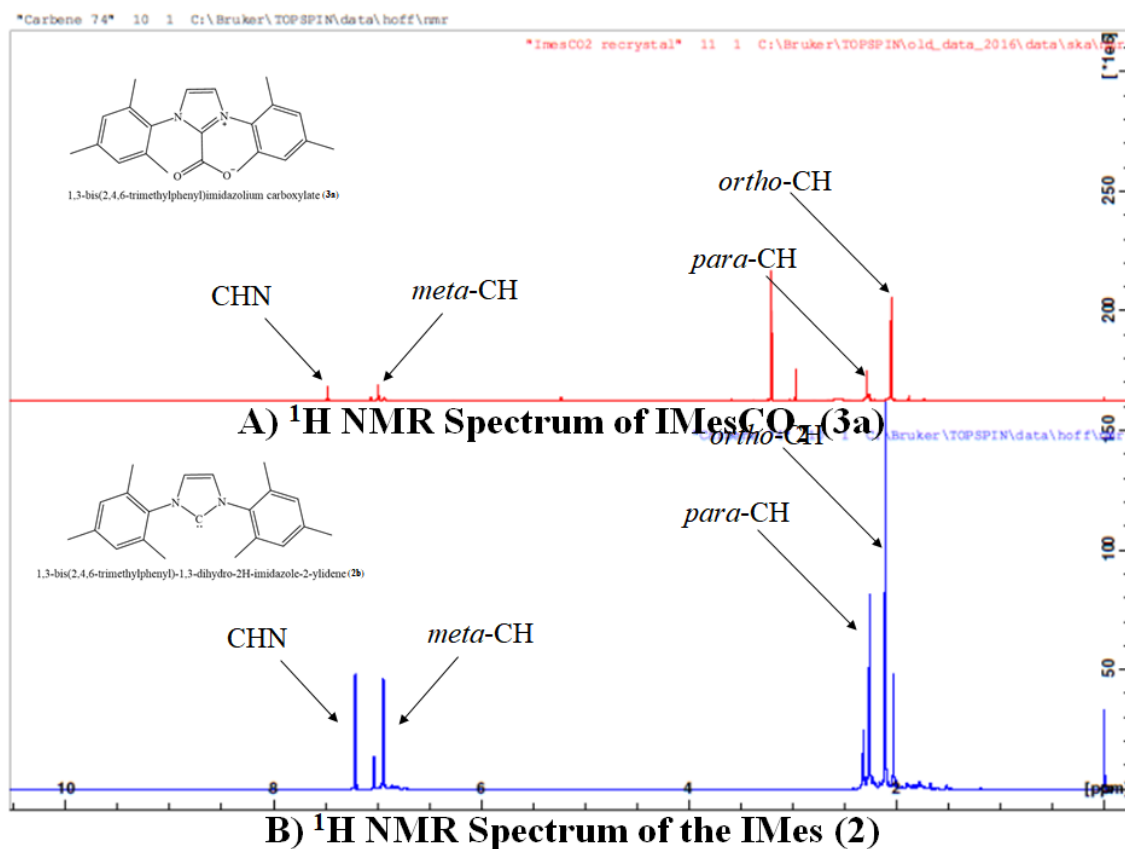
Figure 11: ^{1}H NMR Spectrum of A) the Final Product; B) the Starting Material

A new carbon chemical shift of **3a** was found at 158.47 ppm which is CO_2 chemical shift in **Table 4**. Comparing ^{13}C NMR spectra between **2** and **3a**, chemical shifts for **3a** have moved more downfield than IMes (**2**) due to the CO_2 that has been added onto IMes (**2**).

Table 4: ^{13}C NMR Spectra of IMes (**2**) and IMesCO$_2$ (**3a**)

Assignments	2 (ppm)	3a (ppm)
ortho – CH_3	17.65	17.51
para – CH_3	21.11	21.24
C4	129.90	124.72
C5	130.28	131.29
C7, C9	130.63	130.05
C6, C10	137.08	135.13
C8	141.22	121.70
C2	142.56	141.70
CO_2	N/A	158.47

Figure 12B shows a new transition at 158.47 ppm in ^{13}C NMR spectrum, corresponding to the CO_2 carbon. The peak positions are similar to the NMR chemical shifts that have been published.[35]
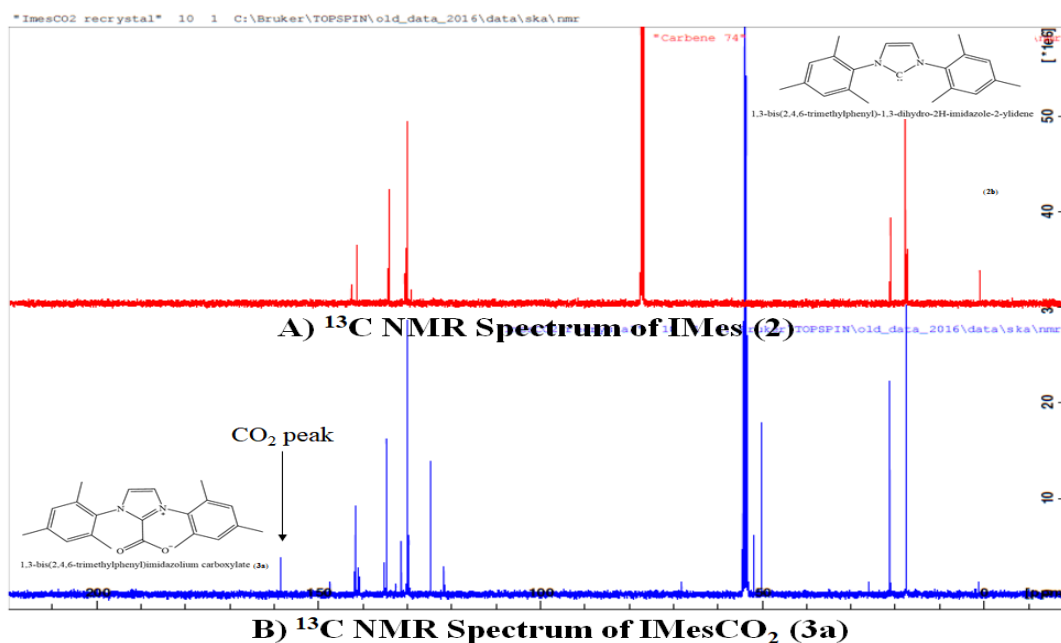
Figure 12: Comparing ^{13}C NMR Spectrum of A) **2** and B) **3a**

Figure 13 is the 2D NOESY NMR spectrum obtained for compound **3a** and it shows that no through–space correlations between the olefin protons and the para methyl protons on the phenyl rings were detected. It is due to their distances that are too far for the Nuclear Overhauser Effect to be detected. However, the *ortho* – CH_3 protons and *meta* – CH_3 protons, separately correlate with imidazolium ring protons (CHN) through space. This indicates that these protons may be less than 5 Å away from each other. To precisely measure the distance between atoms, a single crystal XRD structure would be necessary.
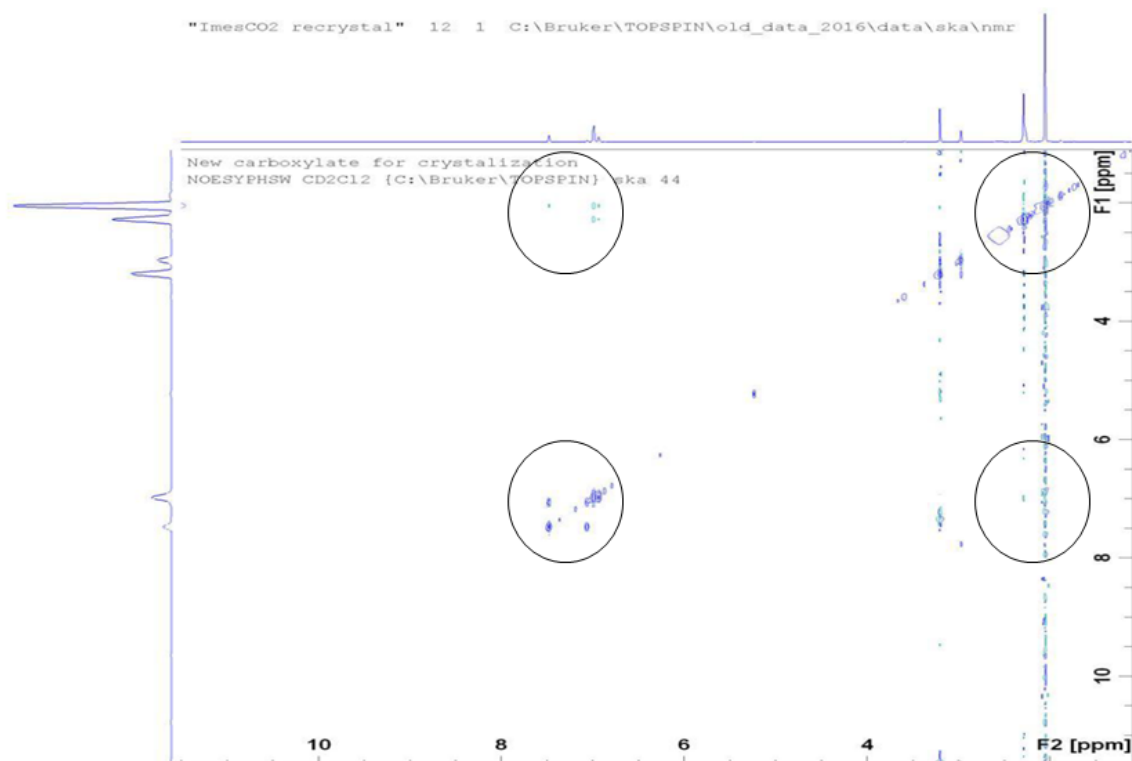
Figure 13: 2D NOESY NMR Spectrum of **3a**

Figure 14 shows that the bond–bond correlations between protons on the phenyl rings are detected. Other protons have bond–bond distances that are too far so that no signals could be detected via 2D COSY NMR spectrum.
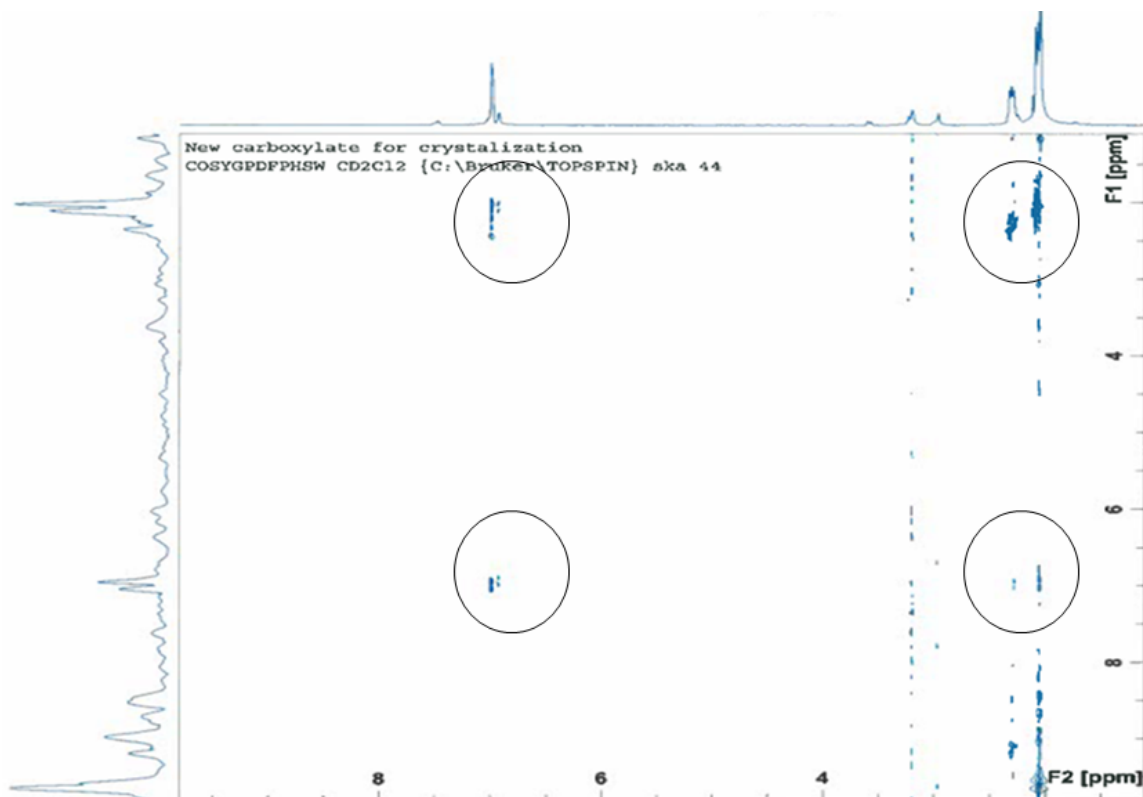
Figure 14: 2D COSY NMR Spectrum of **3a**

The HSQC NMR spectrum of **3a** was obtained (**Figure A12**) and all four H–C correlations were found and are tabulated in **Table 5**.

Table 5: HSQC NMR of IMesCO$_2$ (**3a**)

Assignments	^{1}H NMR (ppm)	^{13}C NMR (ppm)
ortho – CH$_3$	2.049	17.51
para – CH$_3$	2.272	21.24
meta – CH	6.988	129.82
C4	7.476	124.72

IR Characterization and Analysis

For the IR characterization, 2.6 mg of sample and 43.7 mg of KBr were used to make KBr pellets. A full IR spectrum is shown in **Figure B2** and the assignments are as follows: 3159.78 cm^{-1} and 3082.03 cm^{-1} (C$_{phenyl}$=CH), 2956.26 cm^{-1} – 2861.95 cm^{-1} (sp^3 C–H), 1678.50 cm^{-1} (C=O), 1609.10 cm^{-1} and 1550.82 cm^{-1} (C=C), 1488.82 cm^{-1} (C–CH$_3$), 1300.16 cm^{-1} (N–C), 1226.52 cm^{-1} (C$_{phenyl}$–C$_{phenyl}$), and 933.44 cm^{-1} – 658.82 cm^{-1} (C$_{phenyl}$–H).

The IR study of **3a** shows that a new peak at 1678.50 cm^{-1} appears in **Figure 15B** in comparison to the starting compound, IMes (**2**) in **Figure 15A**. Normally, the C=O vibrational stretch of CO$_2$ gas appears at around 667 cm^{-1} and 2349 cm^{-1} when the molecule is isolated. However, when the C=O stretch is present within an organic compound, the peak occurs in the rage 1600 – 1800 cm^{-1}, so that the vibrational stretch at 1678.50 cm^{-1} likely indicates the presence of CO$_2$ at the C(2) carbon of the imidazolium.[20]
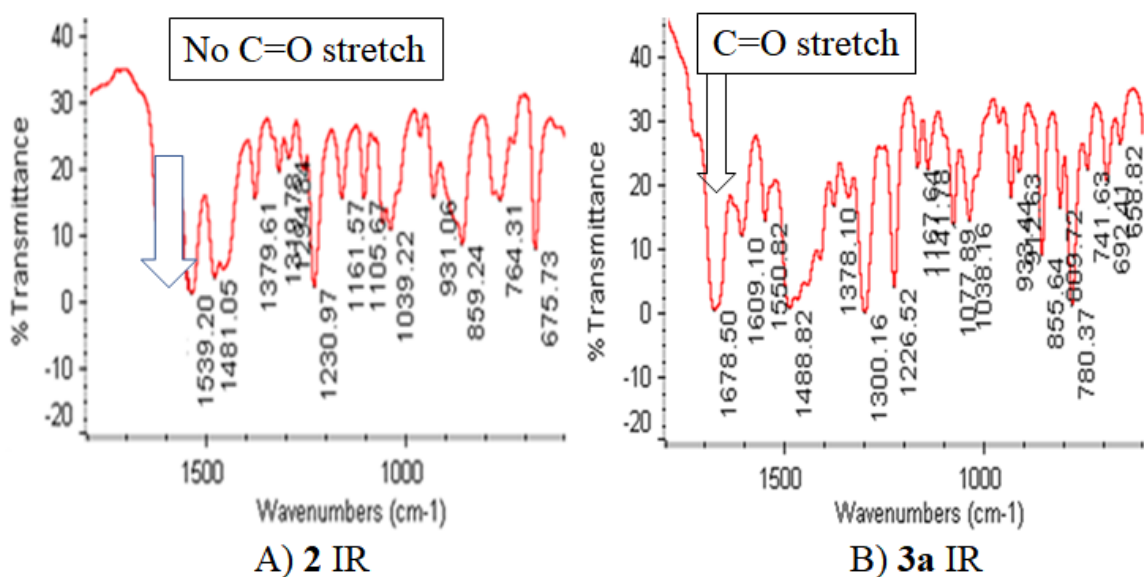
Figure 15: IR Spectra Comparison between **2** and **3a**

TGA Study

For TGA characterization, 3.108 mg of **3a** was finely ground and placed in an aluminum pan. A full TGA profile can be found in Appendix C (**Figure C1**). The published value for the onset of weight loss occurs at 155 °C.[28] However, **Figure 16** shows a continuous weight loss occurred up until around 155 °C. Knowing that the molecular weight of IMesCO$_2$ (**3a**) is 348.446 g/mol, the weight percent of the carbonyl carbon is around 13%. The 13.51% weight loss up until 155 °C indicates the weight loss of CO$_2$ at the C(2) carbon within the molecule.
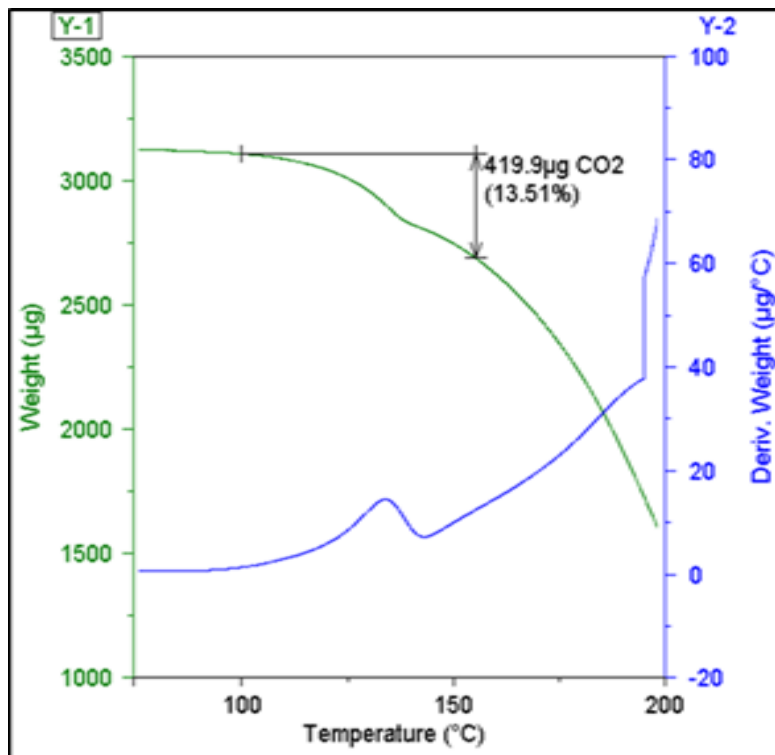
Figure 16: TGA Profile of IMesCO$_2$ (**3a**)

Also, it seems that after 200 °C, the compound becomes pyrolyzed leaving dark carbon residues. The pyrolyzed samples were observed each time the temperature limit was set above 200 °C.

Study of Carbonyl Carbon from IMesCO$_2$ (3a) via Effervescence Test

The gas evolution tests were performed before the GC analysis to narrow down the ideal amount of material for the GC study without wasting product unnecessarily. Neat CH$_3$CN and 5% (v/v) H$_2$O in CH$_3$CN were the solvents used to analyze the effect of water IMesCO$_2$ hydrolysis and CO$_2$ gas evolution. However, the results are described under the GC study using only 5% (v/v) H$_2$O in CH$_3$CN.

The measurement of released gas was made after determining the solubility of IMesCO$_2$ (**3a**) in several types of solvents. Initially, the effervescence was measured with only a few milligrams of **3a**. Once the gas was detected, the theoretical yield was calculated based on the Ideal Gas Law.

Knowing that the molecular weight of the compound **3a** is 348.446 g/mol, the volume of CO$_2$ evolved upon the breakdown of the adduct at 25 °C in L/mol is as follows:

$$PV = nRT$$

Equation 1: The Ideal Gas Law

$$1 \text{ atm} \times V = 1 \text{ mol} \times 0.082 \text{ (L} \times \text{atm / mol} \times \text{K)} \times 298.15 \text{ K}$$

$$V = 24.448 \text{ L/mol} = 24448 \text{ mL/mol}$$

Imidazolium carboxylate (**3a**) amount needed for 1.0 mL CO$_2$ collection:

$$\frac{\text{Amount of imidazolium carboxylate (}\textbf{3a}\text{)}}{348.446 \text{ }^g/_{mol}} * 24450 \text{ }^m/_{mol}$$

$$= 1.0 \text{ mL CO}_2$$

Amount of imidazolium carboxylate (**3a**) = 0.014251 g

$$= 14.251 \text{ mg}$$

First, a general effervescence test was performed. With compound **3a** being a zwitterion, which possesses both a net negative and a net positive charge density region, nonpolar solvents seem to be better solvents to dissolve it. However, polar solvents were studied to check whether **3a** loses its carbonyl carbon. Also, other mixtures and acid/base solvents were used to analyze the dissociation of the carbonyl carbon from IMesCO$_2$ (**3a**). Selection of chemicals was based on articles that had studied carbonyl carbon and NHCs.[20,22-31,34-37,40-43]

The different solvents types used for effervescence tests are listed in **Table 6-8**. Effervescence results obtained when **3a** was exposed to polar aprotic solvents are given in **Table 6**. Repeated trials showed that none of the polar aprotic solvents removed the carbonyl carbon attached at the C(2) carbon. Any measured CO$_2$ may be from the higher pressure that was produced while injecting the solvents.

Table 6: Effervescence Test of IMesCO$_2$ (**3a**) with Polar Aprotic Solvents

Solvents	Amount of **3a** (mg)	Theoretical yield (mL)	Measured CO$_2$ volume (mL)
CH$_2$Cl$_2$	3.7	0.26	0.60
	2.1	0.15	None
DMF	5.8	0.41	None
THF	4.1	0.29	2.1
	2.1	0.15	None
Acetone	3.0	0.21	5.8
	1.5	0.11	None

Results for polar protic solvents are given in **Table 7**. Polar protic solvents proved to be no different from polar aprotic solvents. No consistent measurements of evolved gas were obtained. The measured gas was once again subjected to higher pressure resulting from solvent injection when testing.

Table 7: Effervescence Test of $IMesCO_2$ (**3a**) with Polar Protic Solvents

Solvents	Amount of **3a** (mg)	Theoretical yield (mL)	Measured CO_2 volume (mL)
H_2O	2.3	0.16	None
CH$_3$OH	4.3	0.30	0.40
	3.8	0.27	None
EtOH	1.2	0.08	0.70
	1.5	0.11	None
Isopropanol	3.5	0.25	0.10
	3.9	0.27	None
Acetic Acid	1.7	0.12	None

In **Table 8**, the results were inconsistent with nonpolar solvents. The mixtures, acids, and bases did not yield any gas when the reaction took place even if the amount of compound was increased. However, in general, **3a** is stable in nonpolar solvents and solvent mixtures.

Table 8: Effervescence Test of **3a** with Nonpolar Solvents and Solvent Mixtures

Solvents	Amount of **3a** (mg)	Theoretical yield (mL)	Measured CO_2 volume (mL)
Benzene	5.8	0.41	5.9
	2.8	0.20	None
	2.6	0.28	None
Ethyl Acetate	6.0	0.42	0.60
	3.3	0.23	None
Hexane	2.2	0.15	3.5
	2.5	0.18	None
	2.3	0.16	None
0.01 M HCl	2.4	0.17	None
	6.1	0.43	None
0.01 M NaCl	2.5	0.18	None
	5.1	0.36	None
5% H_2O, 0.01 M NaCl, balance CH_3CN	2.8	0.20	None
	5.0	0.35	None
0.01 M NaOH	2.3	0.16	2.0
	6.1	0.43	None

These experiments show that **3a** does not yield gas when mixed with polar protic, polar aprotic, nonpolar, or even in mixtures, in general. The experimental concentration of the solutions was too low for the reaction to occur, or the scale of the experiment was too small to measure. The results of acetone and benzene showed too much gas which may be due to the vapor pressure of more volatile solvents.

Van Ausdall's dissertation stated that adding water to **3a** showed a new NMR chemical shift for all the methyl protons without losing the carboxylate at C(2) carbon. Both methyl proton shifts moved downfield. Also, adding water to solutions of imidazolium compounds with smaller N–substituents in CH_3Cl instantly removed CO_2.[28]

It has been reported that imidazolium carboxylates with smaller N−substituents, such as the dimethyl carboxylate, i.e., IMeCO$_2$, immediately react with water in CH$_3$Cl solution to form the imidazolium bicarbonate with a new ^{1}H NMR signal at 9.10 ppm for HCO$_3^-$.[28] From this experiment, it was found that methylene chloride does not dissociate the carbonyl carbon. Also, it is unclear whether the solution dissociates carbonyl carbon from imidazolium carboxylate (**3a**). In contrast, another researcher reported that a mixture of water with acetonitrile solution of **3a** hydrogenated the C(2) carbon with HCO$_3^-$ as a byproduct.[25] In order to understand the circumstances to release carbonyl carbon, acetonitrile was employed. Tests were conducted to check whether the solvent dissociates the carbonyl carbon from compound **3a**. Also, to examine how effective water performs in the decarboxylation reaction, another set of experiments was performed with CH$_3$CN containing a trace of water.

Study of Carbonyl Carbon Dissociated from IMesCO$_2$ (3a) via GC Analysis

A GC analysis was performed to study any gas dissociated from IMesCO$_2$ (**3a**). Steady state gas measurements were conducted throughout the experiments. First three small volumes from each sample were tested to determine whether the solvent can dissociate carbonyl carbon from the imidazolium carboxylate (**3a**). Once any form of gas was detected, a larger volume was taken for the GC study.

Measurements of gas evolution from compound **3a** were performed in 5% (v/v) H$_2$O in CH$_3$CN with different quantities of compound **3a** to ensure the validity of the gas evolution experiments. The injection volume was held at a 1.0 mL aliquot solution. Steady state measurements of gas evolution were made in 5% (v/v) H$_2$O in CH$_3$CN

solution. The yielded gas quantity may not be the same as the theoretical yield, but consistent proportions of gas were measured throughout the experiment.

Table 9 below shows that an increase of CO_2 (g) volume was obtained as the quantity of **3a** increases. When **3a** was dissolved in the water itself, no gas was detected. However, the steady evolution of gas was recorded when the sample was dissolved in a water and acetonitrile mixture. The percent deviations from 100% for the 8.5 mg, 15.4 mg, and 51.9 mg samples were +30%, and –37%. Hence, 5% (v/v) H_2O in CH_3CN solution was used for GC analysis of the released carbonyl carbon.

Table 9: CO_2 Evolution Test of Compound **3a** with 5% (v/v) H_2O in CH_3CN

Mass **3a** (mg)	Theoretical yield of CO_2 (mL)	Experimental volume of CO_2 (mL)
51.9	3.64	2.3
15.4	1.08	1.4
8.5	0.60	1.2
7.5	0.53	1.1
5.2	0.36	2.3
3.2	0.22	2.0
1.1	0.077	5.5

For the quantitative measurement of CO_2 gas released from **3a** with N_2 gas purged atmosphere, the GC standards for both N_2 gas and CO_2 gas needed to be measured (Appendix D), since sampling the headspace after reaction would also find some of the purge gas.

The amount of carboxylate (**3a**) for the test was 14.2 mg which was the theoretical mass to collect 1.0 mL of CO_2, according to the Ideal Gas Law. The evolved gas was collected immediately after **3a** was exposed to the solvent. The retention time and integrated peak area were 0.524 min and 19.276 mV•s, respectively. The calculated amount of released CO_2 (g) is 777.0 µL. Thus in practice, a 77.7% yield was observed

44

with 14.8 mg, as shown in **Figure 17**, when the result is compared to the CO_2 standard curve and table (**Figure D1** and **Table D1**). The percent yield is a result of a 2.0 mL gas injection volume. All the standard results of CO_2 (g) and N_2 (g) can be found in Appendix D.
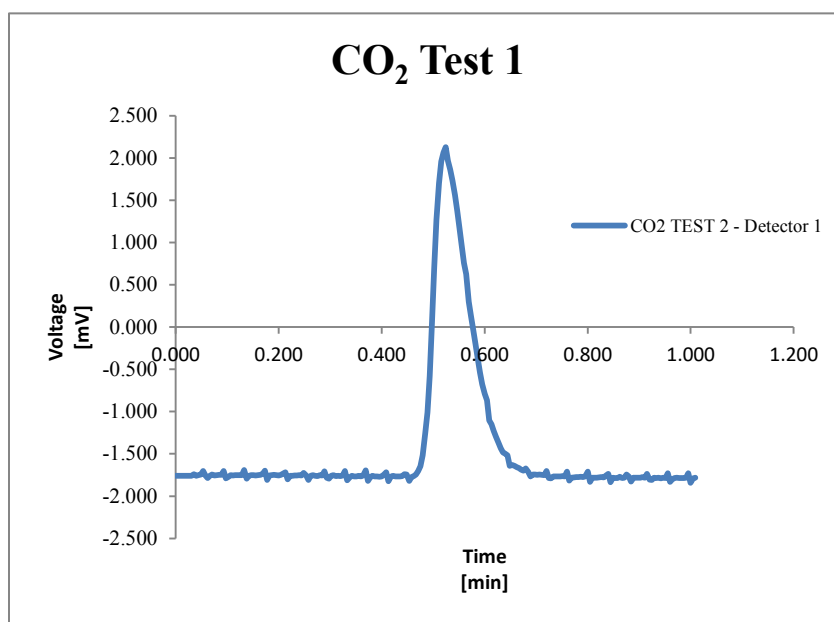

Figure 17: GC Analysis of Detected Gas from **3a**

Nevertheless, to ensure these results for $IMesCO_2$ (**3a**) in acetonitrile, the experiment was performed with no extra water added. The acetonitrile that was used for the experiment had less than 0.3% of water content according to the label from the bottle.

The volumes of CO_2 measured as the reaction took the place for various amounts of carboxylate are shown in **Table 10**. Consistent measurement of carbonyl carbon was detected when **3a** was dissolved in neat CH_3CN solvent in the absence of any extra water. These results may contradict a published journal, where the author[25] stated that 5% (v/v) water in CH_3CN evolved carbonyl carbon the most rapidly. Without adding any extra

water, comparable results were obtained, possibly leaving hydrogen atom at C(2) carbon.

CH_3CN solvent alone could remove the carbonyl carbon from **3a**.

Table 10: CO_2 Evolution from $IMesCO_2$ (**3a**) Dissolved in Dry CH_3CN

Mass of **3a** (mg)	Theoretical yield of CO_2 (mL)	Experimental volume of CO_2 (mL)
58.6	4.11	2.8
10.7	0.751	1.5
5.9	0.41	2.8
5.3	0.37	0.2
2.3	0.16	2.3
1.0	0.070	3.6

Single Crystal Structure Analysis Preparation of IMesCO$_2$ (3a)

For initial recrystallization attempts, a few milligrams of imidazol–2–carboxylate (**3a**) were mixed with one of six different solvents (methylene chloride, chloromethane, THF, acetone, toluene, and hexane) in sanitized and oven–dried test tubes. The amount of solvent added was 1.0 mL throughout. The experiment concentrated on polar protic and polar aprotic solvents. These results shown in **Table 11** indicate that **3a** was more soluble in polar aprotic than polar protic solvents. The dipole moment of the solvent might have been the deciding factor for the solubility of the carboxylate as it dissolved well in solvents with the higher dipole moments. The most suitable dipole moment range of solvent was 1.6D – 3.92D.

Table 11: Solubility Test for Crystal Growth of IMesCO$_2$ (**3a**)

Solvents	Solubility	Dipole Moments (D)[44,45]
Polar aprotic solvents		
CH$_2$Cl$_2$	Soluble	1.60
CHCl$_3$	Soluble	1.78
CH$_3$CN	Soluble	3.92
DMF	Soluble	3.86
THF	Soluble	1.75
Acetone	Soluble	2.88
Polar protic solvents		
H$_2$O	Soluble	1.85
CH$_3$OH	Not soluble	1.69
EtOH	Not soluble	1.69
Isopropanol	Not soluble	1.63
Acetic Acid	Not soluble	1.74
Non-polar solvents		
Benzene	Soluble*	0
Hexane	Soluble*	0
Toluene	Soluble*	0.38
Mixtures, acids, and base		
0.01 M HCl	Not soluble	−
0.01 M NaCl	Not soluble	−
0.01 M NaOH	Not soluble	−

*low heat was applied

Despite the results in **Table 11**, where compound **3a** dissolved better in polar aprotic solvents than the polar protic with higher dipole moments, it also showed IMesCO$_2$ had some solubility towards nonpolar solvents such as benzene, hexane, and toluene, although mild heating of the solvents to increase the solubility was necessary. This was a different type of solvent effect, where the solvents interacted with the aromatic mesityl groups of IMesCO$_2$, which would have an affinity to a nonpolar environment. Nevertheless, the carboxylate compound favored more polar aprotic solvents.

With solubility factors established, attempts to recrystallize **3a** for single crystal XRD were made. First, a 1.0 mL aliquot volume of each hexane and toluene was added to two separate vials with a small amount of **3a** as shown in **Figure 18** and heated. The vials were left on a laboratory bench with the lids on, but not completely fastened. The intent was for slow evaporation of solvent at room temperature to gradually bring the carboxylate to saturation and cause crystal formation.
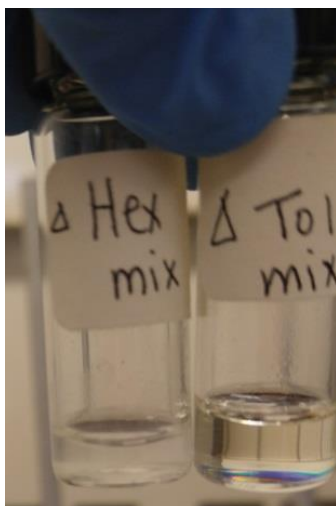

Figure 18: Solubility Tests with Hexane and Toluene

A further attempt on making crystals of **3a** was made with a two-phase mixture of toluene and hexane. The idea was to have a dual–phase condition as in **Figure 19**. The compound was dissolved in a vial of hot toluene, placed in a larger vial containing hexane solvent, and allowed to stand while waiting for solvent interdiffusion to take place.
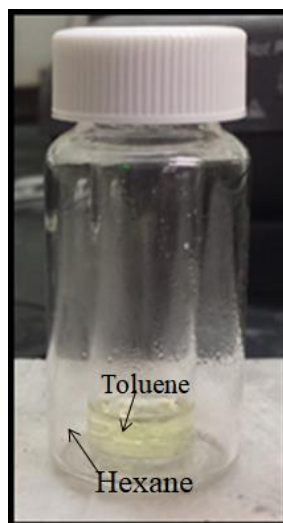

Figure 19: Two-Phase Approach to Crystal Growth Trial with Toluene and Hexane

Another trial involved mixing the two solvents, toluene and hexane, in one vial. Toluene was heated first, but not boiled. A few milligrams of **3a** were added to the heated solvent then cooled to room temperature. Hexane at room temperature was then added. A different trial substituted CH_2Cl_2 for hexane; it was added at room temperature to the heated toluene solution of **3a**. Sample vials from some of the trials are shown in **Figure 20**.

Figure 20: IMesCO$_2$ (**3a**) Recrystallization Attempts

It was difficult to obtain large single crystal structures of **3a**. Each attempt that was performed showed dried-up vials, opaque solution, less volume of solution, or no changes in the vials. The compounds were fully dissolved, yet the no sign of crystals were obtained. **Figure 21** below shows some of the results that were obtained:

Figure 21: Results of IMesCO$_2$ (**3a**) Crystallization Attempts

Another strategy involved scratching the surface of the test tube to promote crystal growth. Compound **3a** was heated in toluene and allowed to cool down to room temperature, and a heated glass rod was used to scratch the surface of the test tube.

Unfortunately, none of the approaches developed larger crystals of IMesCO$_2$ (**3a**) for single crystal XRD, even after many repetitions. It may have been that the compound was not sufficiently pure, so that clean crystal structures of **3a** could not form. Hence, it was necessary to try powder XRD as another step to check whether **3a** is a pure compound.

Powder X–ray Diffraction Study of IMesCO$_2$ (3a)

A finely ground sample of **3a** weighing 26.2 mg was used for the powder XRD study. The XRD pattern is in Appendix F. **Tables F1** and **F2** are measurement conditions and peak list. **Figure F1** is the XRD pattern. A few major 2θ positions are summarized below in **Table 12**.

Table 12: Major Peak List of IMesCO$_2$ (**3a**) PXRD Pattern

Pos. [°2Th.]	d-spacing [Å]	Rel. Int. [%]
10.6304	8.3223	94.1
17.6815	5.01622	9.17
18.6166	4.76631	1.29
23.2107	3.83228	8.92
28.37	3.146	5.67
40.2328	2.24156	1.98
49.1052	1.85532	0.56

Since no publication of 3a powder XRD pattern was found, the obtained powder XRD pattern can be compared to that obtained experimentally after treating with H$_2$ (g) and heat (**6**).

Dry Air Stability Characterization of IMesCO$_2$ (3b)

NMR Characterization

For NMR characterization, 10.7 mg of sample was used to make a 1% CD$_2$Cl$_2$–d_2 solution. Full NMR spectroscopic data are in **Figures A13–17**. Transitions found and their assignments are as follows and chemical shifts comparisons for **3a** and **3b** are found in **Table 13** and **14**:

^{1}H NMR (400 MHz, CH$_2$Cl$_2$–d_2) δ 2.21 ppm (s, 12H, *ortho*–CH$_3$), 2.40 ppm (s, 6H, *para*–CH$_3$), 7.10 ppm (s, 4H, *meta*–CH), 7.53 ppm (s, 2H, CHN)

^{13}C NMR (100 MHz, CH$_2$Cl$_2$–d_2) δ 17.60 ppm (s, *ortho* – CH$_3$), 21.25 ppm (s, *para* – CH$_3$), 121.34 ppm (s, C8), 125.25 ppm (s, C4), 129.60 ppm and 130.17 ppm (s, C7 and C9), 132.51 ppm (s, C6 and C10), 135.18 ppm (s, C5), 140.86 ppm (s, C2), 147.91 ppm (s, CO$_2^-$)

The dry air stability of the bis–mesityl imidazolium carboxylate was examined using NMR. No significant changes in proton NMR chemical shifts were found between **3a** and **3b** as shown in **Table 13**.

Table 13: ^{1}H NMR Chemical Shifts of **3a** versus **3b**

Assignments	**3a** (ppm)	**3b** (ppm)
ortho–CH$_3$	2.05	2.21
para–CH$_3$	2.27	2.40
meta–CH	6.99	7.10
CHN	7.48	7.53

Once again, **3b** is a carboxylate that was studied after a couple of years in a dry air container. Both ^{1}H and ^{13}C NMR chemical shifts have moved downfield from 2.05 ppm to 2.21 (*ortho* – CH$_3$), 2.27 ppm to 2.40 ppm (*para* –CH$_3$), 6.99 ppm to 7.10 ppm (*meta* – CH), and 7.10 ppm to 7.53 ppm (CHN). Over the period, the protons in the

imidazolium carboxylate became more shielded, and so the chemical shifts moved more downfield.

According to the carbon NMR spectrum comparison in **Table 14**, a significant signal for CO_2 was still detected even though the chemical shift had moved from 158.47 ppm to 147.91 ppm. The upfield shift of carbonyl carbon is due to less shielding of the external magnetic field by the protons around the carboxylate. Initially, the intensity of the CO_2 peak observed was barely above the noise in the ^{13}C NMR spectrum. So, the measurement time was increased by changing the signal–to–noise ratio to 4096. The sample had the same concentration for both studies, which may mean that the concentration of the carbonyl carbon at C(2) carbon might have been reduced within the molecule when compared to the carboxylate concentration in **3a** that was measured within one year of its synthesis. The reasons for the peak height differences are not obvious.

Table 14: ^{13}C NMR Chemical Shifts of **3a** versus **3b**

Assignments	**3a** (ppm)	**3b** (ppm)
ortho – CH_3	17.51	17.60
para – CH_3	21.24	21.25
C4	124.72	125.24
C5	131.29	135.18
C7, C9	130.05	130.16
C6, C10	135.13	132.51
C8	121.70	121.35
C2	141.70	141.91
CO_2	158.47	147.91

Higher electronegativity of oxygen atoms on **3b** may have attracted protons from their neighbors, forming a hydrogen bond. It may reduce the bond strength within the carbonyl carbon, CO_2. Also, **3b** is a zwitterion that possesses both positive and negative regions; it is possible that the hydrogen atoms were introduced accidentally when the

container was opened. The proton NMR showed normal intensities comparing to the carbon NMR. It may be due to the lower abundance of ^{13}C in Nature which is about 1%.

According to the 2D NOESY NMR spectrum shown in **Figure 22**, the same through–space correlations exist as they did earlier. Therefore, **3b** was stable in dry air and could be used for further stability analysis.
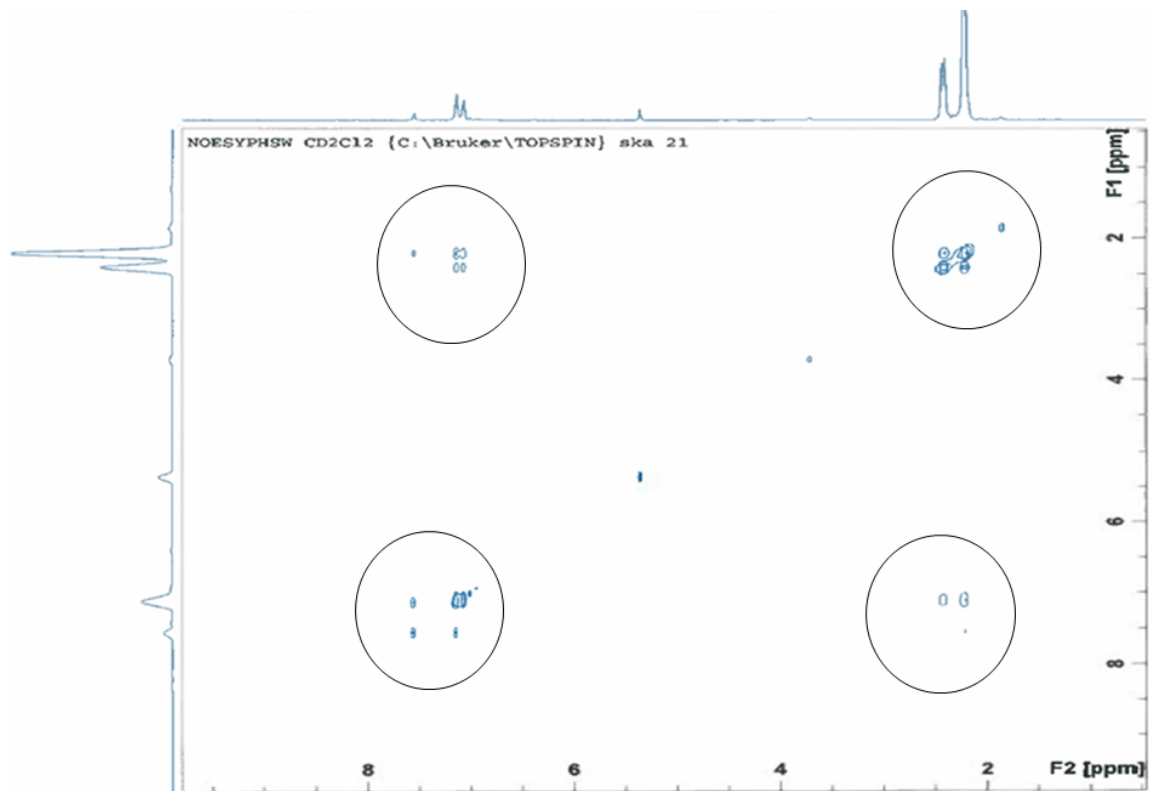

Figure 22: 2D NOESY NMR Spectrum of **3b**

Stronger 2D COSY signals at the methyl groups (2.21 ppm and 2.40 ppm) and

meta – CH group (7.10 ppm) indicate that they are closely correlated to each other, as

shown in **Figure 23**. The methyl groups and *meta* – CH groups are certainly as spatially

close to each other through the bond as it was a couple of years ago in **Figure 14**.
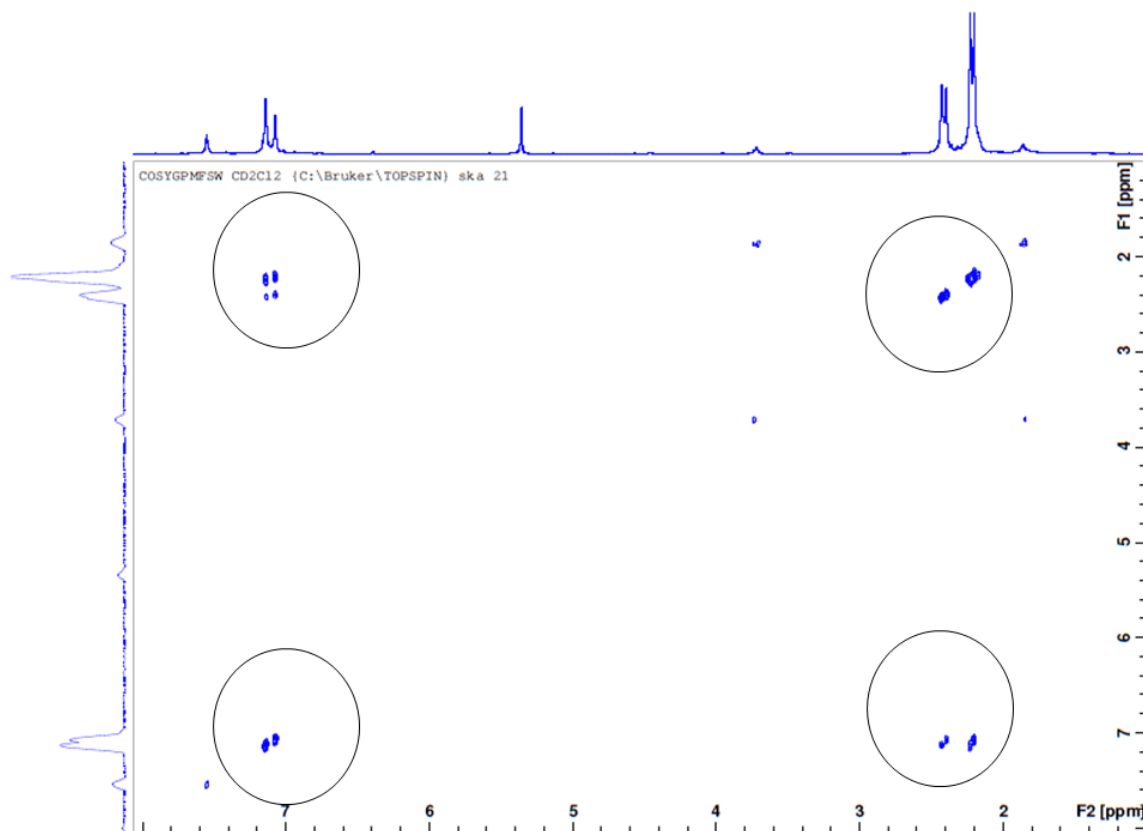

Figure 23: 2D COSY NMR Spectrum of **3b**

According to the 2D HSQC NMR spectrum, all four proton peaks still correlate

with their bonded carbon, as shown in **Table 15** and a full spectrum is found in **Figure**

A17.

Table 15: 2D HSQC NMR Shifts of Compound **3b**

| Assignments	^{1}H NMR (ppm)	^{13}C NMR (ppm)
ortho – CH$_3$	2.21	17.60
para – CH$_3$	2.40	21.25
meta – CH	7.10	130.16
C4	7.53	125.24

55

IR Characterization

For IR characterization, 2.1 mg of **3b** with 30.2 mg of KBr were used to make KBr pellets. A full IR data is available in **Figure B3** and spectroscopic data assignments are as follows: 3158.26 cm^{-1} and 3083.01 cm^{-1} (C$_{phenyl}$=CH), 2954.56 cm^{-1} – 2865.95 cm^{-1} (sp^3 C–H), 1673.42 cm^{-1} (C=O), 1609.10 cm^{-1} and 1549.45 cm^{-1} (C=C), 1490.06 cm^{-1} (C–CH$_3$), 1299.33 cm^{-1} (N–C), 1226.75 cm^{-1} (C$_{phenyl}$–C$_{phenyl}$), and 933.64 cm^{-1} – 691.22 cm^{-1} (C$_{phenyl}$–H).

The IR vibrational stretch of C=O in compound **3a** did not show much change over time from 1678.50 cm^{-1} in **Figure 24A** to 1673.42 cm^{-1} in **Figure 24B**.
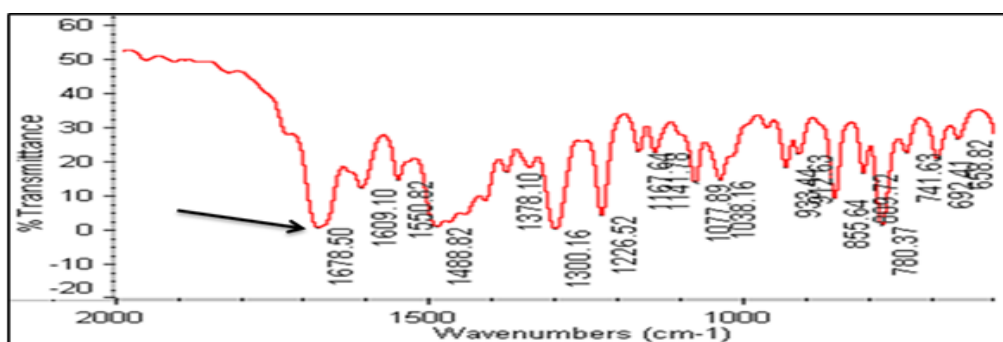
A) IR spectrum of the compound 3a
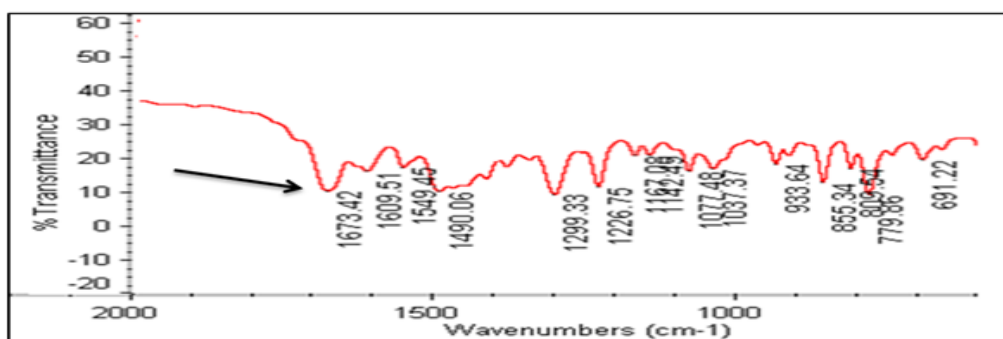
B) IR spectrum of the compound 3b

Figure 24: IR Spectra Comparison of A) **3a** and B) **3b**

All other stretching and bending modes showed similar frequencies to the freshly made imidazolium carboxylate; however, each respective peak intensity was weaker. One

reason is that the collected final sample size was smaller and thus less $C = O$ stretching absorption was obtained in the stored $IMesCO_2$ (**3b**) or the optical density of **3a** was higher due to the differences in experimental amounts: 2.6 mg of **3a** in 43.7 mg KBr versus 2.1 mg of **3b** in 30.2 mg KBr.

TGA Study

Full TGA profiles are in Appendix C (**Figures C2–C4**). Compound **3b** weighed 2.698 mg of finely ground and evenly spread powder. The results for 3.108 mg of **3a** is shown in **Figure 25A** and 2.698 mg of **3b** is shown in **Figure 25B** for comparison.
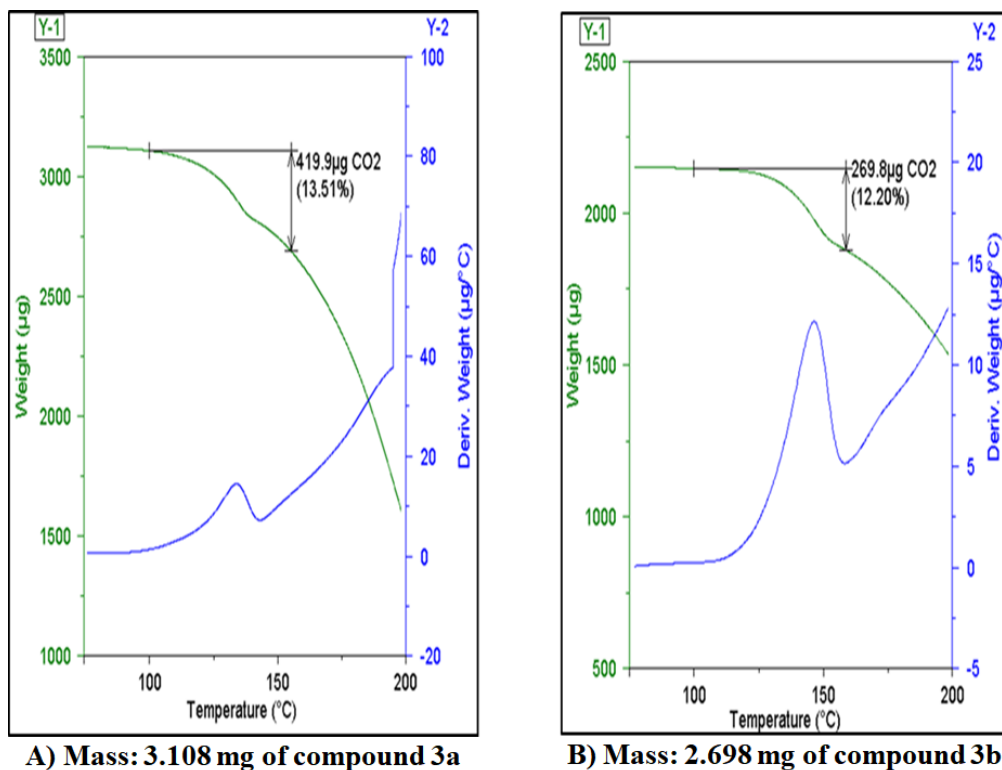

A) Mass: 3.108 mg of compound 3a   B) Mass: 2.698 mg of compound 3b

Figure 25: TGA Profiles of A) **3a** and B) **3b**

Thermogravimetric analysis with a ramping temperature of 5 °C/min up to 200 °C shows a 419.9 µg (13.51%) loss at 155 °C for **3a** in **Figure 25A**. The weight percent loss closely matches with the weight percent of CO_2 (12.59%) attached to the imidazolium.

To check the presence of CO_2 within the ring for the dry air stability characterization, another analysis was done. The thermogravimetric analysis with 5 °C/min up to 250 °C shows a 269.8 µg (12.20%) loss at 155 °C in **Figure 25B**. It is slightly less than the weight percent of carboxylate within the molecule.

Surface area tests were observed in **Figure 26**. The changes in the percent weight loss as the surface areas were changed were 10.5220 mg (1.313%) in **Figure 26A** and 1.4750 mg (22.21%) in **Figure 26B**. The calculated weight loss for **Figure 26A** is 119.0 µg and **Figure 26B** is 327.6 µg. The study proves that 2.0 – 5.0 mg of sample is the optimum amount to analyze the thermal status of compounds.
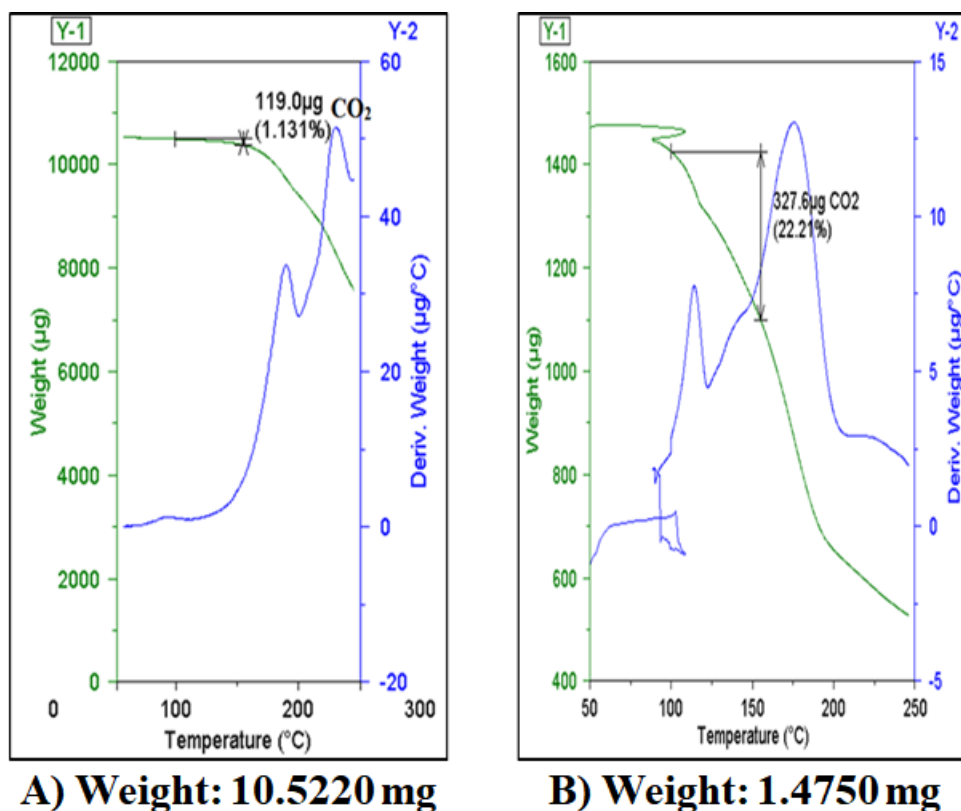

A) Weight: 10.5220 mg   **B) Weight: 1.4750 mg**

Figure 26: TGA Profiles to Study the Surface Area Dependent of **3b**

Study of Carbonyl Carbon Released from IMesCO$_2$ (3b) via GC

The following trials for testing the air stability took 14.2 mg of sample in each trial, so 1.0 mL of CO$_2$ (g) volume could be collected. The results are in Appendix D (**Tables D5–D7** and **Figures D4–D6**). The trial number 2 showed the collected time at 0.569 min and the peak area of 4.050 mV•s. The peak area is 28.8% of the theoretical yield. The third trial exhibited the time of CO$_2$ (g) detected at 0.533 min and the peak area of 4.814 mV•s with 34.2% of CO$_2$ (g) volume. The last trial displayed the CO$_2$ (g) collected time at 0.547 min and peak area of 4.097 mV•s. It represents 29.1% of the CO$_2$ (g) volume.

N$_2$ (g) was also detected from the second trial to the fourth trial: 0.204 minutes with 7.658 mV•s, 0.178 minutes with 7.447 mV•s, and 0.187 minutes with 7.541 mV•s. These numbers correspond to 667.5 µL, 649.1 µL, and 657.3 µL of N$_2$ gas presence inside the Erlenmeyer flask, respectively.

The decarboxylation of CO$_2$ from **3b** test 1 in **Figure D4** showed 4.05 mV•s which is only 287.7 µL of CO$_2$ gas collected. The CO$_2$ test 2 in **Figure D5** showed gas evolution of 342.0 µL of CO$_2$ (g) while test 3 in **Figure D6** showed a collection of 291.1 µL gas evolved. Each trial is summarized in **Table D5** for test 2, **Table D6** for test 3, and **Table D7** for test 4. These numbers may indicate the carbonyl carbon is still attached, but it is strongly attached to the molecule that the solution used, 5% (v/v) H$_2$O in CH$_3$CN was weak to break the C(2)–CO$_2$ bond.

Each volume is a result of a 1.0 mL gas injection volume. Knowing the collected the head space volume of **3b** GC test was a half of the removed volume, an average of two–third (Average 613.8 µL) of the theoretical amount was collected by doubling the

CO_2 gas evolution volume. As the stability of the carboxylate increases, breaking the C(2) and CO_2 bond becomes more difficult with 5% (v/v) H_2O in CH_3CN.

Study of Carbonyl Carbon Released from IMesCO$_2$ (3b) via Effervescence Test

To study the CO_2 removal from compound **3b**, several distinct types of solvents: polar protic solvents, polar aprotic solvents, and non–polar solvents were examined. The compound still dissolved well in both acetonitrile with 1.3 mL of gas and a 5% (v/v) H_2O in acetonitrile mix with 1.7 mL of gas (**Table 16**). Also, the volumes of gas evolved are similar to a theoretical yield.

Table 16: General Effervescence Test of Compound **3b**

Solvents	Amount of **3b** used (mg)	Theoretical CO_2 yield (mL)	CO_2 evolved (mL)
CH_2Cl_2	2.3	0.16	None
CH_3CN	2.2	0.15	1.3
Acetone	2.4	0.17	None
H_2O	1.5	0.11	None
CH_3OH	1.5	0.11	None
Acetic Acid	2.1	0.15	None
Benzene	1.5	0.11	None
Hexane	1.6	0.11	None
5% (v/v) H_2O in CH_3CN	2.1	0.15	1.7

The gas evolution tests of compound **3a** showed that the 5% (v/v) H_2O in CH_3CN mixture had similar efficiency to remove the carbonyl carbon. Compound **3b** still dissolved well in both acetonitrile and an acetonitrile in water mix with detection of gas. However, nonpolar solvents could not remove CO_2 from the compound. Also, no gas was evolved with several polar protic solvents such as water and methanol. The gas detection test proved that compound **3b** still behaved in the same manner as compound **3a**.

Single Crystal Structure Analysis Preparation of IMesCO$_2$ (3b)

Table 17: Solubility Test of IMesCO$_2$ (**3b**)

Solvents	Solubility	Dipole Moments (D)[43,45]
CH$_2$Cl$_2$	Soluble	1.60
CH$_3$CN	Soluble	3.92
Acetone	Soluble	2.88
H$_2$O	Soluble	1.85
CH$_3$OH	Not Soluble	1.69
Acetic Acid	Not Soluble	1.74
Toluene	Soluble	0.38
Benzene	Soluble^	0
Hexane	Soluble^	0

^Dissolved once and then low heat applied

Solubility tests of compound **3b** was necessary to examine whether the compound still dissolved in similar types of solvents and the results are summarized in **Table 17**. The results showed that **3b** was still soluble in all tested polar aprotic and nonpolar solvents, plus water. The study showed that **3b** had similar solubility characteristics as **3a**. Compound **3b** was soluble in both polar and nonpolar solvents. It was more soluble in polar aprotic solvents than compound **3a**. Over the two years, compound **3a** was kept away from moisture, so the property of interest for compound **3b** that was studied after a couple of years stayed similar to compound **3a**.

Toluene and hexane were heated before mixing with **3b** for better solubility. Also, mixing **3b** in hexane did not dissolve homogeneously, so stirring the solution was necessary while a gentle heat was applied to the solution. The lids for all vials were closed, but not tightly closed. The vials were left inside of the hood for the crystal growth. Since both hexane and toluene are highly volatile, the results were recorded within 12-hour period. However, no notable change was observed other than the reduce amount of solution.

The experimental amounts were increased about twice more than the amounts used in previous recrystallization attempts (**Figure 27**). When observing the results of CH_2Cl_2 and CH_2Cl_2 in toluene, the crystal growth study for the single crystal structure resulted in only dried out test tubes. The solutions in the experimental test vials evaporated overnight and no crystalline forms were found. Even if crystalline forms were found, they were too small for a single crystal XRD.

Figure 27: Crystal Growth Trial of **3b** in CH_2Cl_2 and CH_2Cl_2 in Toluene Mix

Water Stability Characterization of 3b (4)

<u>NMR Characterization</u>

According to the effervescence test result in **Table 16**, no effervescence was observed when bis-mesityl imidazolium carboxylate (**3b**) was dissolved in water. To understand this behavior, 10.7 mg of compound **4**, prepared as described in Chapter 2, was dissolved in deuterated DMSO solvent to make a 1% DMSO–d_6 solution and analyzed via NMR. A full NMR spectroscopic data are found in **Figures A18–A21**.

^{1}H NMR (400 MHz, DMSO–d_6) δ at 2.12 ppm (s, 12H, *ortho*–CH$_3$), 2.36 ppm (s, 6H, *para*–CH$_3$), 7.21 ppm (s, 4H, *meta*–CH), 7.85 ppm (s, 1H, C(2)), 8.26 ppm (s, 2H, CHN), 9.67 ppm (s, 1H, HOCOO⁻).

^{13}C NMR (100 MHz, CH$_2$Cl$_2$–d_2) δ 17.32 ppm (s, *ortho* – CH$_3$), 21.08 ppm (s, *para* – CH$_3$), 122.36 ppm (s, C8), 125.29 ppm (s, C4), 129.29 ppm and 129.83 ppm (s, C7 and C9), 131.44 ppm (s, C5), 134.75 ppm and 135.16 ppm (s, C6 and C10), 138.97 ppm (s, C2), 141.09 ppm (s, CO$_2$⁻)

Figure 28 shows that the 4 hydrogen atoms (*ortho*- and *para*-methyl groups, *meta*-CH, and the olefin) were still visible in compound **4**. The chemical shift at *meta* hydrogen is 7.21 ppm, and 8.26 ppm is the proton chemical shifts at C(3) and C(4) carbon. The result is consistent with $IMesCO_2$ (**3b**). However, two new different proton chemical shifts were found at 7.85 ppm and 9.67 ppm, which are slightly different from other chemical shifts. These chemical shifts could have resulted from the H_2O exposure.
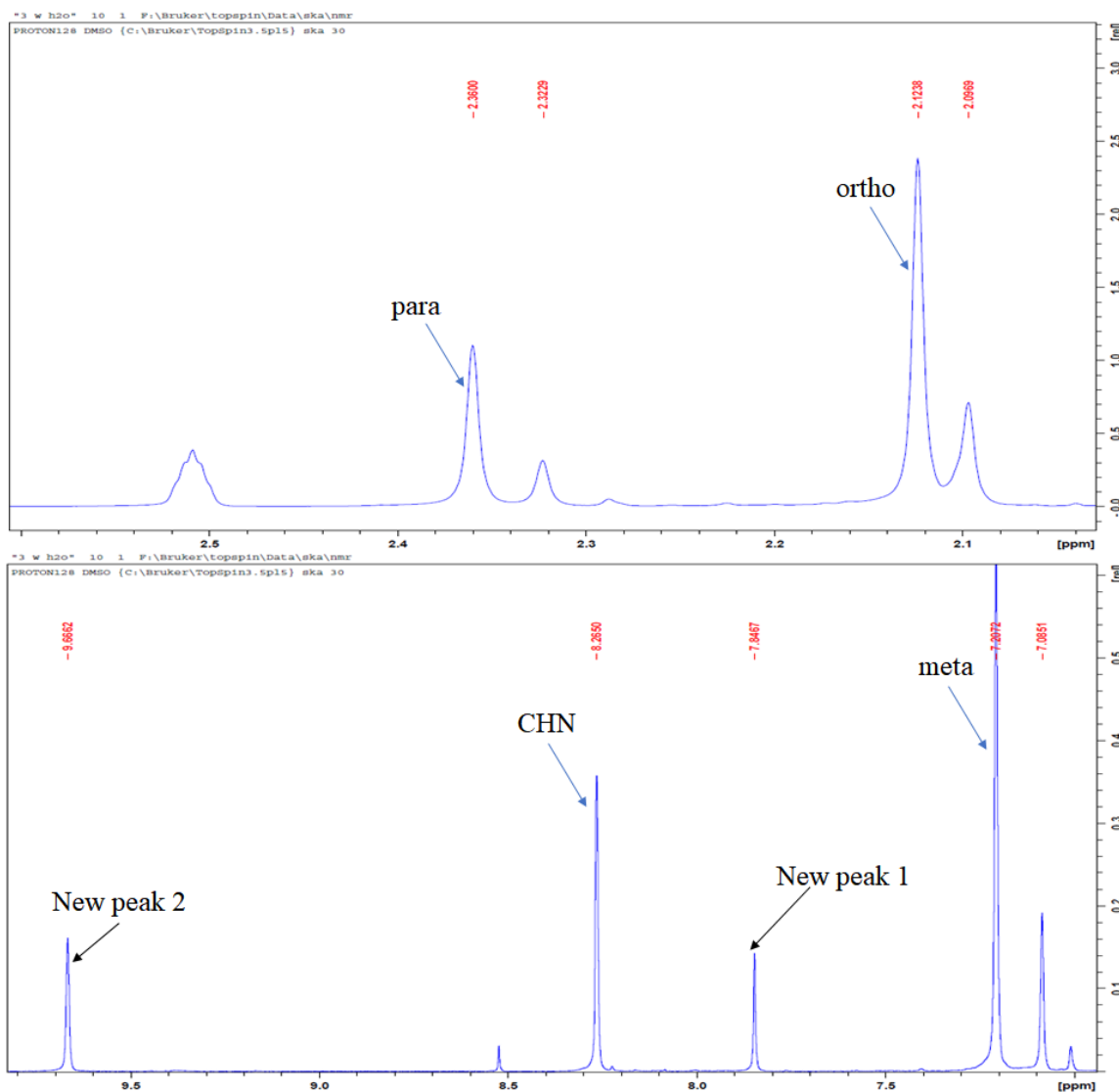
Figure 28: ^1H NMR Spectrum of Compound **4**

Introducing D_2O to a CD_3CN solution of imidazolium carboxylate with smaller

N-substituents showed different chemical shifts according to D.M. Denning and D.E. Falvey.[25] Addition of water instantly showed protonation with new two singlets. The backbone hydrogen atoms were shifted downfield and new chemical shifts at around 7.1 ppm and 7.3 ppm were found. However, introducing water to **3b** powder showed two different chemical shifts (7.85 ppm and 9.67 ppm) according to the experiment.

A speculative structure is drawn in **Figure 29** and an unconfirmed ^{1}H NMR prediction is shown in **Figure 30** running the unconfirmed structure via *ChemDraw Professional*.[26]
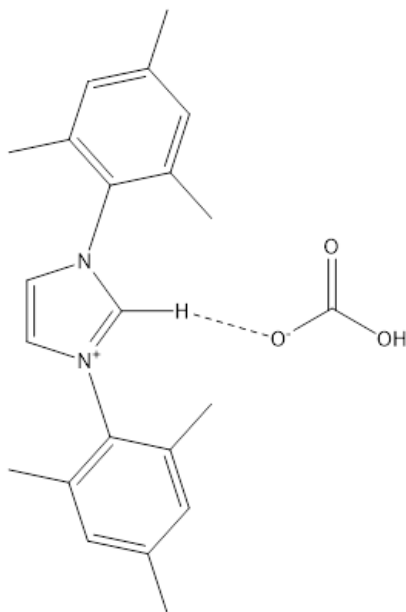
Figure 29: A Hypothetical Structure of **4**

The ^{1}H NMR chemical shifts are roughly similar to the experimental results when the chemical shifts are compared with **Figure 30**. The chemical shifts of two chemical shifts at 8.92 ppm and 12.09 ppm which were generated by *ChemDraw Professional*[26] could be found in different chemical shifts according to the cleanness of both examined compound and the NMR solvent. The chemical shifts imidazolium ring is majorly

affected by the purity of the experiments. Two new peaks from the experiment, which are 7.85 ppm and 9.67 ppm in **Figure 28**, may represent hydrogen bonds at C(2) carbon and carbonyl carbon. The chemical shift for the experimental result at 9.67 ppm may be hydrogen from bicarbonate at the carbonyl carbon. Nevertheless the differences in chemical shifts, a byproduct of bicarbonate could an unsubstantiated result for water stability of **3b** due to a lack of protonating reagent.
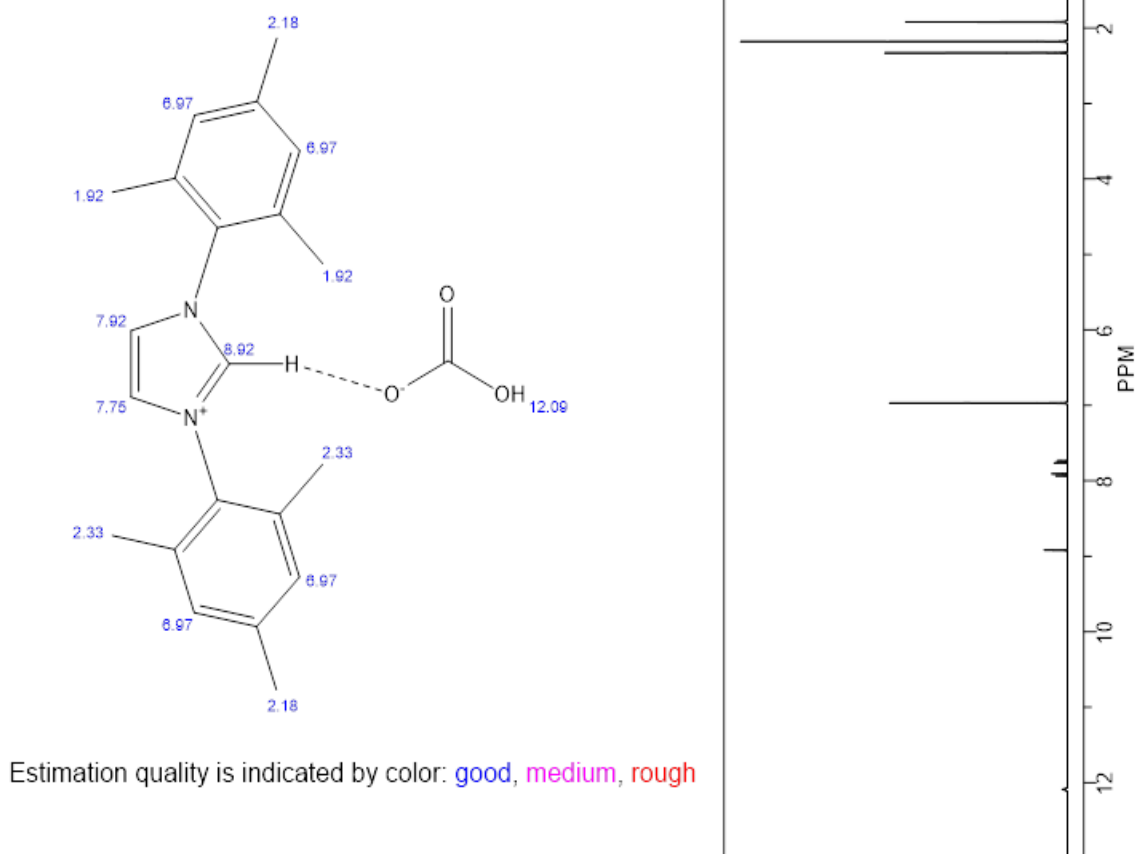

Figure 30: Unconfirmed Software-Generated ^{1}H NMR Spectrum of Imidazolium Bicarbonate[26]

The proton correlations between *meta – CH*, *ortho – methyl*, *para – methyl*, and

C(4) still exist after compound **3b** was dissolved in water (**Figure 31**).
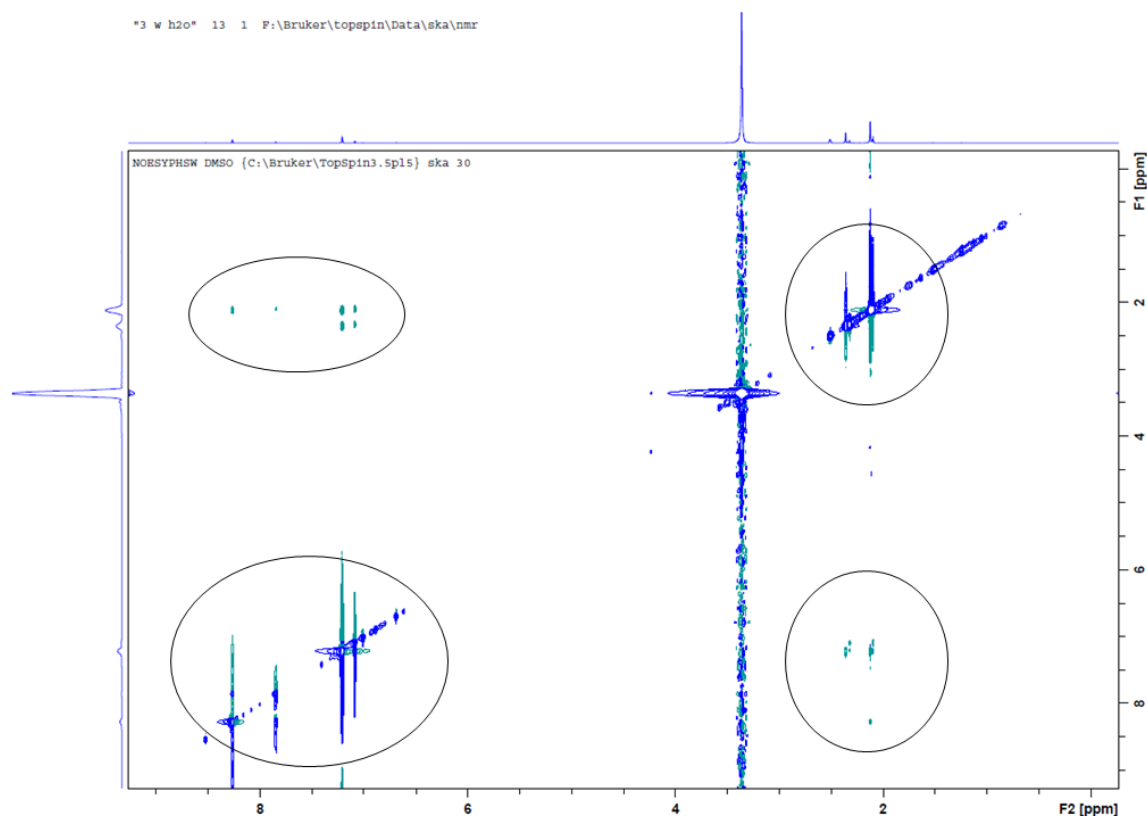
Figure 31: 2D NOESY NMR Spectrum of Compound **4**

According to the ^{13}C NMR chemical shifts in **Figure A23**, no byproduct of carbonic anhydride was observed since a large peak of a feasible CO_2 chemical shift was found at 141.09 ppm. It may indicate that the C(2) carbon could be now bonded to hydrogen and the proton is forming a hydrogen bond to the carbonic anhydride¨s oxygen. Or water must have kept the carbonic anhydride just close enough that the imidazolium structure could be hydrogen bonded to water. Most of the chemical shifts moved upfield. A higher proton concentration around the carbon could be the reason why the carbon chemical shifts of C(6) and C(10) are more downfield than C(5).

According to the 2D HSQC NMR spectrum in **Figure A21**, only 3 correlations were observed instead of 4 correlations for **3b**. Dissolving **3b** in water might have

disturbed **3b** by forming bicarbonate at the C(2) carbon. Thus the structure may not be the same as shown in **Figure 29**. If the carbonyl carbon was released as soon as compound **4** was dissolved in deuterated DMSO but was somehow trapped within compound **4**, it is possible that only three correlations were observed. However, if CO_2 is being released due to deuterated DMSO, at least two more C–H correlations should be observed in 2D HSQC NMR spectrum.

The results indicate that either compound **4** may not be as pure. Or addition of another solvent (deuterated DMSO) to compound **4** may have caused the carbonyl carbon to be protonated, and that would explain why the reasonable CO_2 chemical shift was detected at 141.09 ppm, which is about 20 ppm farther upfield than **3a** CO_2 chemical shift. Interpretation of the NMR results could have benefited from a higher signal–to–noise ratio.

Hydrogen Gas Stability Characterization of 3b (5)

NMR Characterization

The characterization of **5** was done via NMR. For NMR characterization of compound **5**, 10.9 mg was dissolved to make a 1% DMSO–d_6 solution. Full NMR spectra of **5** are found in **Figures A22–A25**.

^{1}H NMR (400 MHz, DMSO–d_6) δ 2.12 ppm (s, 12H, *ortho* – CH$_3$), 2.36 ppm (s, 6H, *para* – CH$_3$), 7.09 ppm (s, 4H, *meta* – CH), 7.88 ppm (s, 2H, CHN), 8.29 ppm (s, 1H, C(2)), 9.65 ppm (s, 1H, HCOO$^-$)

^{13}C NMR (100 MHz, CH$_2$Cl$_2$–d_2) δ 17.35 ppm (s, *ortho* – CH$_3$), 21.09 ppm (s, *para* – CH$_3$), 122.07 ppm (s, C8), 124.19 ppm (s, C4), 127.32 ppm (s, C7 and C9), 129.29 ppm (s, C5), 129.82 ppm (s, C6 and C10), 135.10 ppm (s, C2), 146.82 ppm (s, CO$_2^-$)

Table 18 summarizes how the chemical shifts have changed as hydrogen gas was introduced to **3b**. Nitrogen and oxygen atoms withdrew electrons by deshielding hydrogen atoms at C4 while protons at the *ortho*–CH$_3$, *meta*–CH, and *para*–CH$_3$ became shielded. Hence, an introduction of hydrogen gas to **3b** caused structural changes at the C(2) carbon leading a removal of CO$_2$.

Table 18: ^{1}H NMR Shifts of **3b** and **5**

Assignments	3b (ppm)	5 (ppm)
ortho–CH$_3$	2.21	2.12
para–CH$_3$	2.40	2.36
meta–CH	7.10	7.09
CHN	7.53	7.88

In **Figure 32**, the ^{1}H NMR spectrum of compound **5** shows a more intense singlet at the C4 carbon (CHN) on the imidazolium ring than compound **3b**. The methyl groups on the phenyl rings show cleaner peaks at 2.12 ppm and 2.36 ppm. The relative heights of

the proton peaks are in general related to the proportion of each type of proton present within the molecule, which makes sense since compound **3b** was purged with hydrogen gas. The whole compound has a higher proton concentration than before, hence, all protons on the methyl groups on the phenyl ring and imidazolium ring show better defined peaks at the same signal–to–noise ratio as it was in **3b**.
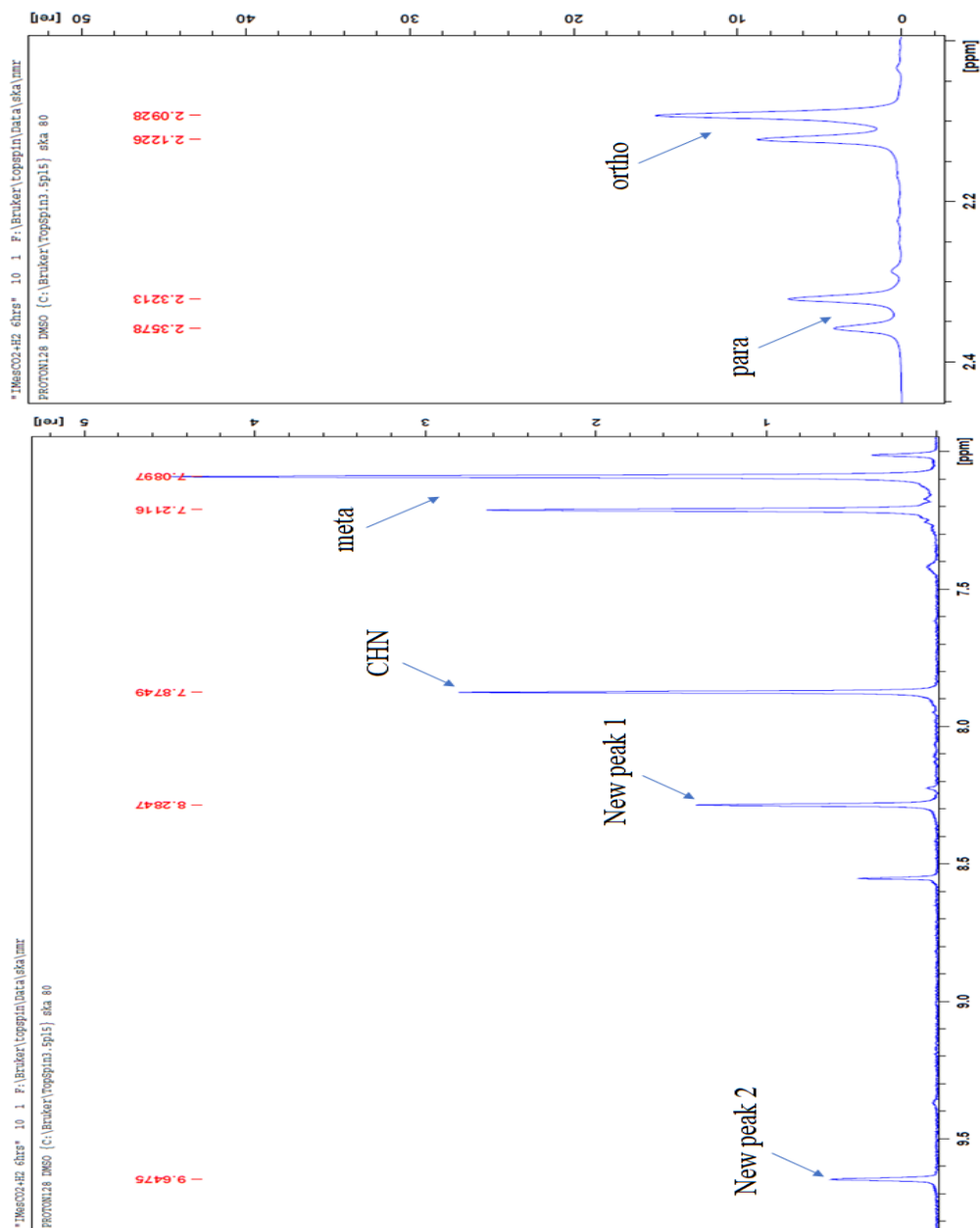

Figure 32: ^{1}H NMR of Compound **3b** Purged with H$_2$ (g)

Furthermore, a couple of new chemical shifts were observed apart from the four chemical shifts that have already been discussed. A hypothetical structure is drawn in **Figure 33** for compound **3b** was purged with H_2 (g).
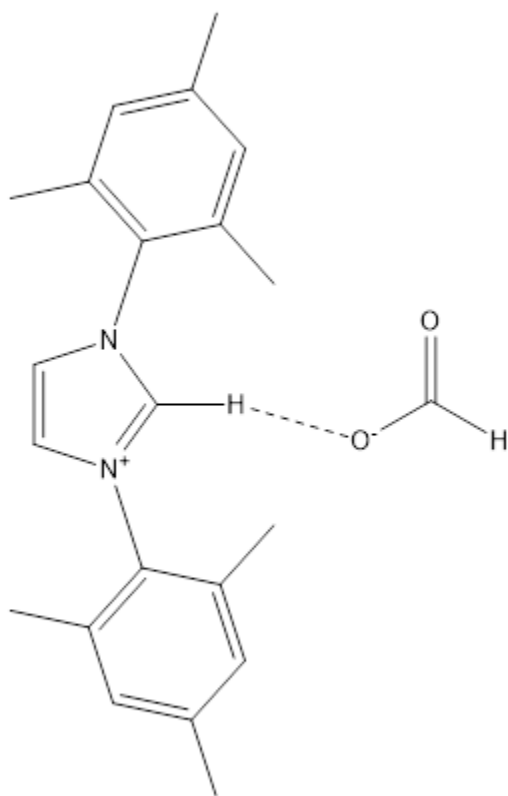
Figure 33: A Speculative Structure of **5**

Also, an approximately calculated ^{1}H NMR was obtained via *ChemDraw Professional*[26] in **Figure 31** and the experimental chemical shifts at 8.28 ppm and 9.65 ppm look similar to the computational chemical shifts of imidazolium formate in **Figure 34**. The C(2) carbon might be bonded to a hydrogen atom showing a chemical shift at 8.55 ppm. The most downfield chemical shift at 9.65 ppm may be a hydrogen shift that is attached to a carbonyl carbon.

ChemNMR [1]H Estimation
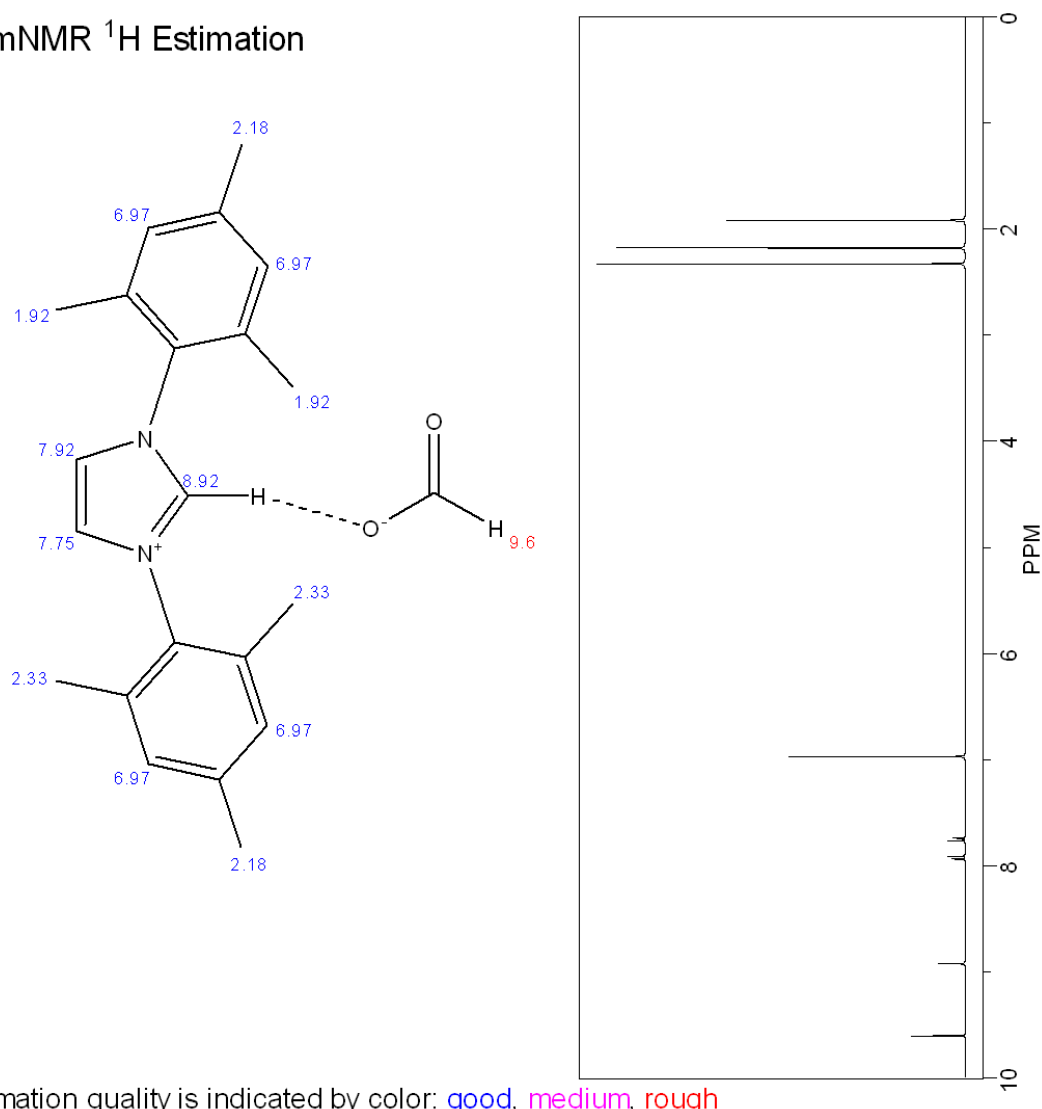
Estimation quality is indicated by color: good, medium, rough

Figure 34: An Unconfirmed Software-Generated ^{1}H NMR Spectrum of Imidazolium Formate

When studying the 2D NOESY NMR spectrum in **Figure 35**, the hydrogen atoms on the phenyl rings show through–space correlations with each other. The hydrogen atoms on C(3) and C(4) showed a correlation with the newly found peak at 8.28 ppm. It is a possible hydrogen peak at the C(2) carbon correlating with the hydrogen atoms at C(3) and C(4). Exposing **3b** to H_2 (g) might cause intermolecular structural changes to the imidazolium ring.
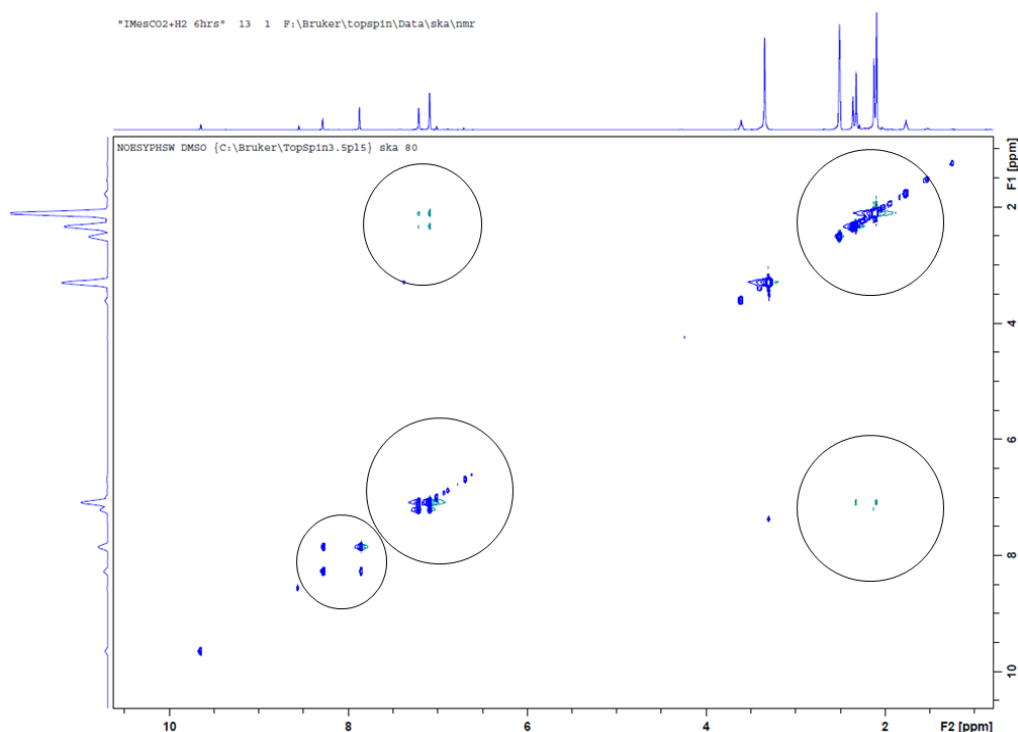
Figure 35: 2D NOESY NMR Spectrum of Compound **5**

The ^{13}C NMR spectral data in **Table 19** compares the chemical shifts between **3b** and **5**. All the chemical shifts are similar except for the carbons that are closer to the new hydrogen atoms, i.e. the C(2) and carbonyl carbons. As more hydrogen atoms were added to the environment, these carbons become more shielded, causing a weaker effective magnetic field. Also, the increase in the proton concentration near the molecule shifted the C(5) carbon peaks more upfield as was seen in the water stability test. These weaker

chemical shifts may be the result of slow water uptake during the compound"s prolonged storage period.

Table 19: ^{13}C NMR Chemical Shifts for **3b** and **5**

Assignments	**3b** (ppm)	**5** (ppm)
ortho – CH_3	17.60	17.32
para – CH_3	21.25	21.09
C4	125.25	124.19
C5	135.18	129.29
C7, C9	130.17	127.32
C6, C10	132.51	129.82
C8	121.34	122.07
C2	140.86	135.10
CO_2	147.91	146.82

The correlation between the olefin H with its corresponding carbon is studied at a very low resolution. Despite the period of storage and the changes of chemical shifts, 4 distinctive correlations between hydrogen atoms and carbon atoms were observed in the 2D HSQC NMR in **Figure A29**. Peak correlations are summarized in **Table 20** below.

Table 20: 2D HSQC NMR Spectrum for Compound **5**

^1H (ppm)	^{13}C (ppm)
2.09	17.35
2.32	21.09
7.21	127.32
7.88	122.07

If the redox occurred between **3b** and H_2 (g), two more C–H correlations should have been observed in HSQC NMR. One is C–H correlation between the C(2) carbon with a hydrogen atom attached to it. The other possible C–H correlation is from the released carbonyl carbon with a hydrogen atom. Hence, the final product structure possesses a similar **3b** structure even after **3b** was purged with H_2 (g). The structural changes might have happened, but it is difficult to characterize the changes without a single crystal XRD study.

Effervescence Test and Single Crystal Structure Analysis of 5

In order to study the crystallographic pattern of **5**, a few milligrams of compound **5** was dissolved in hexane, toluene, CH_2Cl_2, a mixture of toluene with hexane, and mixtures of toluene with CH_2Cl_2 (**Table 21**). The solvents were chosen according to their solubility tests in **3b**. If the compound was dissolved in the solvent mix, the solvent was chosen for an attempt to recrystallize the compound.

Table 21: Solubility Test of **5**

Solvents	Solubility	CO_2 evolved (mL)
CH_2Cl_2	Soluble	None
CH_3CN	Soluble	2.3
Acetone	Opaque, Partial soluble	5.8
H_2O	Soluble	None
CH_3OH	Soluble	None
Acetic Acid	Insoluble	None
Toluene	Soluble	None
Benzene	Partial soluble	None
Hexane	Partial soluble	None

Slightly different solubility results were obtained between **3b** and **5**. Both

compounds **3b** and **5** gave the same results when dissolved in CH_2Cl_2, CH_3CN, H_2O,

acetic acid, and toluene. In contrast, compound **5** was partially soluble in acetone,

benzene, and hexane. Purging **3b** with H_2 (g) to produce **5** might have reduced the

carbonyl carbon to a possible formate; compound **5** became more soluble in nonpolar

without heating (**Figure 36**).
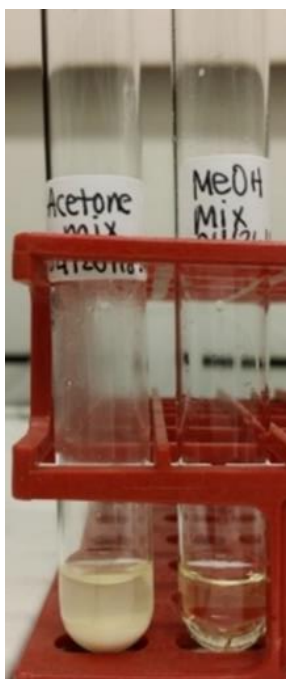
Figure 36: Solubility of **5** in Acetone and Methanol

Because compound **5** was partially soluble in acetone, acetone could be used for a dual–phase recrystallization study with toluene. Once compound **5** was completely dissolved in toluene, acetone was added. The vials were left inside of a laboratory bench for crystal growth. However, only a reduced amount of the solution was observed. (**Figure 37**)

Figure 37: Crystal Growth Results of **5** in Dual–Phase Solution of Acetone and Toluene

Since compound **5** showed better solubility in toluene than either hexane or

CH_2Cl_2, it was dissolved in toluene first and the second solvent, either hexane or CH_2Cl_2,

was added to the solution (**Figure 38A**). Compound **5** was dissolved in different

temperature toluene for better solubility and faster crystal growth. One was at room

temperature and the other one was heated toluene (**Figure 38B**). The experimental test

tubes were left on the laboratory bench overnight for crystal growth. However, no crystal

growth of compound **5** was observed in either a hexane plus toluene mix or a CH_2Cl_2 plus

toluene mix. Only reduced amounts of solution were observed for the toluene trials.
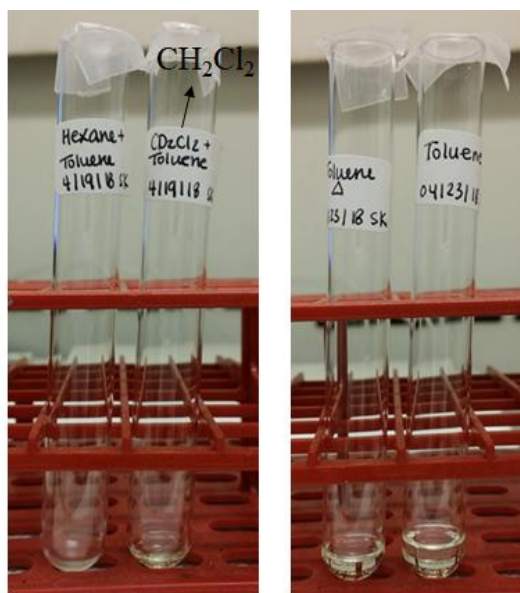
Figure 38: Crystal Growth Results of **5** in A) Phase Change; B) Temperature–Dependent

Heat Resistance and Stability Characterization of 5

<u>NMR Characterization</u>

Compound **5** was gently heated for 3 hours to study what happens right before the

removal of carbon dioxide at the C(2) carbon. Full NMR spectroscopic data are available

in Appendix A (**Figures A26–A29**).

For NMR Characterization of **5** with heat (**6**), 30.50 mg were collected to make a

3.0% DMSO–d_6 solution.

^{1}H NMR (400 MHz, DMSO–d_6) δ 2.13 ppm (s, 12H, $ortho$ – CH$_3$), 2.36 ppm (s, 6H,

$para$ – CH$_3$), 7.21 ppm (s, 4H, $meta$ – CH), 7.86 ppm (s, 1H, C(2)), 8.29 ppm (s, 2H,

CHN), 9.71 ppm (s, 1H, COOH$^-$)

^{13}C NMR (100 MHz, CH$_2$Cl$_2$–d_2) δ 17.34 ppm (s, $ortho$ – CH$_3$), 21.08 ppm (s, $para$ –

CH$_3$), 122.18 ppm (s, C8), 125.29 ppm (s, C4), 129.28 ppm and 129.82 ppm (s, C7 and

C9), 131.46 ppm (s, C5), 134.76 ppm and 135.16 ppm (s, C6 and C10), 139.01 ppm (s,

C2), 141.06 ppm (s, CO$_2^-$)

Heating compound **5** to 95 °C did not show significant changes in the four peaks

(**Table 22**). However, each peak became broadened after compound **5** was heated

(**Figure A30**).

Table 22: ^{1}H NMR Shifts of **5** and **6**

Assignments	**5** (ppm)	**6** (ppm)
$ortho$–CH$_3$	2.09	2.13
$para$–CH$_3$	2.32	2.36
$meta$–CH	7.21	7.21
CHN	7.88	7.86

When three different stability tests were compared, the peaks were observed at

similar chemical shifts except for a few variances (**Figure 39**). The heights at around 9.5

ppm became smaller and the intensity of the proton peak on the imidazolium ring became weaker as $H_{2 (g)}$ and heat were added to compound **3b**. It could be due to the increase in hydrogen concentration near the molecule that is destabilizing the carbonyl carbon. It may indicate that the H_2 (g) alone could remove the carbonyl carbon, eventually.
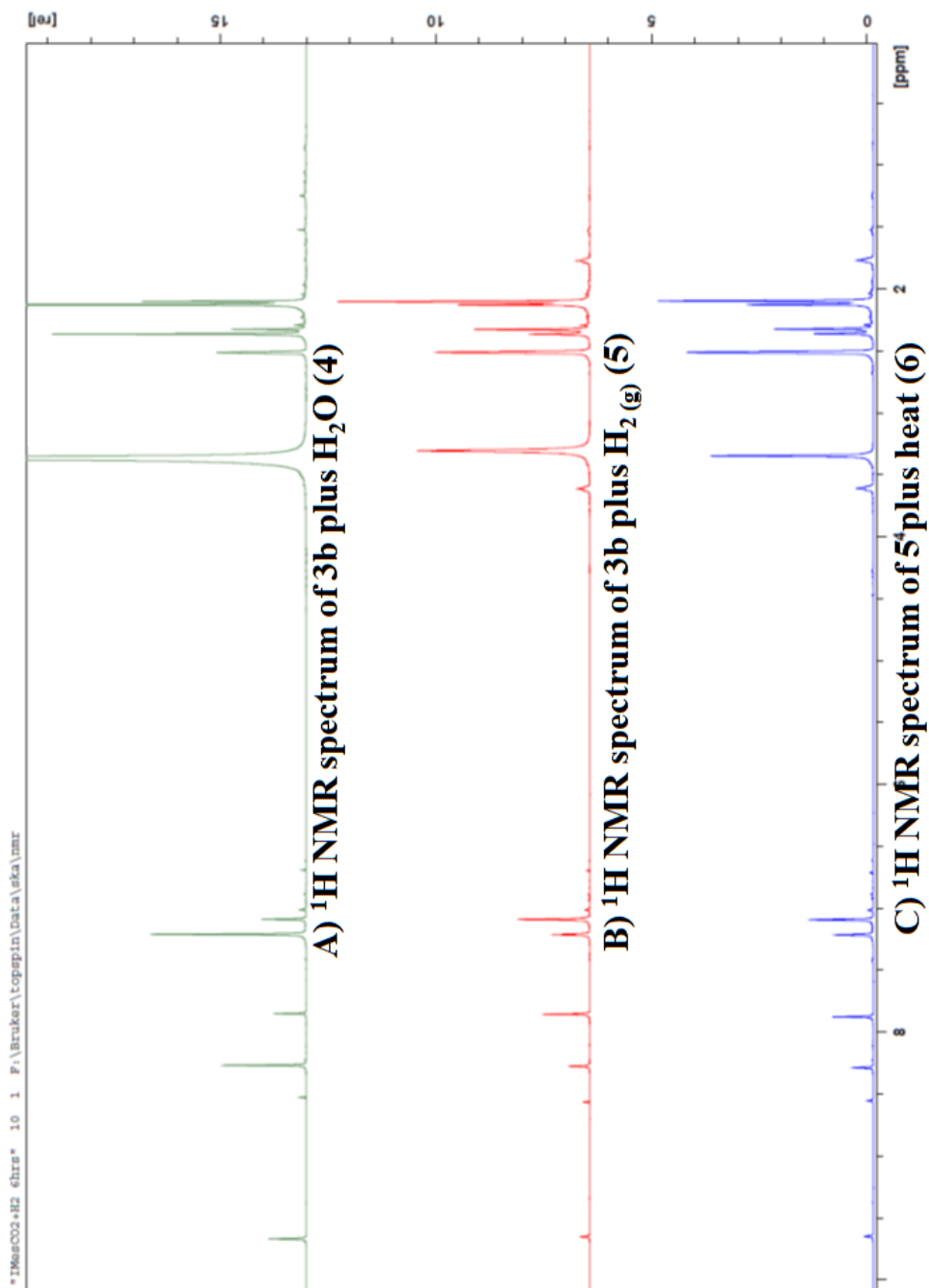
Figure 39: Comparison of ^{1}H NMR Spectra of **3b** Stability in H_2O, H_2, and Heat

Also, the 2D NOESY NMR characterization in **Figure 40** shows that heating

compound **5** caused the disappearance of the protons'' correlations between the

imidazolium ring and the phenyl rings. The 2D NOESY NMR spectrum should have

been more symmetric by canceling the noise, but there was no correlation observed

between hydrogen atoms at the C(2) and C(4) carbons. The distance between the protons

is farther than 5 Å and that is why they were not correlated. Recrystallization of

compound **6** could show what exactly happens when heat was added to compound **5**.
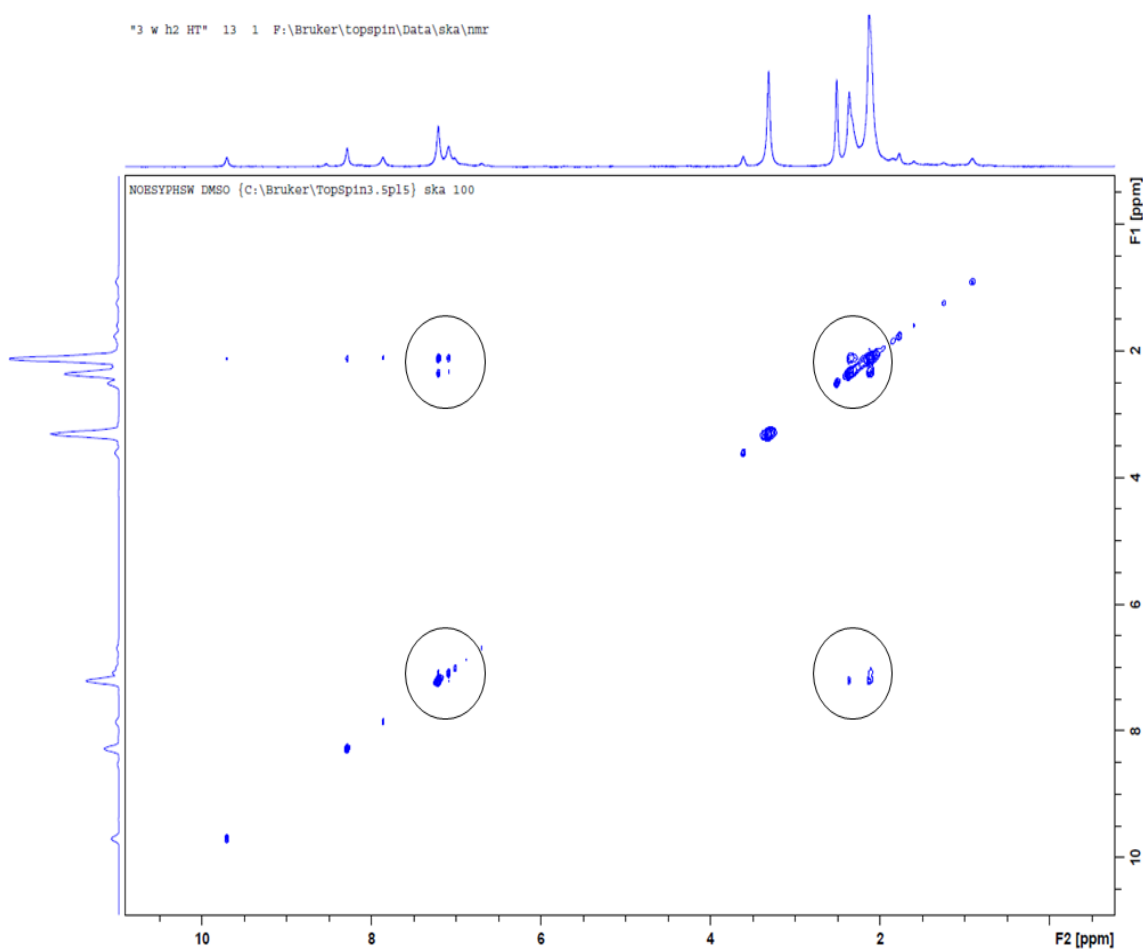
Figure 40: 2D NOESY NMR Spectrum of **5** with Heat (**6**)

The comparison of carbon NMR chemical shifts for **5** and **6** are shown in **Table**

23 with all nine expected peaks, including a possible carbonyl carbon peak at 141.06

ppm. The carbon chemical shifts on the imidazolium ring for compound **6** had moved

farther downfield. It may be due to the stabilization of the imidazolium ring as the

powder form of **5** was heated, so the carbonyl carbon can be released to eventually

become a byproduct.

Table 23: ^{13}C NMR Shifts of **5** and **6**

Assignments	**5** (ppm)	**6** (ppm)
ortho – CH$_3$	17.32	17.34
para – CH$_3$	21.09	21.08
C4	124.19	125.29
C5	129.29	131.46
C7, C9	127.32	129.82
C6, C10	129.82	135.16
C8	122.07	122.18
C2	135.10	139.01
CO$_2$	146.82	141.06

The 2D HSQC NMR correlations in **Figure A33** showed that the C(4) – H

correlation has disappeared even though the proton correlations in the 2D NOESY NMR

spectrum were still present. It could indicate that heating compound **5** disturbed the

molecule to remove CO$_2$. The changes were studied using powder XRD and the result

was compared to the result of compound **3a** powder XRD.

Powder XRD Study

Powder XRD characterization used 42.7 mg of **6**. The full XRD pattern is available in **Figure F2**. **Tables F3** and **F4** are measurement conditions and peak list. A simple comparison of the PXRD pattern for **6** to the previously obtained PXRD pattern for **3a** was used to determine the changes in **6**.

When the peak lists of **3a** and **6** were compared, position [2θ] at 10.63 with 94.1% intensity in **3a** was absent in compound **6** (**Tables F2** and **F4**). Also, some of the peak positions [2θ] have changed and several new peaks that were only found in **6** showed exceptionally low relative intensity summarized in **Table 24**. Otherwise, both patterns displayed similarities.

Table 24: PXRD Pattern Only Found in **6**

Pos. [°2Th.]	d-spacing [Å]	Rel. Int. [%]
7.281	12.13151	0.43
8.1777	10.80309	0.12
30.7429	2.90596	1.23
56.1933	1.63559	0.89
58.6275	1.57335	0.22
61.5391	1.50571	0.78
66.0438	1.4135	0.5
69.1827	1.35683	0.09
71.5776	1.3172	0.09
75.1181	1.26366	0.88
77.8818	1.22558	11.19
83.7248	1.15428	0.4

First, a structure compound **3b** was disturbed by H_2 (g), and then it was heated which slightly interrupted the bonds according to the collected powder XRD patterns. However, it is difficult to understand how exactly the structures have changed only using the powder X–ray pattern without any reference database.

CHAPTER 4: DISCUSSION

Synthesis and Characterization of 1,3–bis(2,4,6–trimethylphenyl)imidazolium–2–carboxylate (3a)

A previously published procedure for the synthesis of **3a** was adopted for the reaction of bis-mesityl imidazolyl carbene intermediate toward CO_2 (g). A successful synthesis of compound **3a** was achieved. A new CO_2 peak was observed at 159.47 ppm in the ^{13}C NMR spectrum. A vibrational stretch at 1678 cm^{-1} was observed via IR spectroscopy. The presence of CO_2 was also confirmed via TGA where **3a** lost 13.51% of its mass at 155 °C. To study further on releasing CO_2, GC analysis was performed with 5% H_2O in CH_3CN; it successfully generated CO_2 in 75% of the theoretical yield. Various types of solvents were tested for their effectiveness toward CO_2 effervescence from **3a**. No significant differences were observed between 5% H_2O in CH_3CN or neat CH_3CN. Higher water concentrations in CH_3CN may or may not accelerate adducts dissociation. Generally, polar solvents have a higher tendency to remove CO_2 from compound **3a**. However, some inconsistent results were obtained, so additional work needs to be performed. If every step of removing CO_2 from **3a** had been performed inside a glove box instead of a glove bag, more reproducible results might have been obtained. To check the purity of the compound, powder XRD pattern was taken; however, no reference spectrum was available for comparison. Also, a close examination of a single crystal diffraction pattern for **3a** failed to yield a structure even though various types of solvents were used to recrystallize it.

Stability Characterization of 1,3–bis(2,4,6–trimethylphenyl)imidazolium–2–carboxylate (3b)

Air Stability

When sample **3a** was studied after it had been stored in a Drierite container for two years (**3b**), no significant changes were observed. However, slight chemical shifts were detected in both ^{1}H and ^{13}C NMR spectra. The proton signals shifted downfield where the nucleus is less shielded from the external magnetic field. Also, the chemical shift for CO_2 bonded to the C(2) carbon appeared upfield from its original position. Both IR spectroscopic data and the TGA profile showed CO_2 still attached to the bis-mesityl imidazolyl carbene intermediate. However, the GC study of compound **3b** showed that less CO_2 gas was detected than when the original procedure was performed on **3a**. It is uncertain what happened to the CO_2 attached to **2**, but it is possible that the bond length between C(2) carbon and CO_2 became weaker, which could be due to a trace of water accumulated over 2–year period so that hydrogen atoms could have broken the adduct bond during the procedures. Hence, single crystal XRD was attempted. Even if compound **3b** dissolved well in the selected solvents, producing crystals was unsuccessful. Also, no significant difference was found using a 5% H_2O in CH_3CN solution or neat CH_3CN during the GC study. Other H_2O/CH_3CN proportions may prove to be more effective at separating and driving off the CO_2. Nevertheless, even after more than two years of storage, **3a** was stable in air and could be used for further analysis.

Stability in Water

Dissolving **3a** and **3b** in water did not generate any gas during effervescence tests. The *ortho*–methyl protons showed two different types of chemical shifts when the

coupling constants were calculated. However, the ^{1}H NMR study of **3b**'s stability in water (**4**) showed that a possible bicarbonate formed at the C(2) carbon and carbonyl carbon. A 2D NOESY NMR spectrum showed correlations between the hydrogen atom on the C(2) carbon and hydrogen atoms on the *ortho*–CH$_3$. It is an indication that the water tried to break the carbonyl carbon off from the C(2) carbon, but the higher electronegativity might have drawn the hydrogen at the C(2) carbon closer to the oxygen on the carbonyl carbon. Hence, no gas was detected even if two new peaks were detected.

Stability under H$_2$ (g)

When compound **3b** was purged with H$_2$ (g) (**5**), the ^{1}H NMR characterization showed the formation of formate at or around the C(2) carbon. Because of the 4 correlations shown in the 2D HSQC NMR spectrum, it is believed that all hydrogen atoms were still in proximity to the corresponding carbons.

Stability under H$_2$ (g) and Heat Resistance

When compound **5** was heated to 95 °C (**6**), it still seemed to be stable, in that the carbonyl carbon peak in the ^{13}C NMR spectrum was still observed. The powder XRD pattern did change when compared to compound **3a**. The powder X–ray diffraction results of **3a** and **6** showed that the H$_2$ (g) and heat changed the structure of **3a**.

CHAPTER 5: CONCLUSION

1,3–bis(2,4,6–trimethylphenyl)imidazolium carboxylate (**3a**) was successfully

synthesized via CO_2 addition to 1,3–bis(2,4,6–trimethylphenyl)imidazolyl carbene (**2b**)

in THF under N_2 atmosphere. A variety of analytical methods showed that the final

compound, 1,3–bis(2,4,6–trimethylphenyl)imidazolium carboxylate (**3a**), was formed and

could be used for further analysis. NMR spectroscopy and IR spectroscopy were

employed to confirm the compound"s structure. The ratio of hydrogen atoms from the

integration of peak areas on the ^{1}H NMR spectrum corresponded to the number of

hydrogen atoms present in compound **3a**. Clear chemical shift values for the carbons on

the imidazolium and phenyl rings were detected. The CO_2 adduct showed a new carbon

peak for CO_2 at 158.47 ppm. IR spectra data analysis revealed a new absorption at

1678.50 cm^{-1}, which corresponds to the C=O vibrational stretch. A PXRD pattern for **3a**

was generated, but no published diffraction pattern could be found to use as a reference.

Attempts at growing crystals sufficiently large for single crystal diffraction analysis were

unsuccessful.

The TGA profile showed that the percent weight loss at 155 °C corresponded

precisely to the weight percent of CO_2 present in **3a**. Several solvents were used to test

the solubility of the final product **3a** and showed better solubility in polar aprotic

solvents. Effervescence tests, followed by GC analysis, proved that CO_2 was bound to the

carbene (**2b**). A 5% (v/v) H_2O in CH_3CN mixture and neat CH_3CN were two solvents

used to give off about 1 mL of gas, which is the theoretical yield. It was determined that

no significant differences were studied between two mixture and solvent at dissociating

the carboxylate.

An air stability test of **3a** was effectively performed by storing it in a desiccator for over two years (**3b**). An NMR study of **3b** showed that the same number of hydrogen atoms was present and chemical shifts of protons remained similar to what they were 2 years ago. The bonding relationships between protons and carbons remained correlated. The $C = O$ vibrational stretch remained at similar wavenumbers. CO_2 was removed at 155 °C according to TGA study. A reduced CO_2 concentration when studying the decarboxylation of **3b** was observed via GC analysis.

Reactions between water and compound **3b** were designed for checking hydrolytic stability. NMR spectroscopy was employed to study any changes in the compound"s structure. It was stable in water; however, the solution may contain bicarbonate in addition to **3b**, since new downfield proton peaks were found in the ^{1}H NMR spectrum. Similar shifts were found in the ^{1}H NMR spectrum of compound **3b** after exposure to hydrogen gas (**5**), which contains formate in addition to **3b**.

When analyzing the heat resistance, 2D HSQC NMR showed that the olefin protons have lost their correlations with the previous corresponding carbons. It indicated that **3b** is not stable at an increased temperature, as thermal energies begin to exceed the bond energy between the C(2) and carbonyl carbon. Also, the powder X–ray pattern showed possible structural changes, which may involve formate formation. Hence, the starting reactant (**2**) could be employed for the storage of renewable hydrogen energy and for generating fuel. The experimental results in this thesis are reproducible and further research in crystallization, hydrogenation or electrochemical reduction of the imidazolium carboxylate is highly recommended.

Future Work

Future work should involve further characterization of pure $IMesCO_2$ powder and an attempt to recrystallize it to obtain the single crystal XRD pattern of pure $IMesCO_2$, which has yet to appear in the open literature. This will provide a more complete structural understanding of how the atoms interact with each other and what the resulting compound would look like after losing CO_2. XRD pattern of $IMesCO_2$ dissolved and recrystallized from H_2O and after reaction with H_2 gas could show what chemistry has occurred. Also, more acid and base solvents could be used to study the stability of $IMesCO_2$. Structural analysis of the imidazolium compound after the CO_2 is removed could be studied via single crystal XRD and NMR. It would be of value to demonstrate that the bis-mesityl imidazolyl carbene intermediate was regenerated so that a possible catalytic cycle for CO_2 activation could be considered for renewable energy conversion. Additionally, CO_2 bonded to **2** might be electrochemically reducible to formate for further subsequent renewable energy conversion. All experiments were performed on a laboratory bench after the stable $IMesCO_2$ (**3**) was formed. PXRD pattern showed that the powder may not be completely pure. XRD pattern related to water and hydrogen gas stability may be obtained to identify any possible byproducts formed during CO_2 reduction procedures.

REFERENCES

1. Climate Change. https://19january2017snapshot.epa.gov/climate–change–science/causes–climate–change_.html (accessed Mar 5, 2017).

2. Gerlach, T. Comment: Volcanic versus anthropogenic carbon dioxide: The missing science. https://www.earthmagazine.org/article/comment–volcanic–versus–anthropogenic–carbon–dioxide–missing–science?page=1 (accessed Mar 5, 2018).

3. Sneed, A. Get Ready for More Volcanic Eruptions as the Planet Warms. https://www.scientificamerican.com/article/get–ready–for–more–volcanic–eruptions–as–the–planet–warms/ (accessed Apr 23, 2018).

4. Arnell, N.W.; Livermore, M. J. L.; Kovats, S.; Levy, P. E.; Nicholls, R.; Parry, M. L.; Gaffin, S. R. *NATO ASI Ser., Ser. I: Global Environmental change*. **2004**, *14*, 3–20.

5. Global Warming. http://www.ucsusa.org/global_warming#.VUhUgZVFBMt (accessed Apr 17, 2015).

6. Global Warming 101. Natural Resources Defense Council. http://www.nrdc.org/globalwarming/ (accessed Apr 17, 2015).

7. Hayashi, A.; Akimoto, K.; Sano, F.; Mori, S.; Tomoda, T. *Climate Change*. **2010**, *98*, 87–112.

8. Bastasch, M. 25 Years of Predicting The Global Warming „Tipping Point". http://dailycaller.com/2015/05/04/25–years–of–predicting–the–global–warming–tipping–point/ (accessed May 24, 2015).

9. What are El Nino and La Nina? National Ocean Service: National Oceanic and Atmospheric Administration U.S. Department of Commerce. https://oceanservice.noaa.gov/facts/ninonina.html (accessed Jul 18, 2018).

10. What is Green Chemistry? ACS Chemistry for life. https://www.acs.org/content/acs/en/greenchemistry/what-isgreenchemistry.html (accessed Jan 12, 2018.)

11. Ho, M. T.; Allinson, G. W.; Wiley, D. E. *International Journal of Greenhouse Gas Control 5*. **2011**, 49–60.

12. Kukreja, R. What are Greenhouse Gases? Conserve Energy Future. https://www.conserve–energy–future.com/greenhouse–gases.php (accessed May 15, 2015).

13. Greenhouse Gas (GHG) Emissions. EPA. https://www.epa.gov/ghgemissions (accessed Jun 26, 2018).

14. Qiyong, X. U.; Jiaoju, G. E. *ScienceDirect: Energy Procedia 5*. **2011**, 1026–1031.

15. Compound Summary for CID 280: Carbon Dioxide. http://pubchem.ncbi.nlm.nih.gov/compound/carbon_dioxide#section=Top (accessed May 24, 2015).

16. Why does CO_2 get most of the attention when there are so many other heat–trapping gasses? Union of Concerned Scientists Science for a healthy planet and safer world. http://www.ucsusa.org/global_warming/science_and_impacts/science/CO2–and–global–warming–faq.html#.VUgeNJOHHIU (accessed Apr 17, 2015).

17. Takeshita, T.; Yamaji, K. *Environ. Econ. Policy Stud*. 2006, *8*, 55.

18. Shahbazi, A.; Nasab, B. R. *J. Pet. Environ. Biotechnol.* **2016**, *7*, 291.

19. Carbon Recycling International. http://www.carbonrecycling.is/ (accessed May 24, 2015).

20. Sarve, A. N.; Ganesphpure, P. A.; Munshi, P. *Ind. Eng. Chem. Res.* **2012**, *51*, 5174–5180.

21. Mori, H.; Yamamoto, H.; Kwan, T. *Chem. Pharm. Bull.* **1972**, *20* (11), 2440–2444.

22. Sharp, J. T. *Ann. Rep. Prog. Chem. Sect. B: Org. Chem.* 1971, *68*, 217–239.

23. Carbenes. https://chem.libretexts.org/Core/Organic_Chemistry/Fundamentals/Reactive_Inter mediates/Carbenes (accessed Feb 2, 2018).

24. Denning, D. M.; Falvey, D. E. *J. Org. Chem*. **2017**, *82*, 1552–1557.

25. Denning, D. M.; Falvey, D. E. *J. Org. Chem*. **2014**, *79*, 4293–4299.

26. *ChemDraw Professional*, version 16.0; PerkinElmer: Cambridge, MA, 2017.

27. Duong, H. A.; Tekavec, T. N.; Arif, A. M.; Louie, J. *Chem.Commun*., **2004**, 112–113.

28. Van Ausdall, B. R. An investigation of *N*–heterocyclic carbene carboxylates: insight into decarboxylation, a transcarboxylation reaction, and synthesis of hydrogen bonding precursors. Ph.D. Dissertation, The University of Utah, UT, 2012.

29. Van Ausdall, B. R.; Glass, J. L.; Wiggins, K. M.; Aarif, A. M.; Louie, J. *J. Org. Chem*. **2009**, *74*, 7935–7942.

30. Fevre, M.; Coupillaud, P.; Miqueu, K.; Sotiropoulos, J.; Vignolle, J.; Taton, D. *J. Org. Chem.* **2012**, *77*, 10135–10144.

31. Domyati, D.; Hope, S. L.; Latifi, R.; Hearns, M. D.; Tahsini, L. *Inorg Chem*. **2016**, *55*, 11685–11693.

32. Lalaoui, N.; Reuillard, B.; Philouze, C.; Holzinger, M.; Cosnier, S.; Le Goff, A. *Organometallics.***2016**, *35*, 2987–2992.

33. Schleicher, D.; Leopold, H.; Borrmann, H.; Strassner, T. *Inorg. Chem*. **2017**, *56*, 7217–7229.

34. Arduengo, A. J.; Harlow, R. L.; Kline, M. *J. Am. Chem. Soc.,* **1991**, *113*, 361–363.

35. Zhang, J.; Wang, Y.; Du, G.; Gu, C-Z.; Dai, B. *Chin. J. Chem*. **2015**, *33*, 1211–1215.

36. Tudose, A.; Demonceau, A.; Delaude, L. *J. Organomet. Chem*. **2006**, *691*, 5356–5365.

37. Ramnial T.; Taylor, S. A.; Bender, M. L.; Gorodetsky, B.; Lee, P. T. K.; Dickie, D. A.; McCollum, B.M.; Pye, C. C.; Walsby, C. J.; Clyburne, J. A. C. *J. Org. Chem*. **2008**, *73*, 801–812.

38. Rao, R. K.; Pishgar, S.; Strain, J.; Kumar, B.; Alta, V.; Kumari, S.; Spurgeon, J. M. *J. Mater.Chem. A*. **2018**, *6*, 1736–1742.

39. Fatima, T.; Haque, R. A.; Razali, M. R. *J. Mol. Struct.* **2017**, *1141*, 346–350.

40. Kim, S.; Jung, Y.; Park, S. *Journal of Power Sources*. **2005**, *152*, 272–277.

41. Zargari N.; Jung, E.; Lee, J – H.; Jung, K. W. *Tetrahedron Lett.* **2017**, *58*, 3330–3332.

42. Gorodetsky, B.; Ramnial, T.; Branda, N. R.; Clyburne, J. A. C. *ChemComm*. **2004**, 1972–1973.

43. Merlic, C. A; Strouse, J. Introduction to IR Spectra. https://webspectra.chem.ucla.edu/irintro.html (accessed Jul 12, 2018).

44. Movassaghi, M.; Schmidt, M. A. *Org. Lett.* 2005, *7*, 4

45. Dipole mements. Chemistry LibreTexts. https://chem.libretexts.org/Textbook_Maps/Physical_and_Theoretical_Chemistry _Textbook_Maps/Supplemental_Modules_(Physical_and_Theoretical_Chemistry)/Physical_Properties_of_Matter/Atomic_and_Molecular_Properties/Intermolecul ar_Forces/Specific_Interactions/Dipole_moments (accessed Aug 3, 2018).

APPENDIX A: NMR DATA

Figure A1: ^{1}H NMR Spectrum of **1** in THF–d_8

Original Carbene check in THF
PROTON128 THF {C:\Bruker\TOPSPIN} ska 41

96
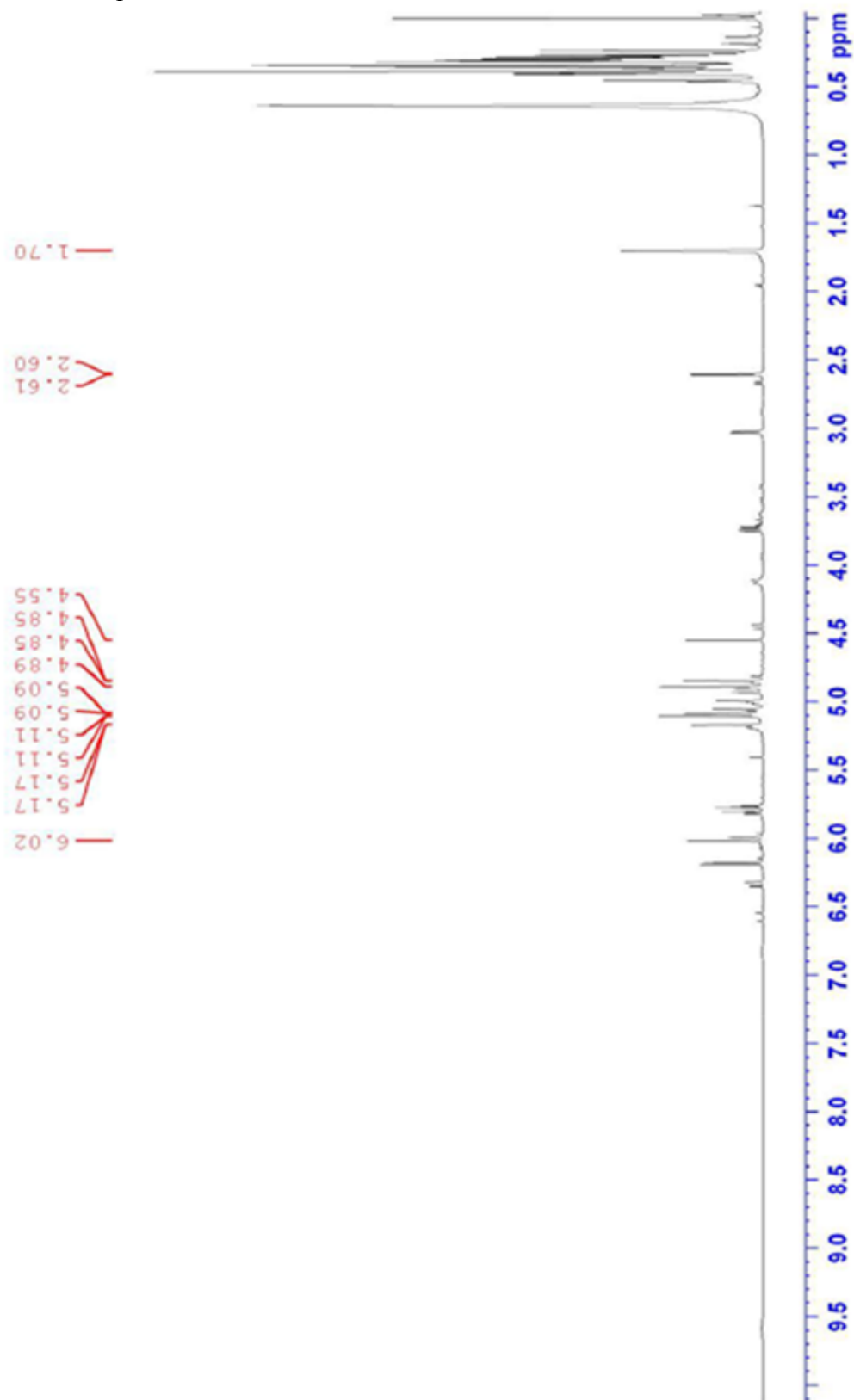
Figure A2: ^{13}C NMR Spectrum of **1** in THF–d_8
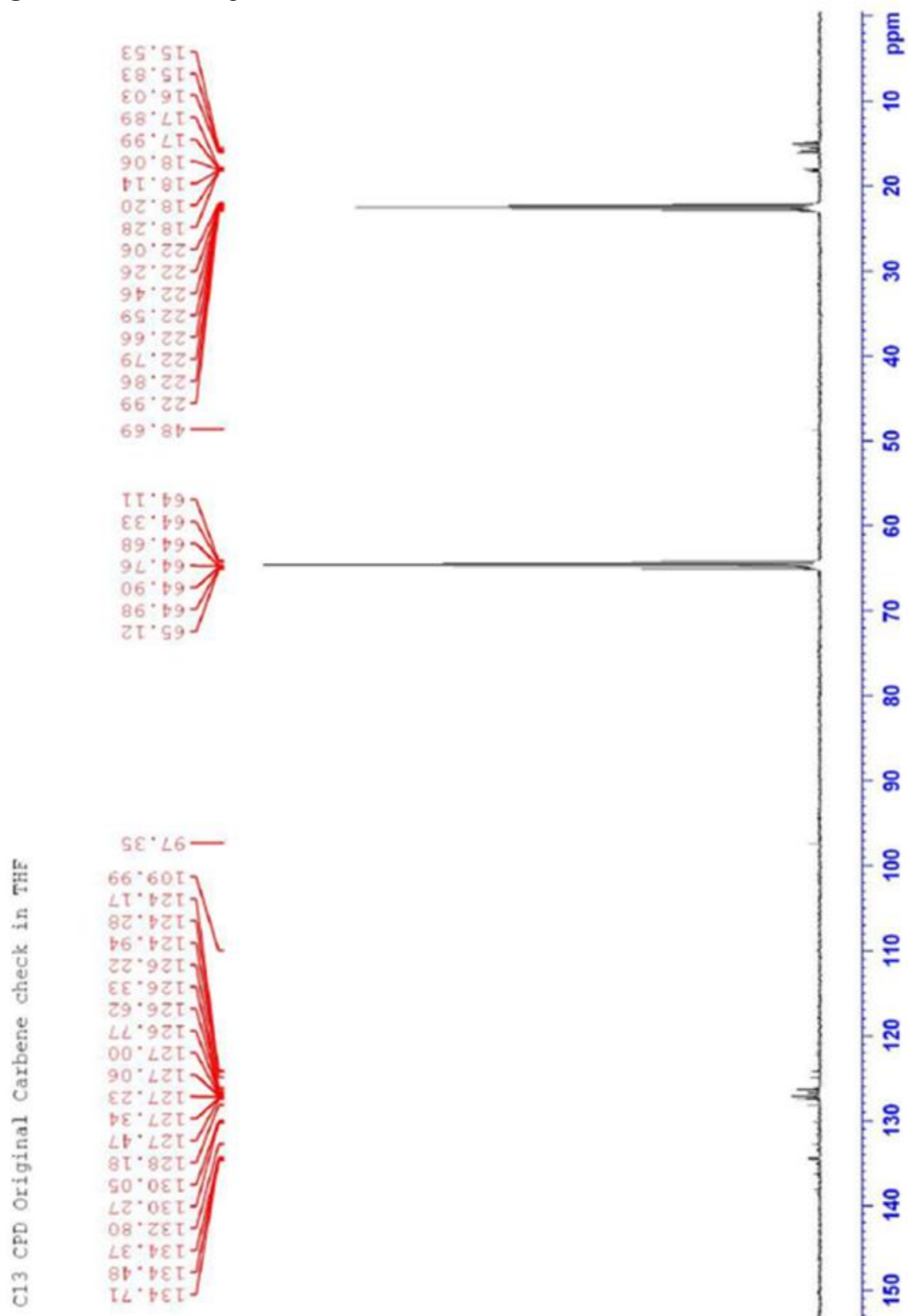
Figure A3: ^{1}H NMR Spectrum of **2** in CDCl$_3$–d_2
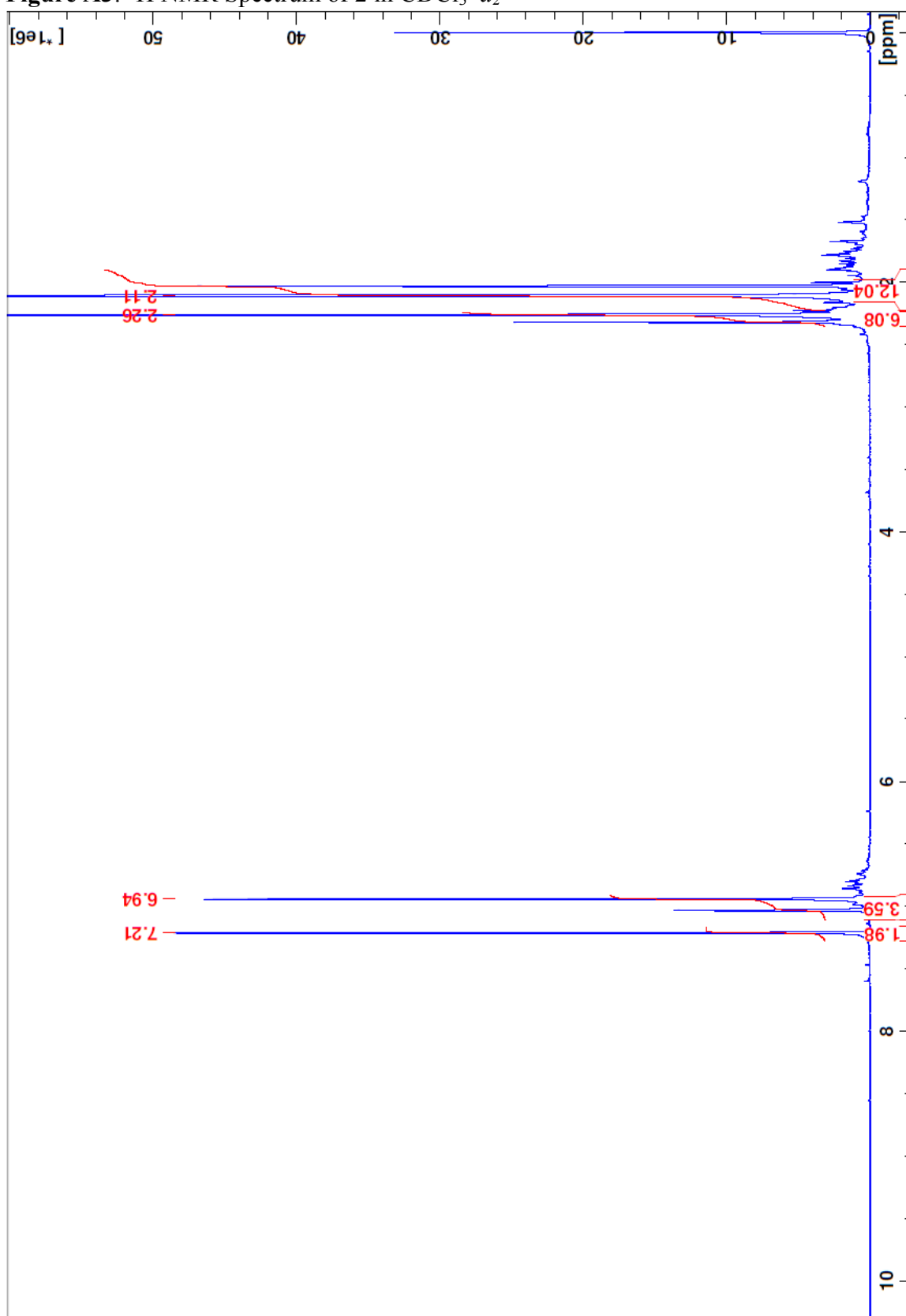
Figure A4: ^{13}C NMR Spectrum of **2** in CDCl$_3$–d_2

99
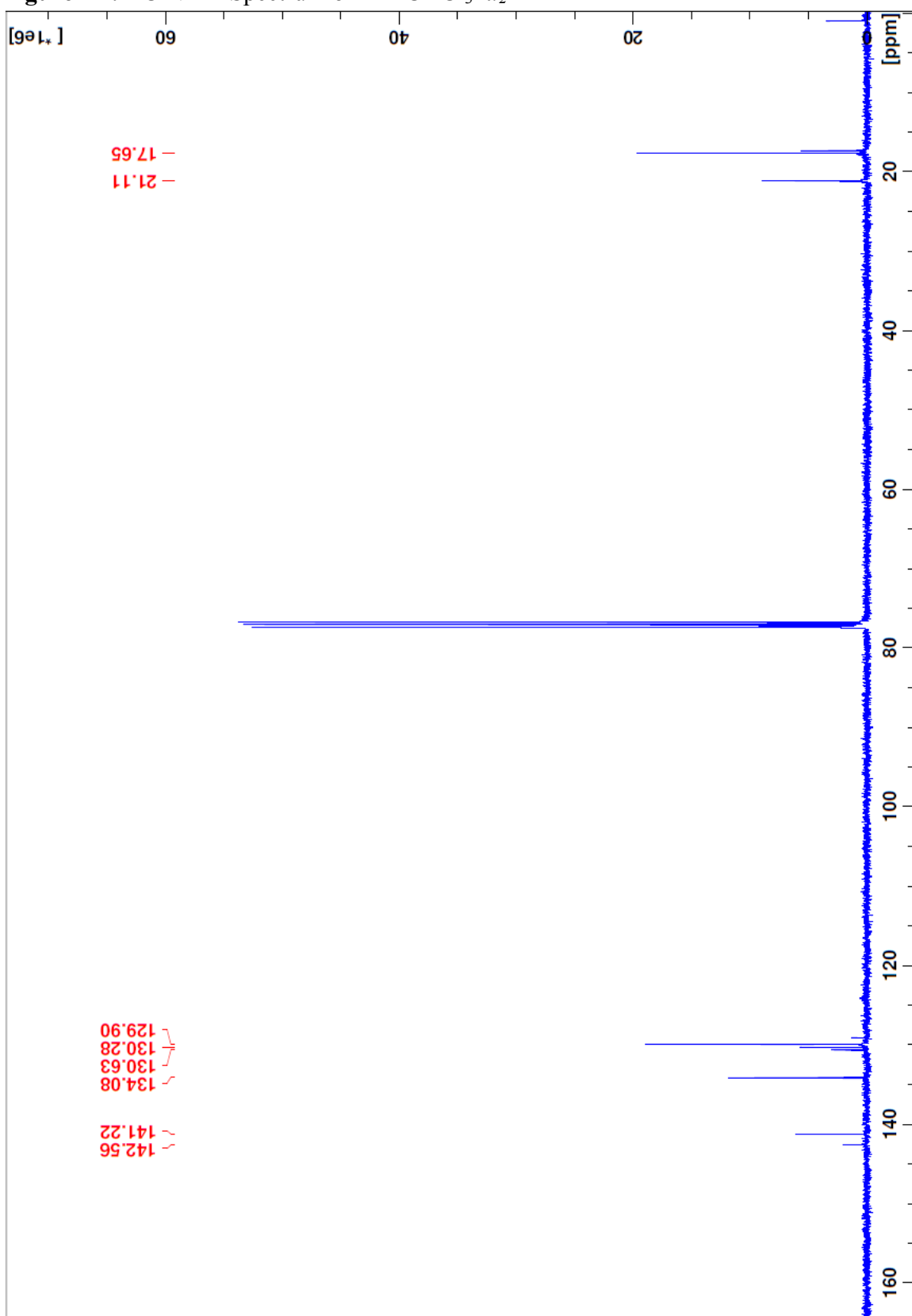
Figure A5: 2D COSY NMR Spectrum of **2** in CDCl$_3$–d_2
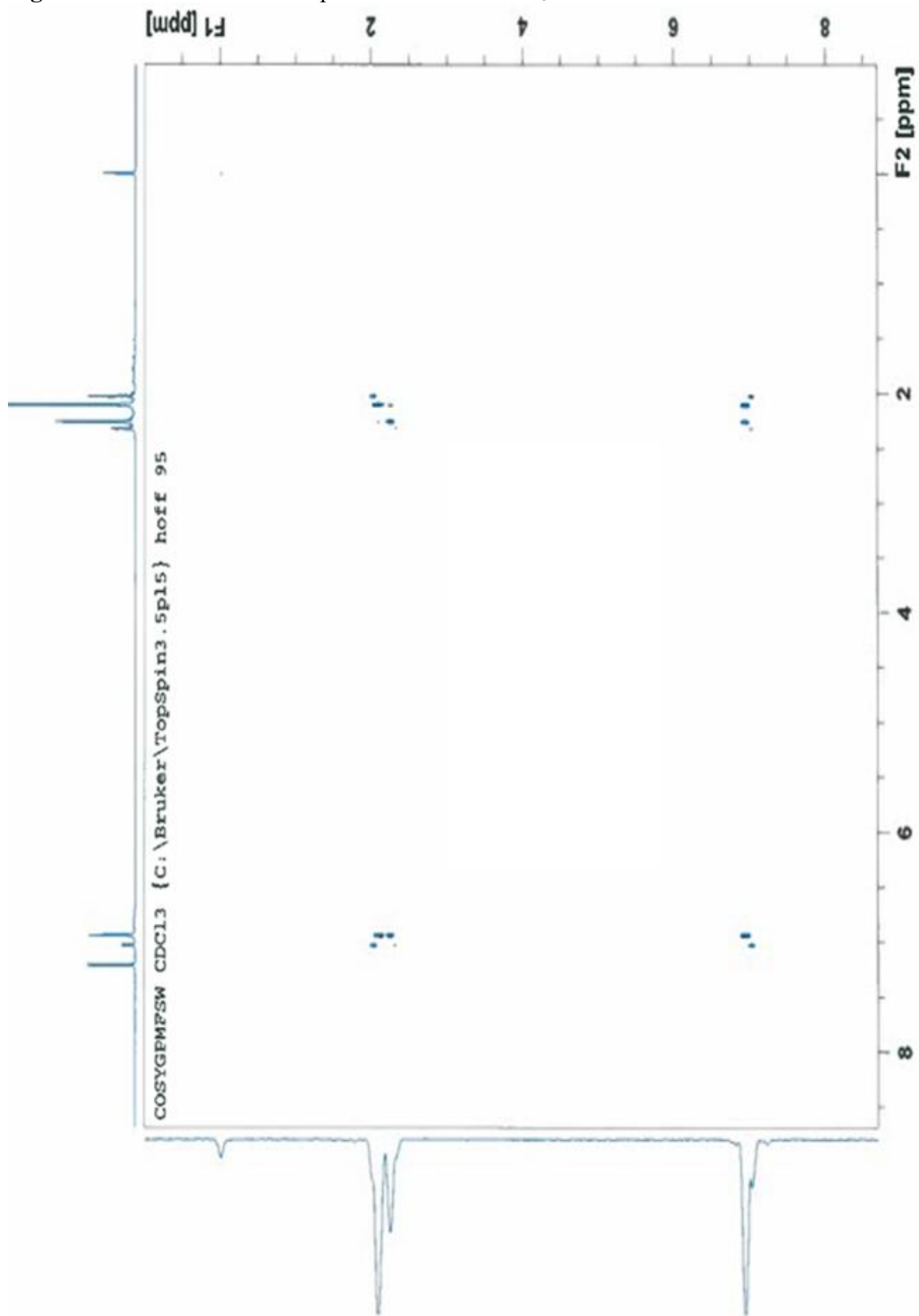
Figure A6: 2D NOESY NMR Spectrum of **2** in CDCl$_3$–d_2
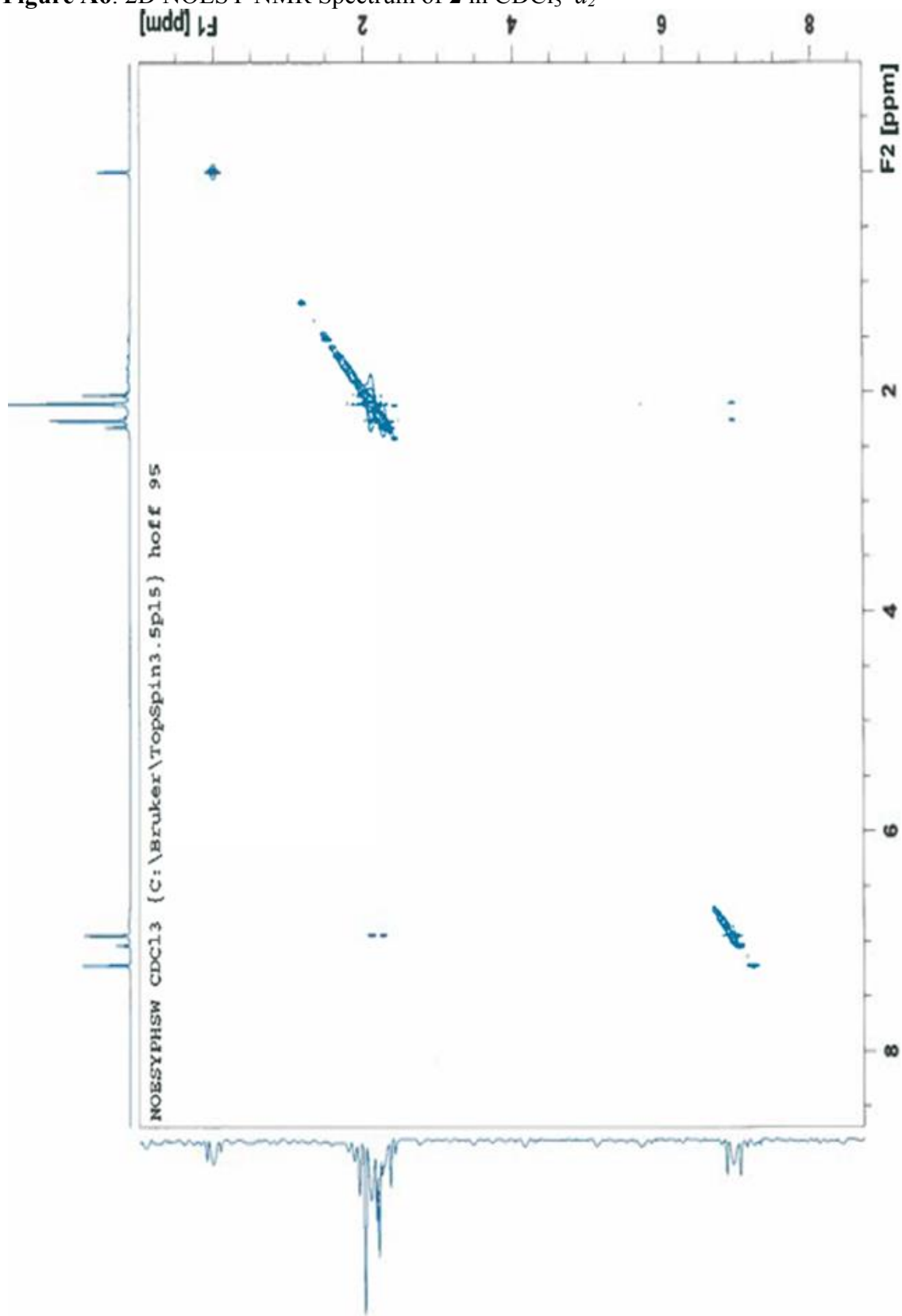
Figure A7: 2D HSQC NMR Spectrum of **2** in CDCl$_3$–d_2
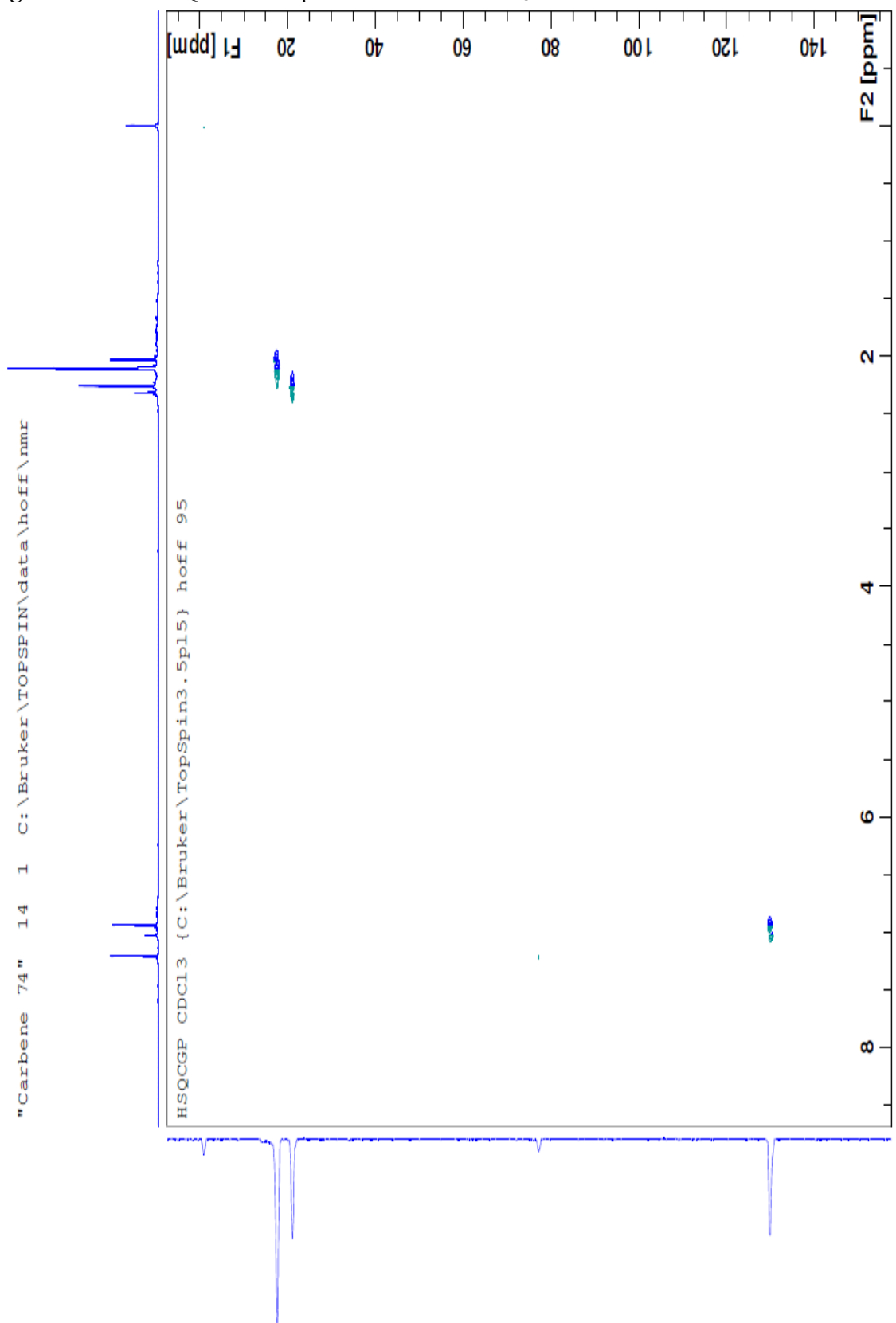
Figure A8: ^{1}H NMR Spectrum of **3a** in CD$_2$Cl$_2$–d_2
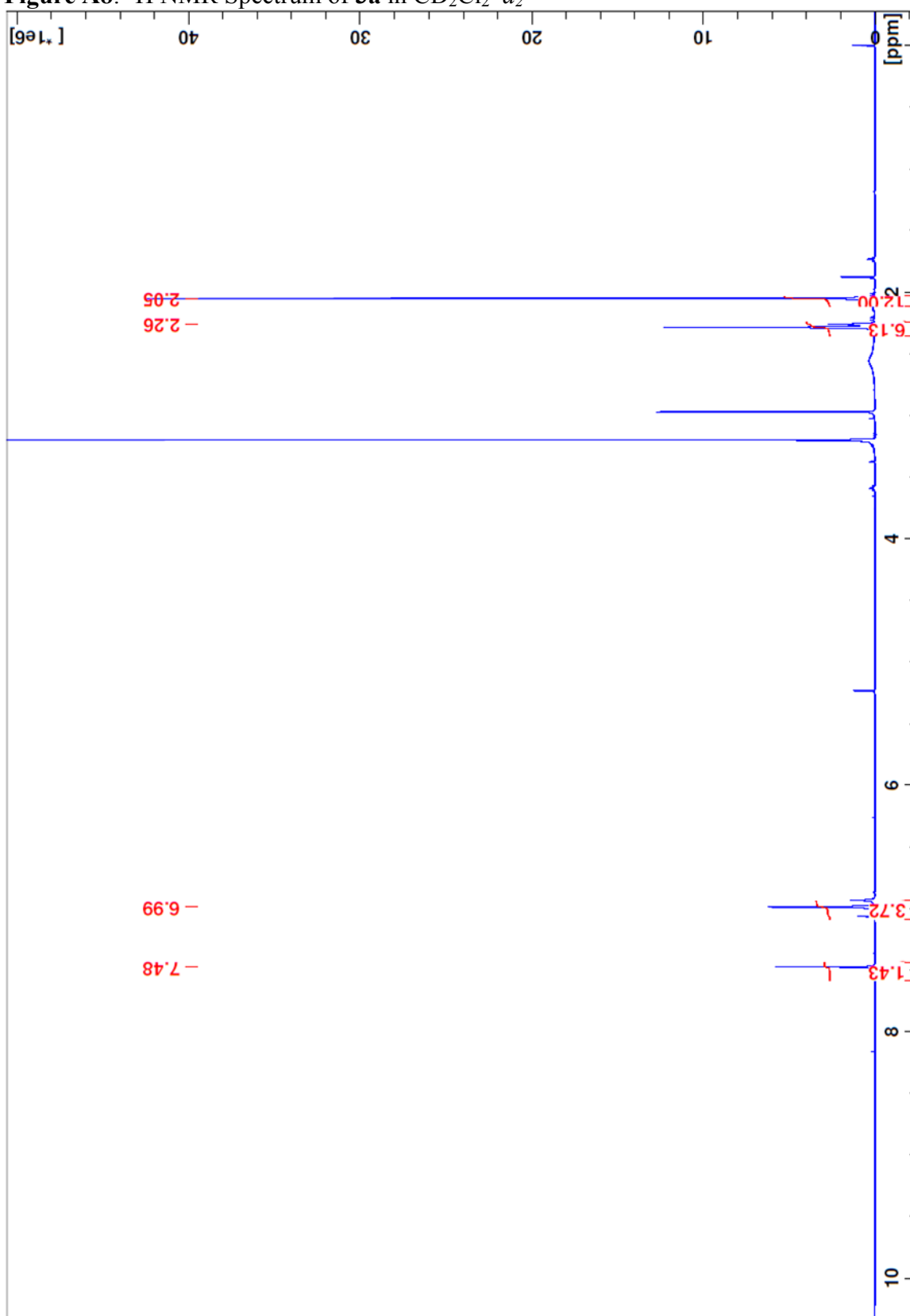
Figure A9: ^{13}C NMR Spectrum of **3a** in $CD_2Cl_2–d_2$
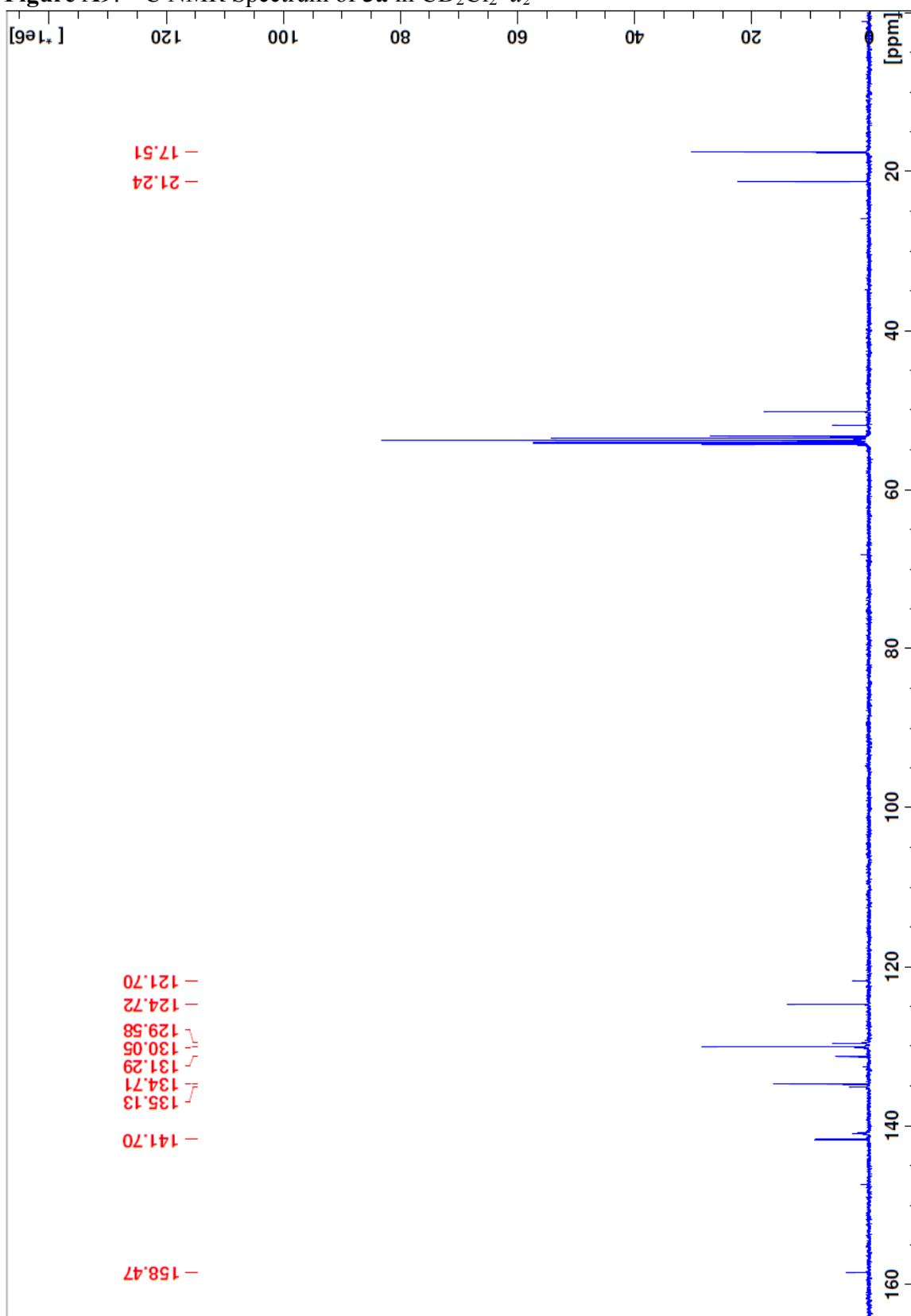
Figure A10: 2D NOESY NMR Spectrum of **3a** in CD$_2$Cl$_2$–d_2
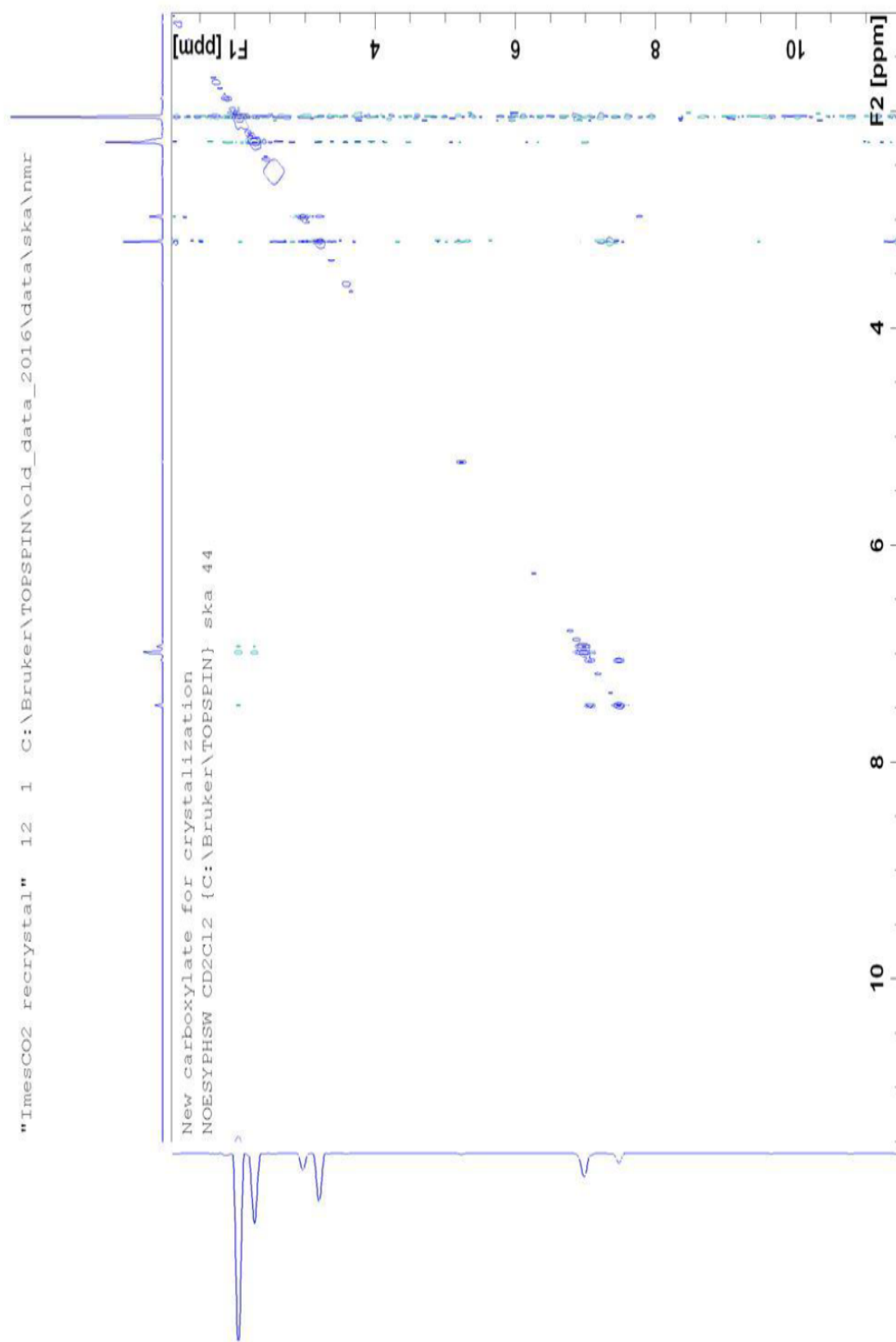
Figure A11: 2D COSY NMR Spectrum of **3a** in $CD_2Cl_2-d_2$
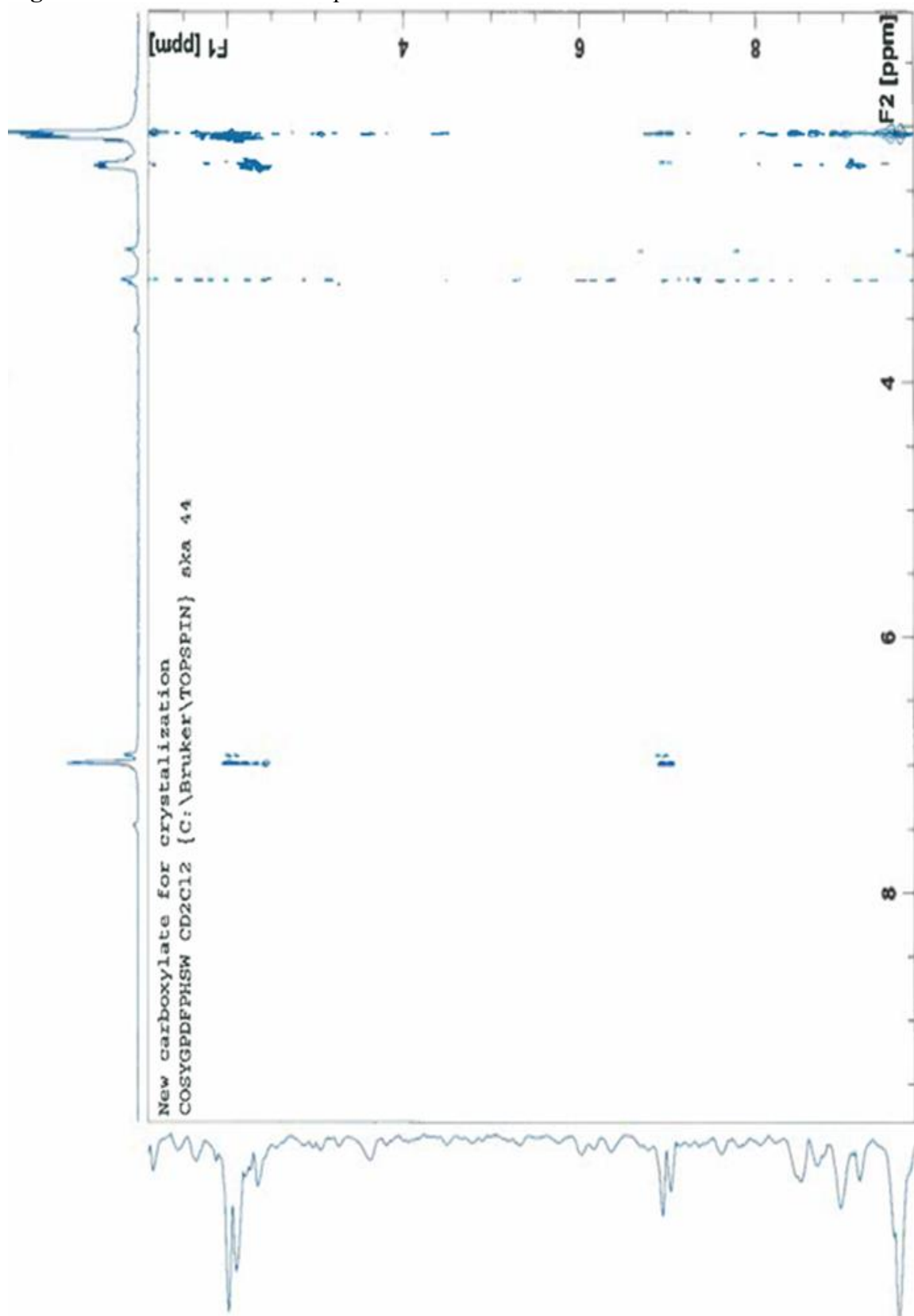
Figure A12: 2D HSQC NMR Spectrum of **3a** in CD_2Cl_2–d_2

New carboxylate for crystalization
HSQCGP CD2Cl2 (C:\Bruker\TOPSPIN) ska 44
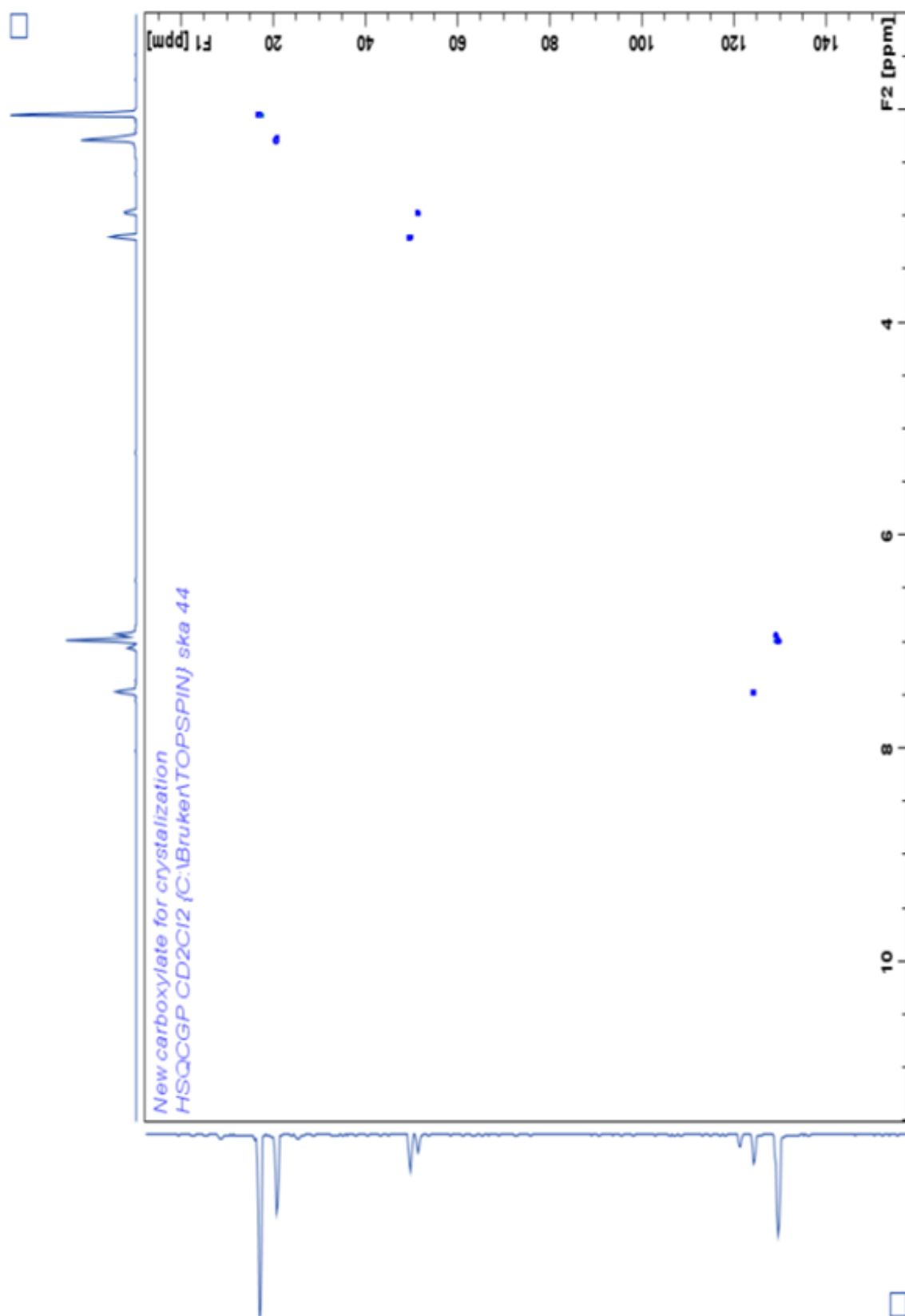
Figure A13: ^{1}H NMR Spectrum of **3b** in CD_2Cl_2–d_2
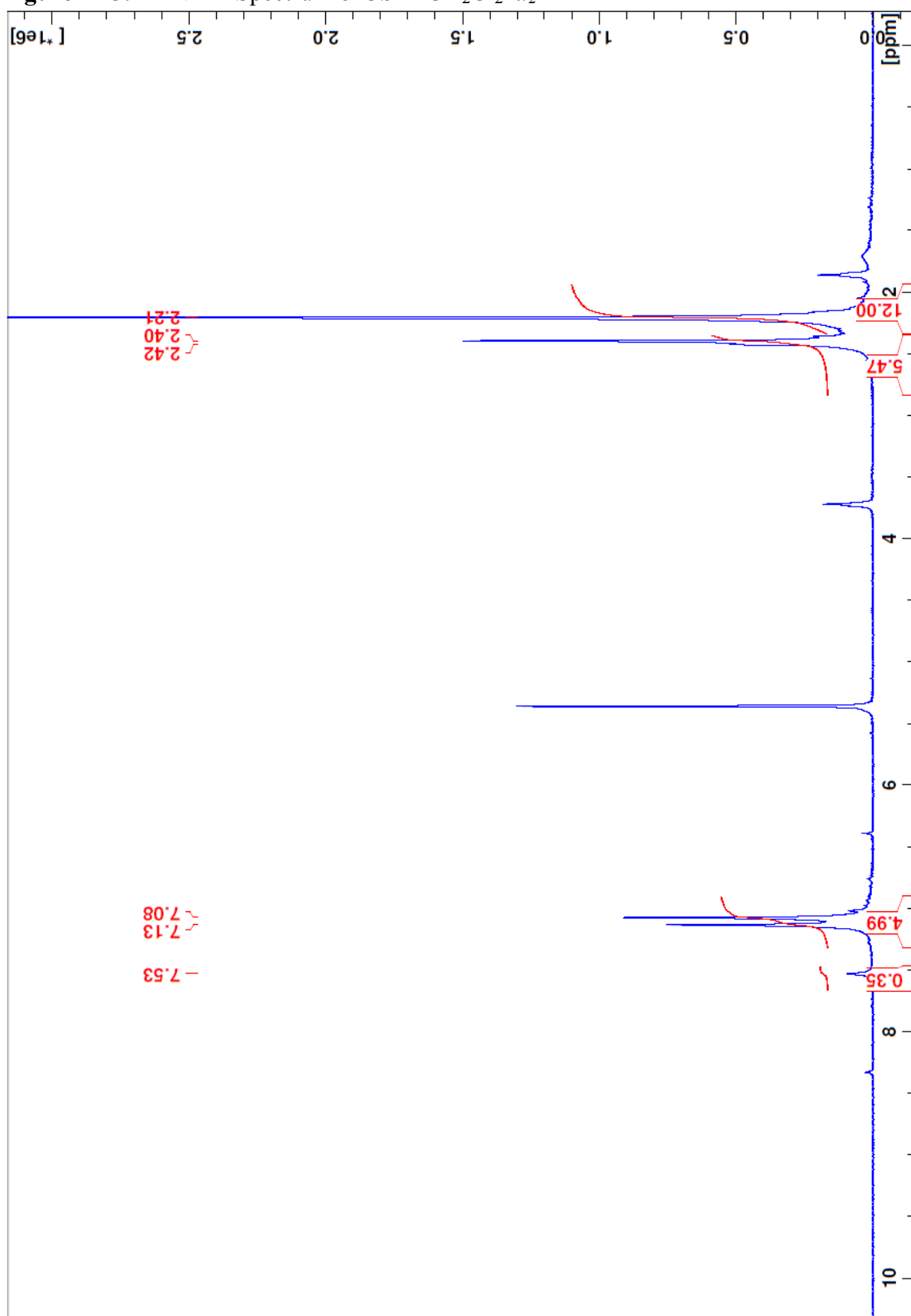
Figure A14: ^{13}C NMR Spectrum of **3b** in CD_2Cl_2–d_2
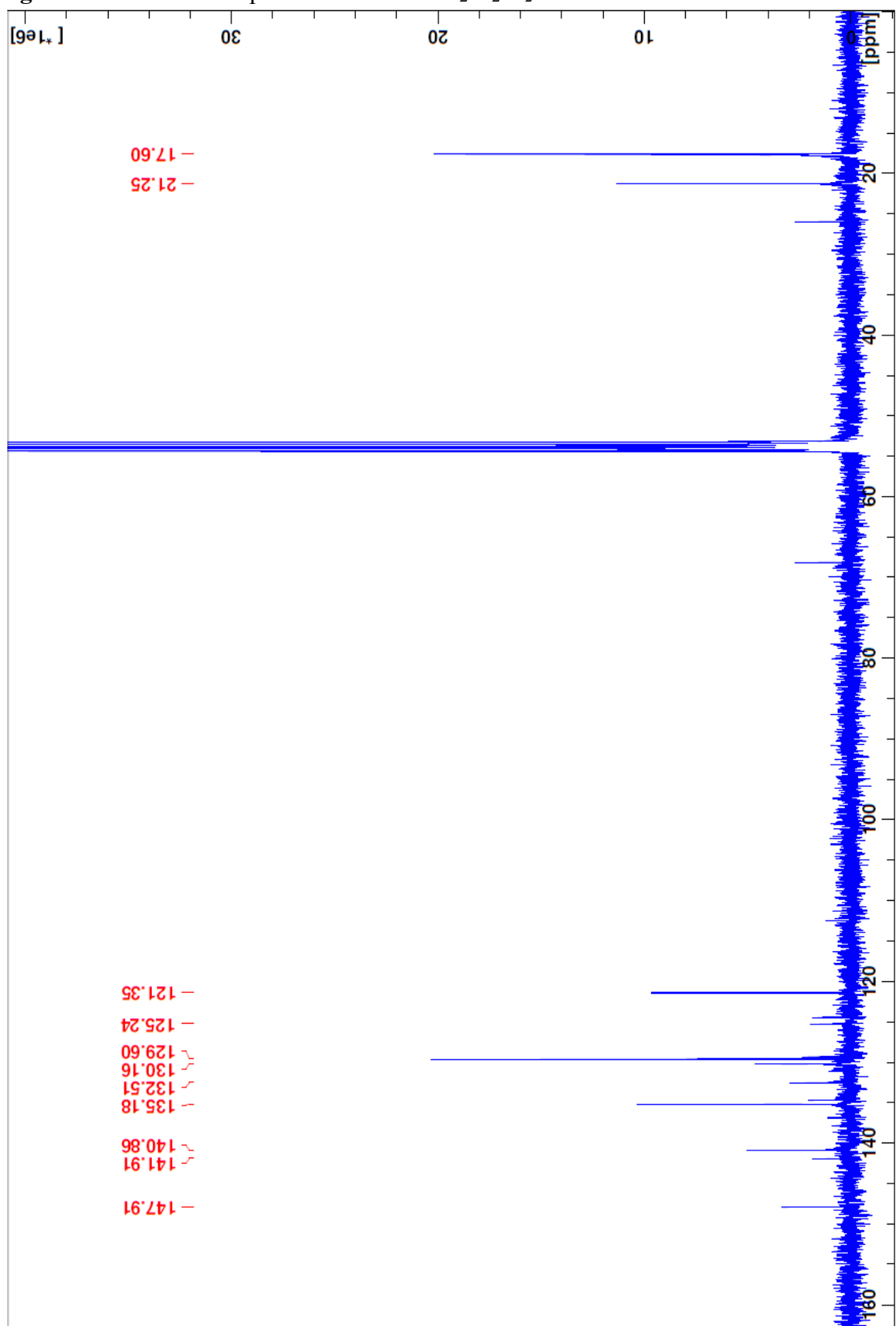
Figure A15: 2D NOESY NMR Spectrum of **3b** in $CD_2Cl_2-d_2$

Figure A16: 2D COSY NMR Spectrum of **3b** in CD_2Cl_2–d_2
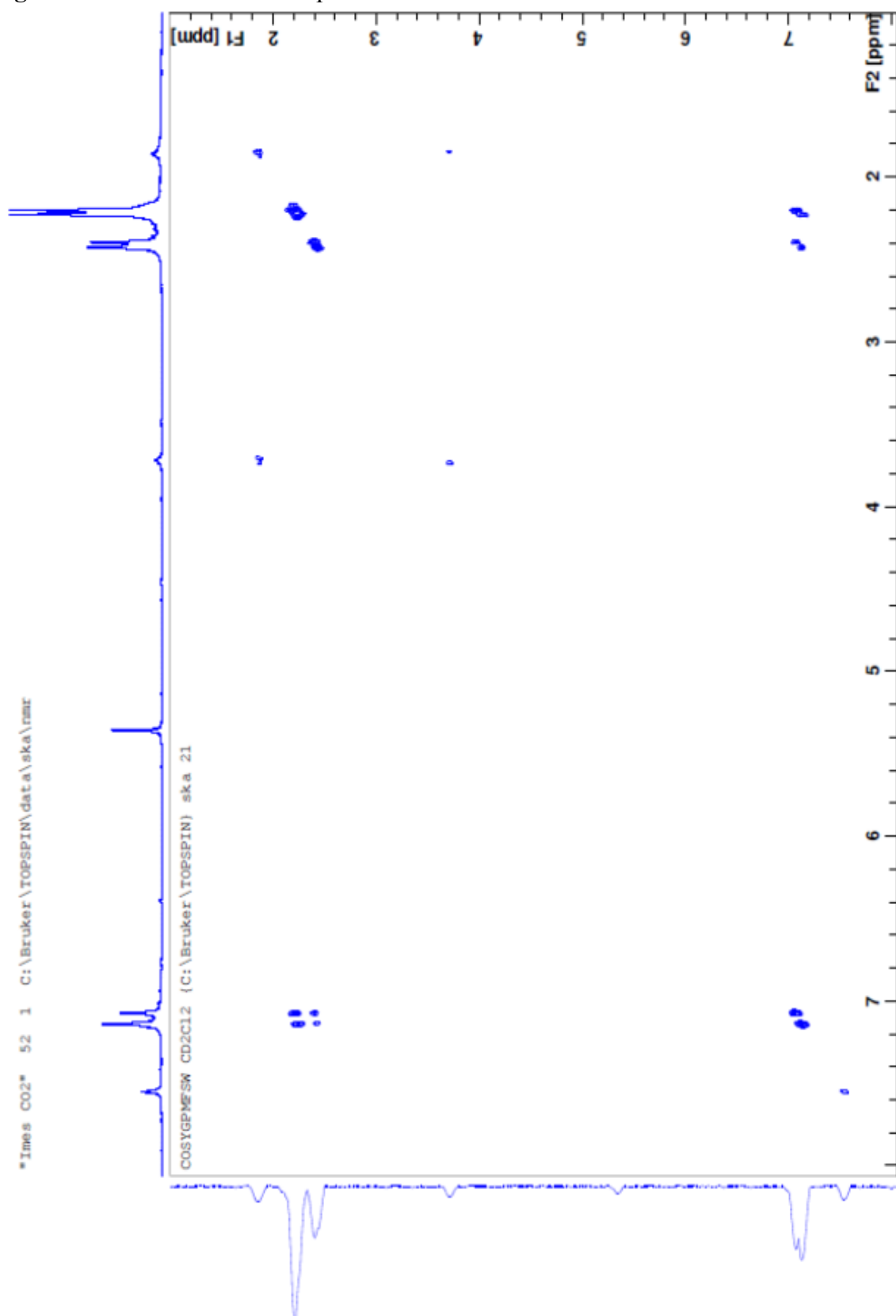
Figure A17: 2D HSQC NMR Spectrum of **3b** in $CD_2Cl_2–d_2$
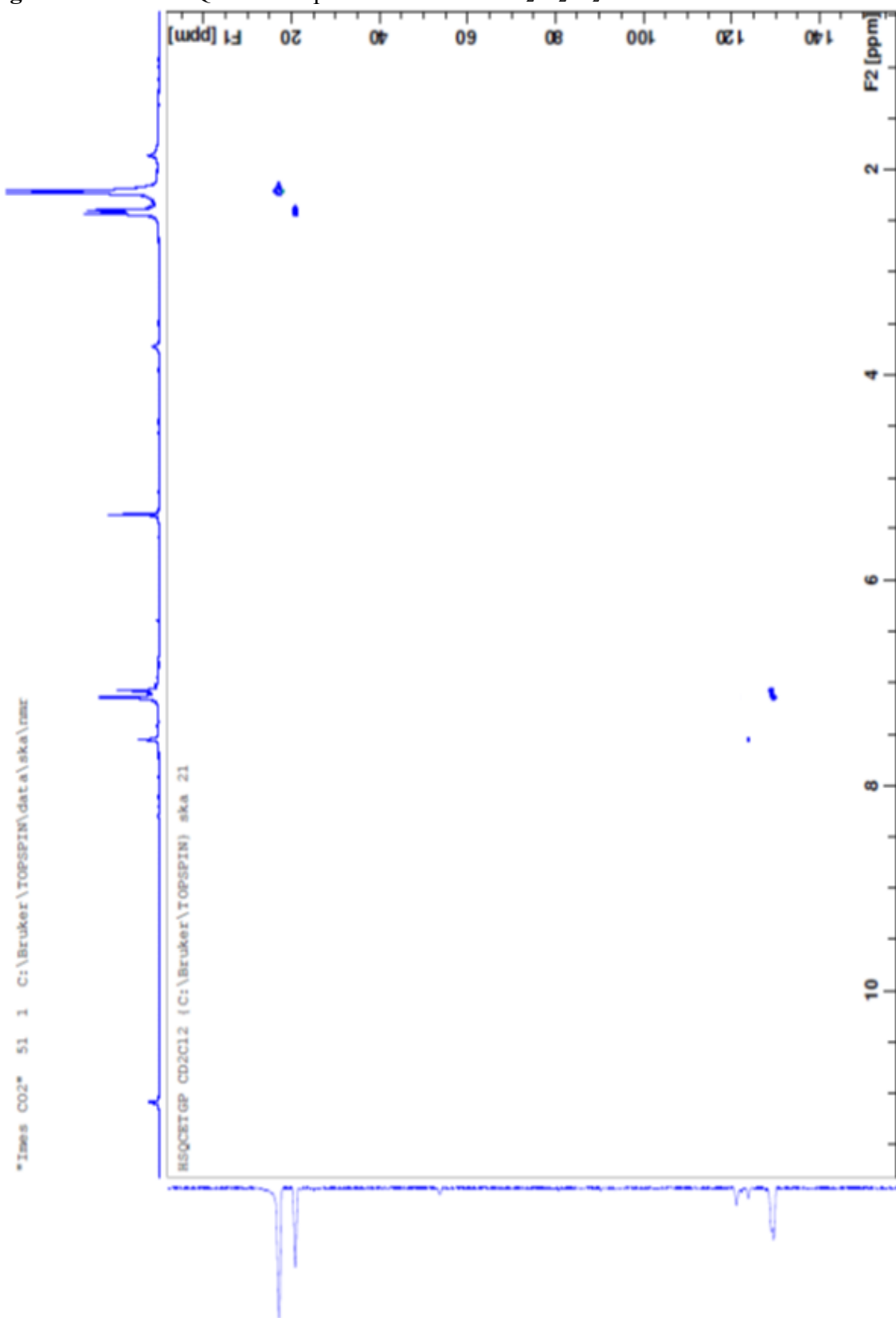
Figure A18: ^{1}H NMR Spectrum of **4** in DMSO–d_6
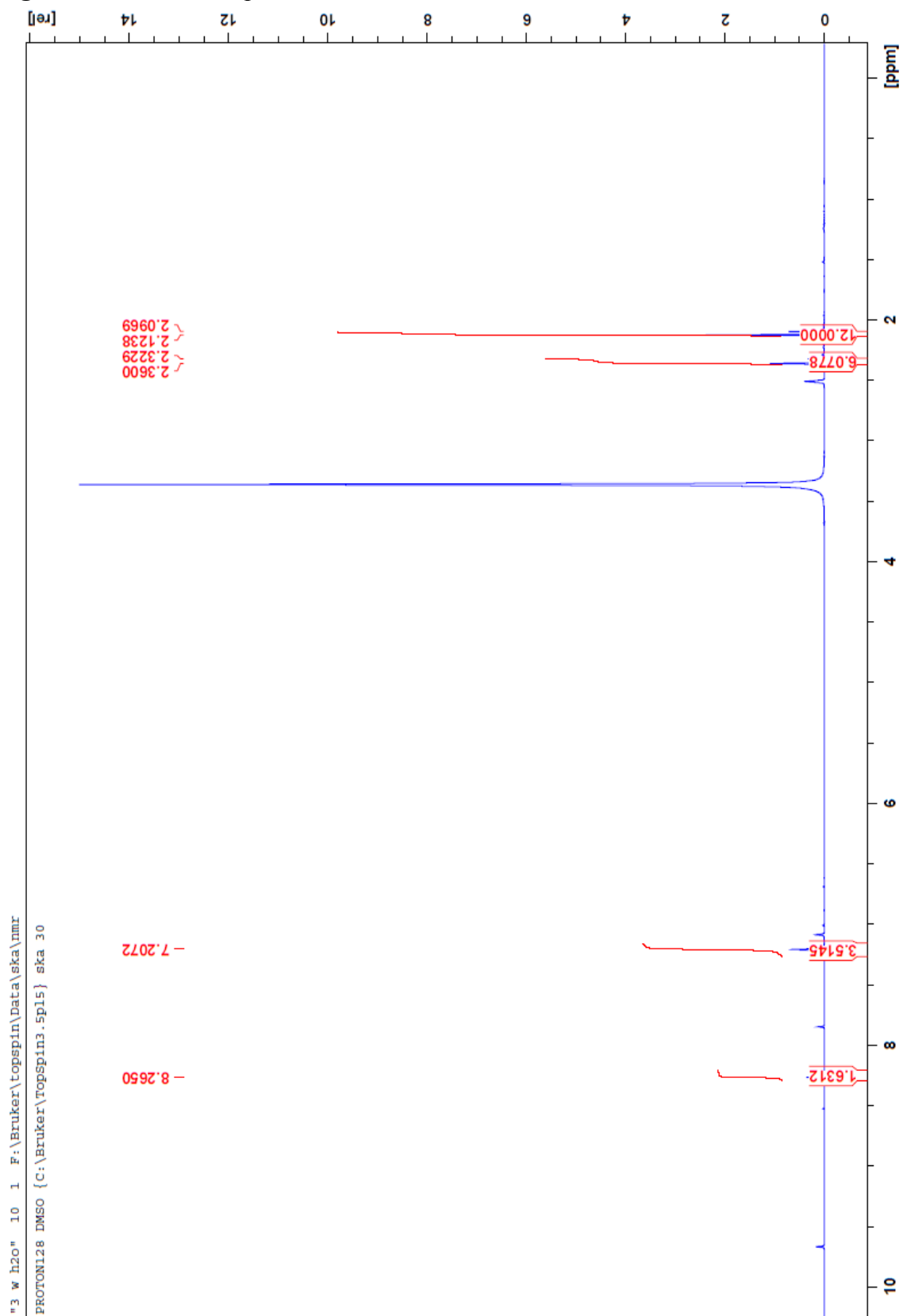
Figure A19: 2D NOESY NMR Spectrum of **4** in DMSO–d_6
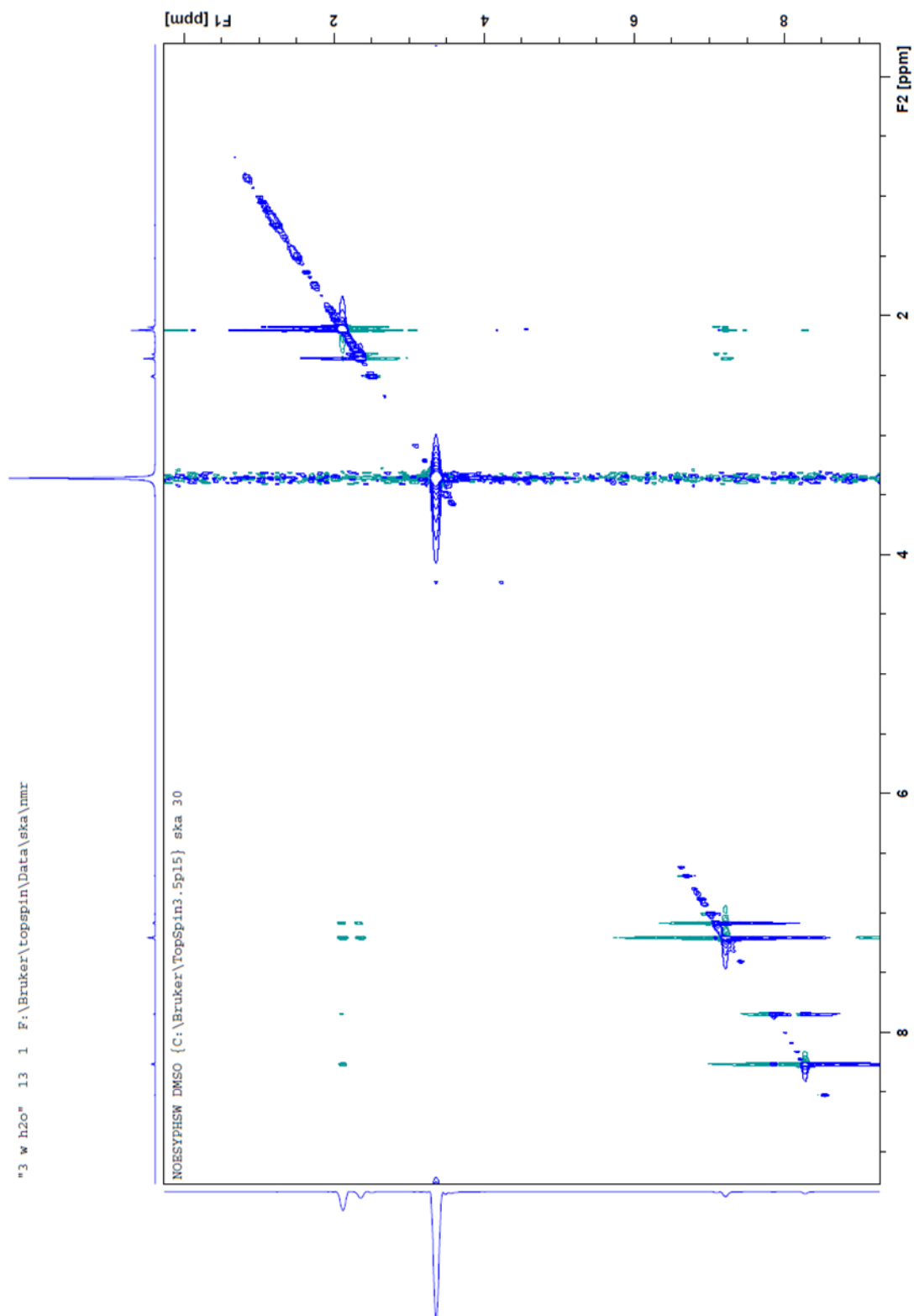
Figure A20: ^{13}C NMR Spectrum of **4** in DMSO–d_6

115
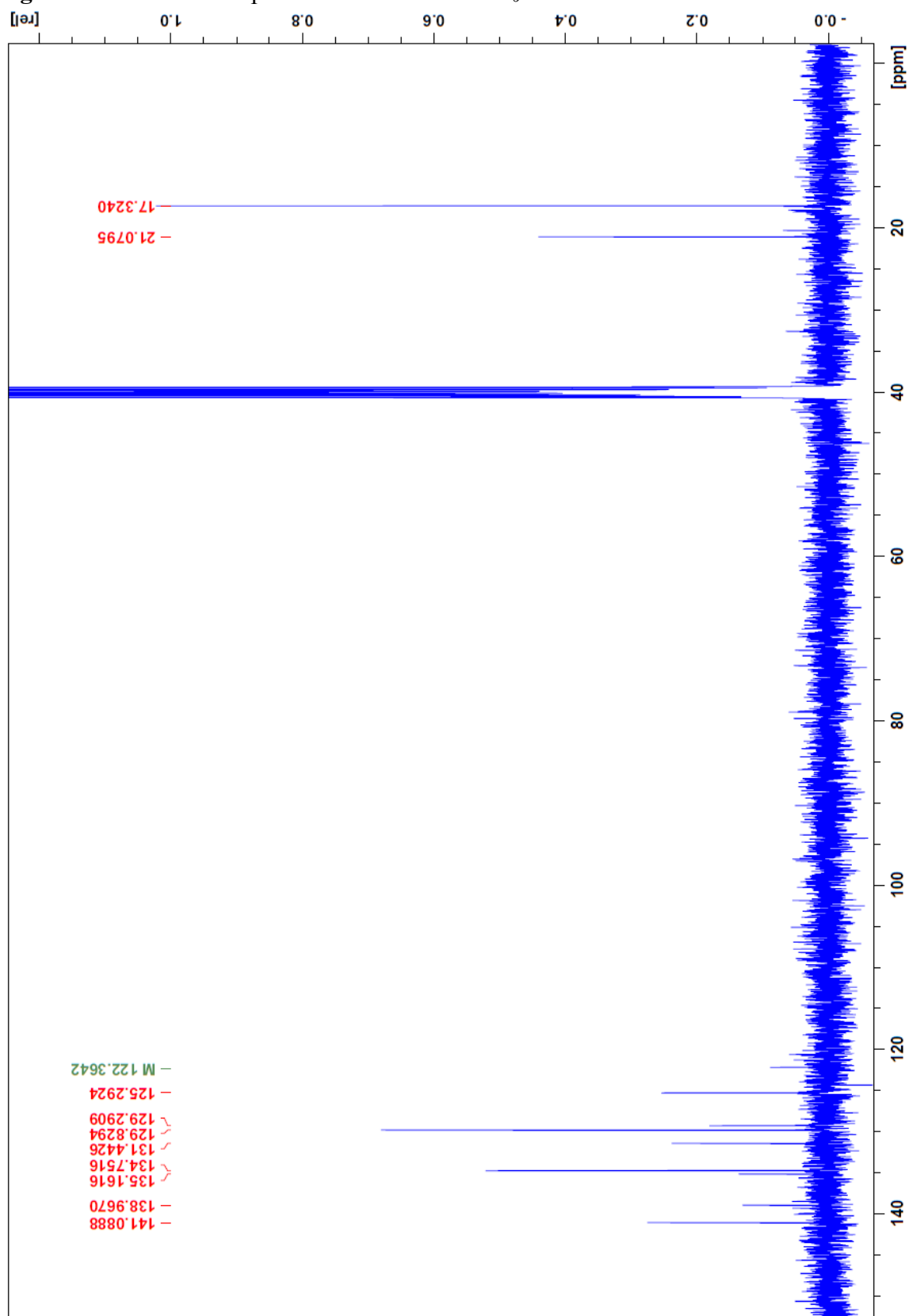
Figure A21: 2D HSQC NMR Spectrum of **4** in DMSO–d_6
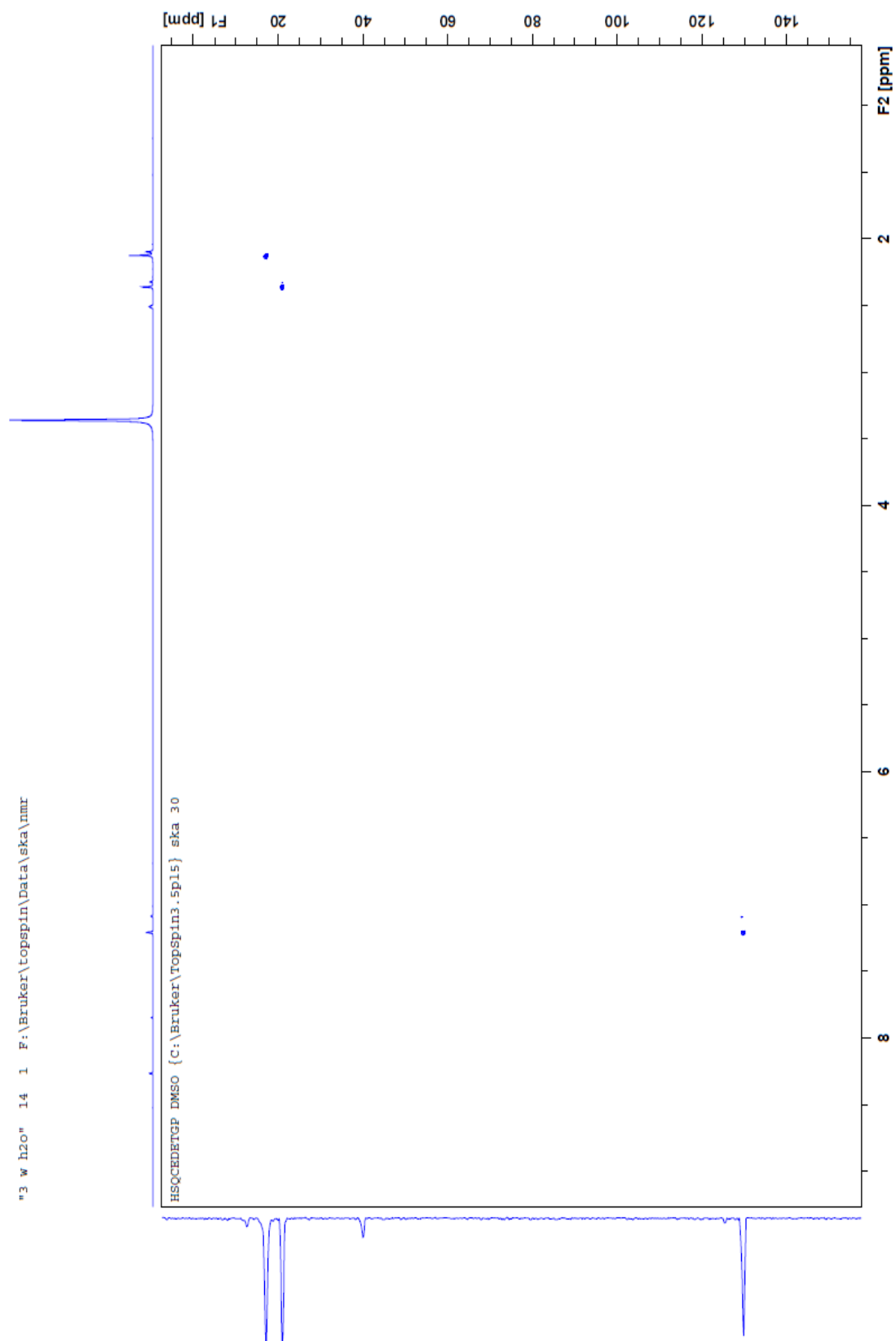
Figure A22: ^{1}H NMR Spectrum of **5** in DMSO–d_6
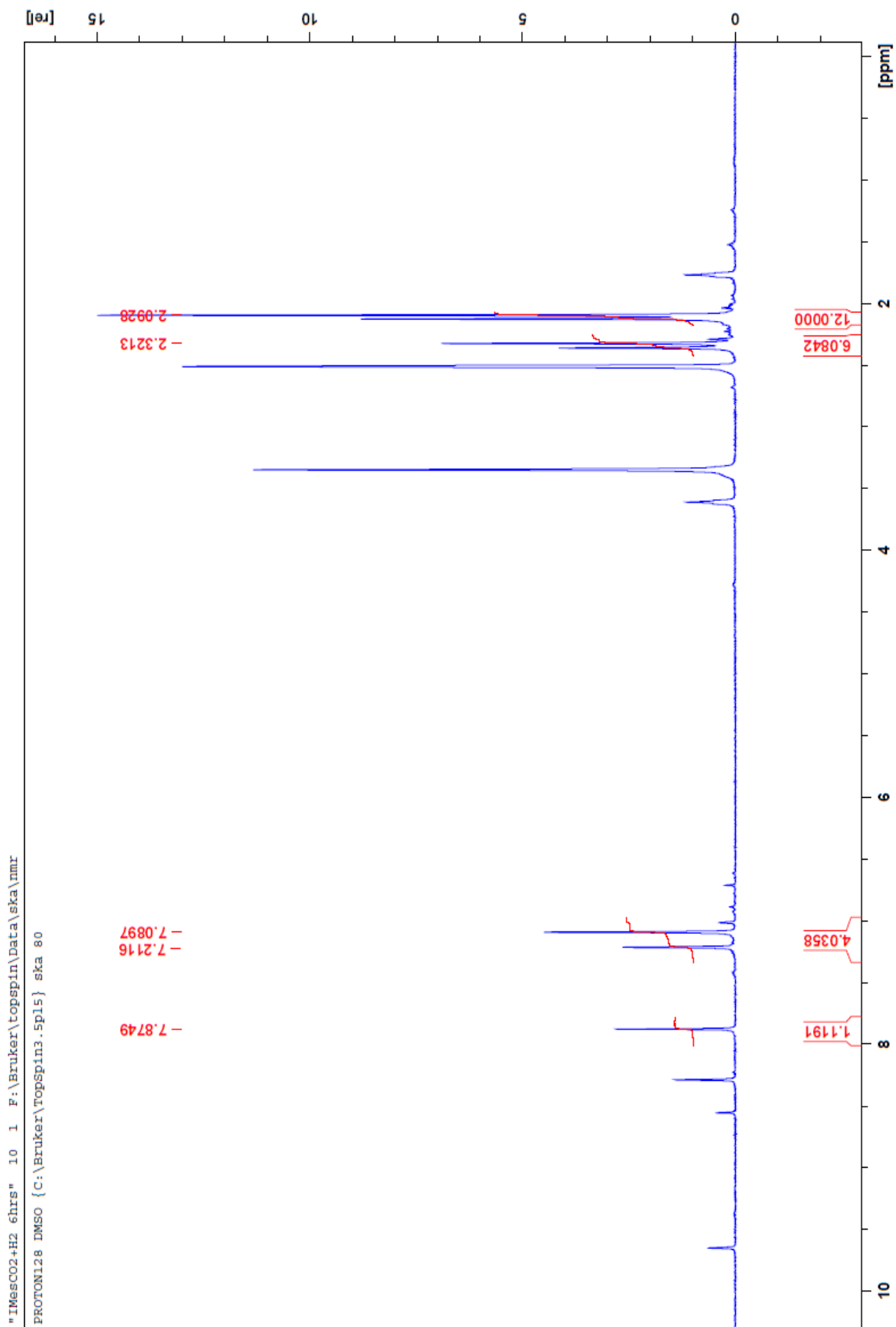
Figure A23: ^{13}C NMR Spectrum of **5** in DMSO–d_6
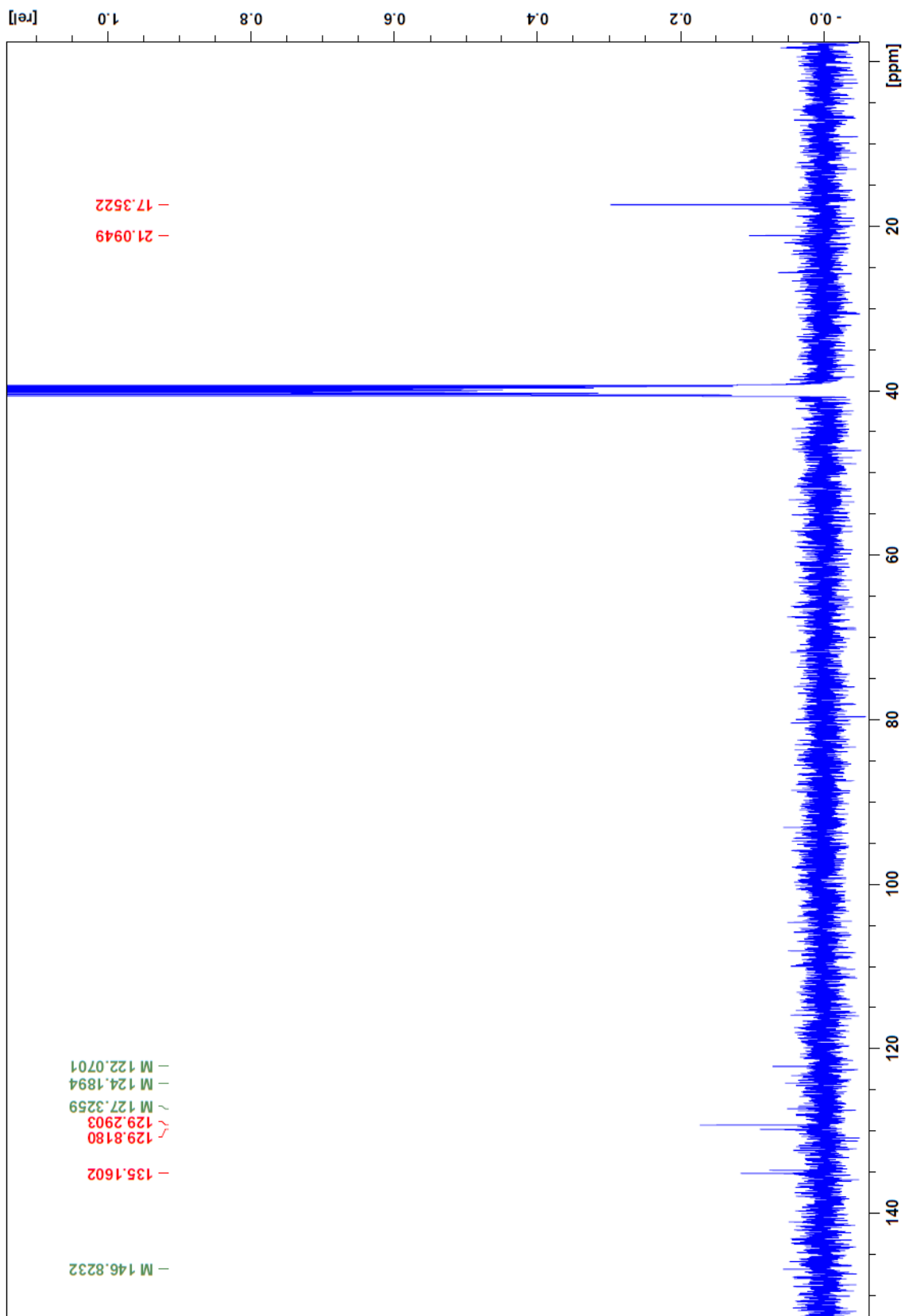
Figure A24: 2D NOESY NMR Spectrum of **5** in DMSO–*d₆*
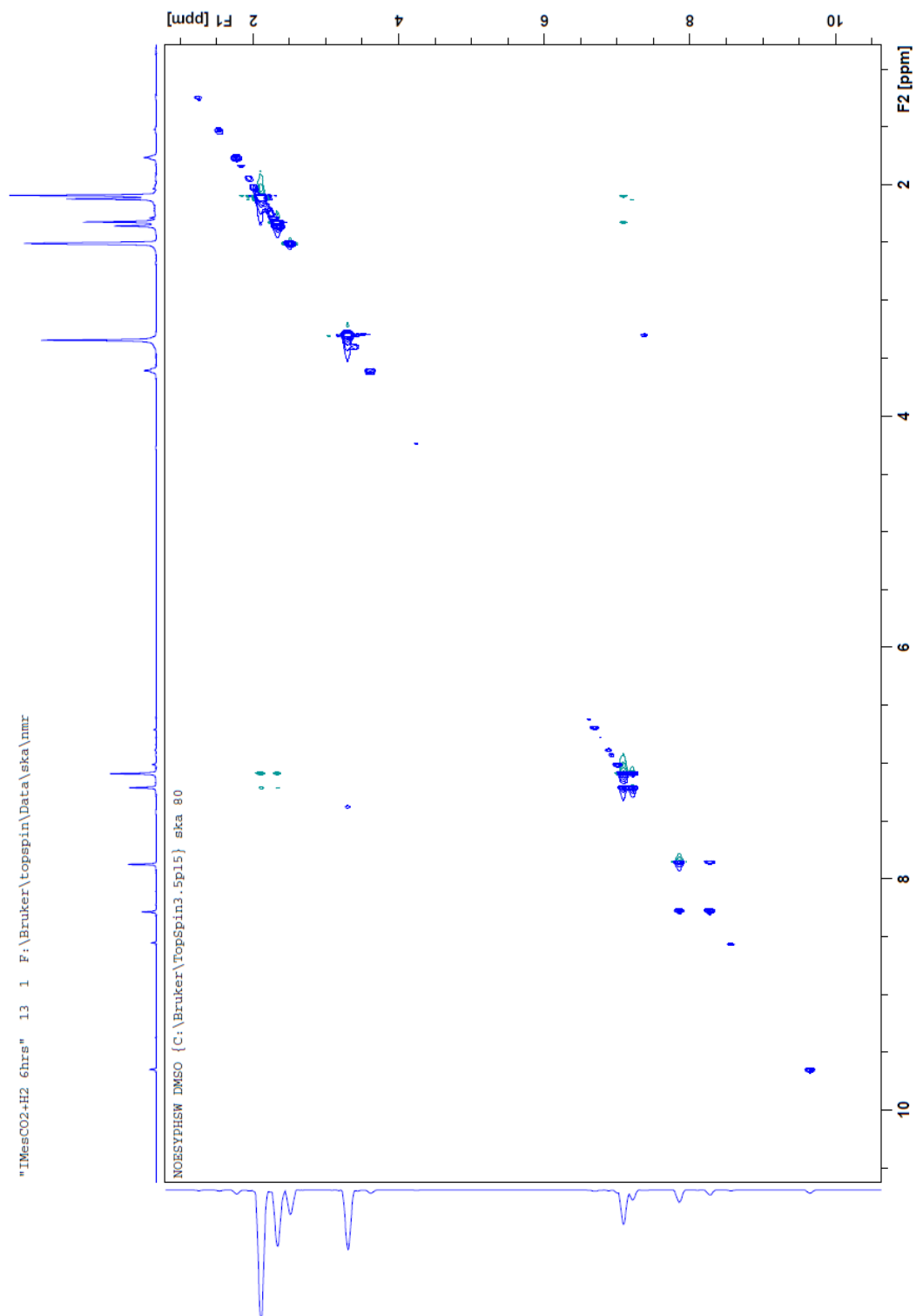
Figure A25: 2D HSQC NMR Spectrum of **5** in DMSO–d_6
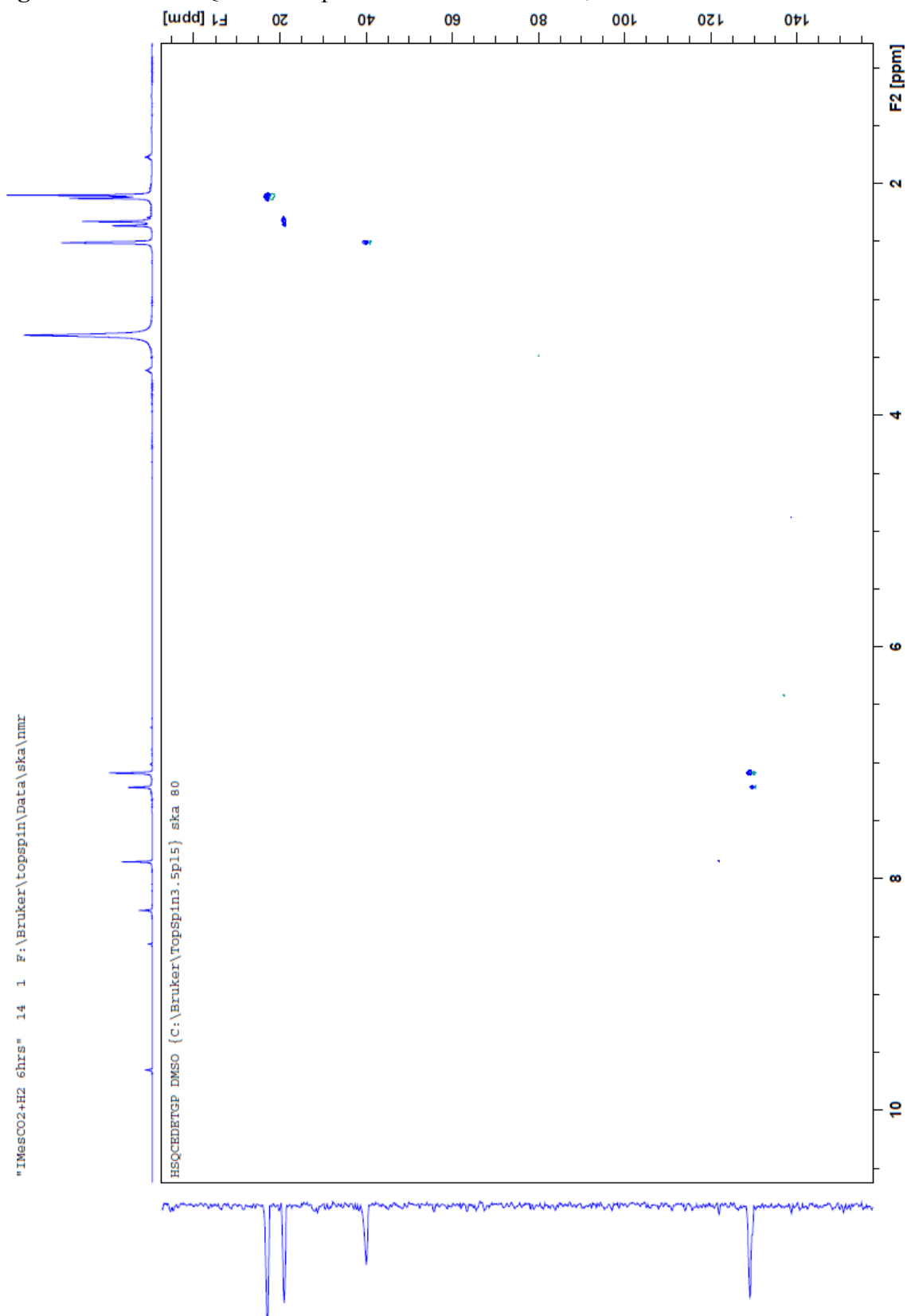
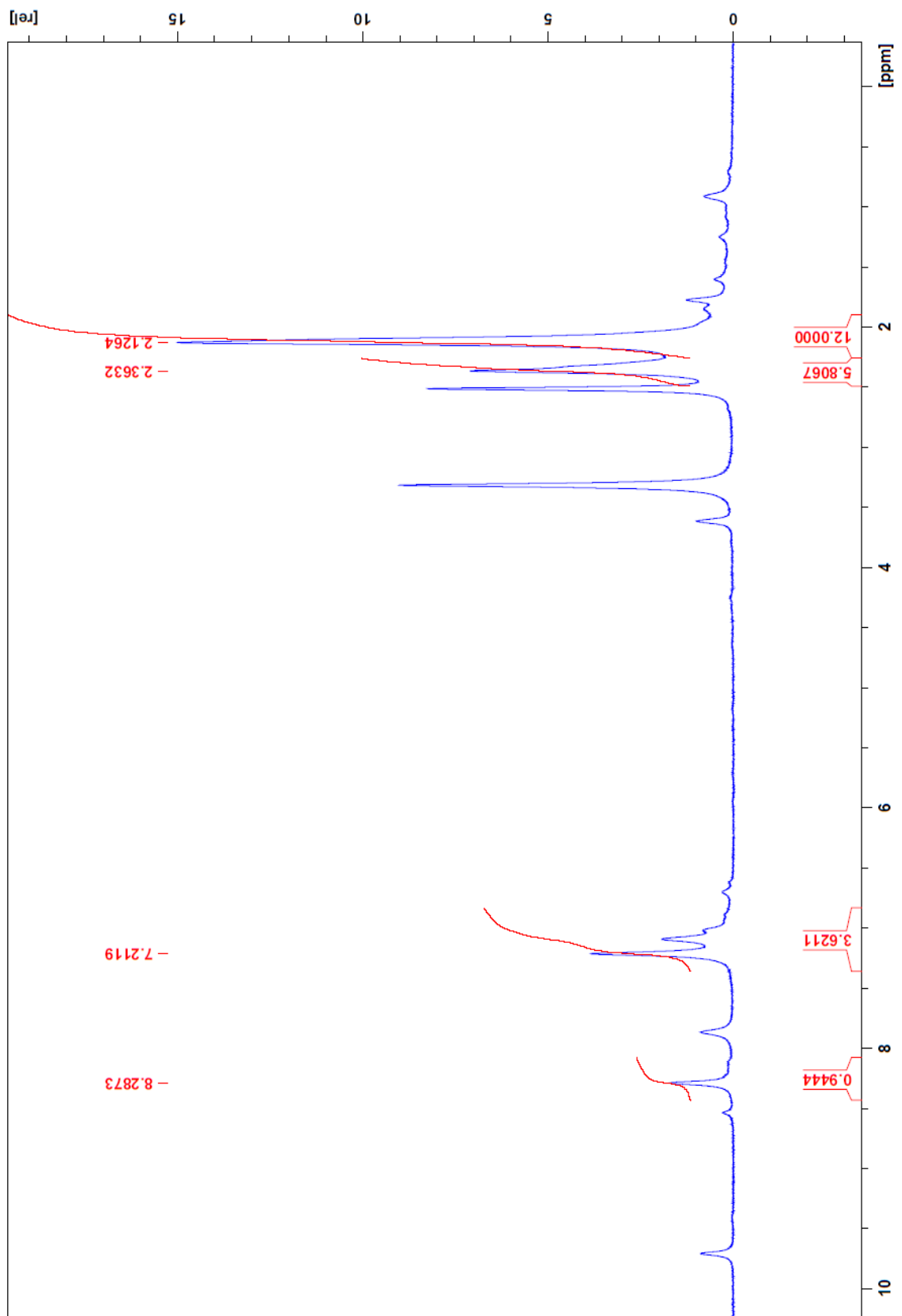**Figure A26**: ^{1}H NMR Spectrum of **6** in DMSO–d_6

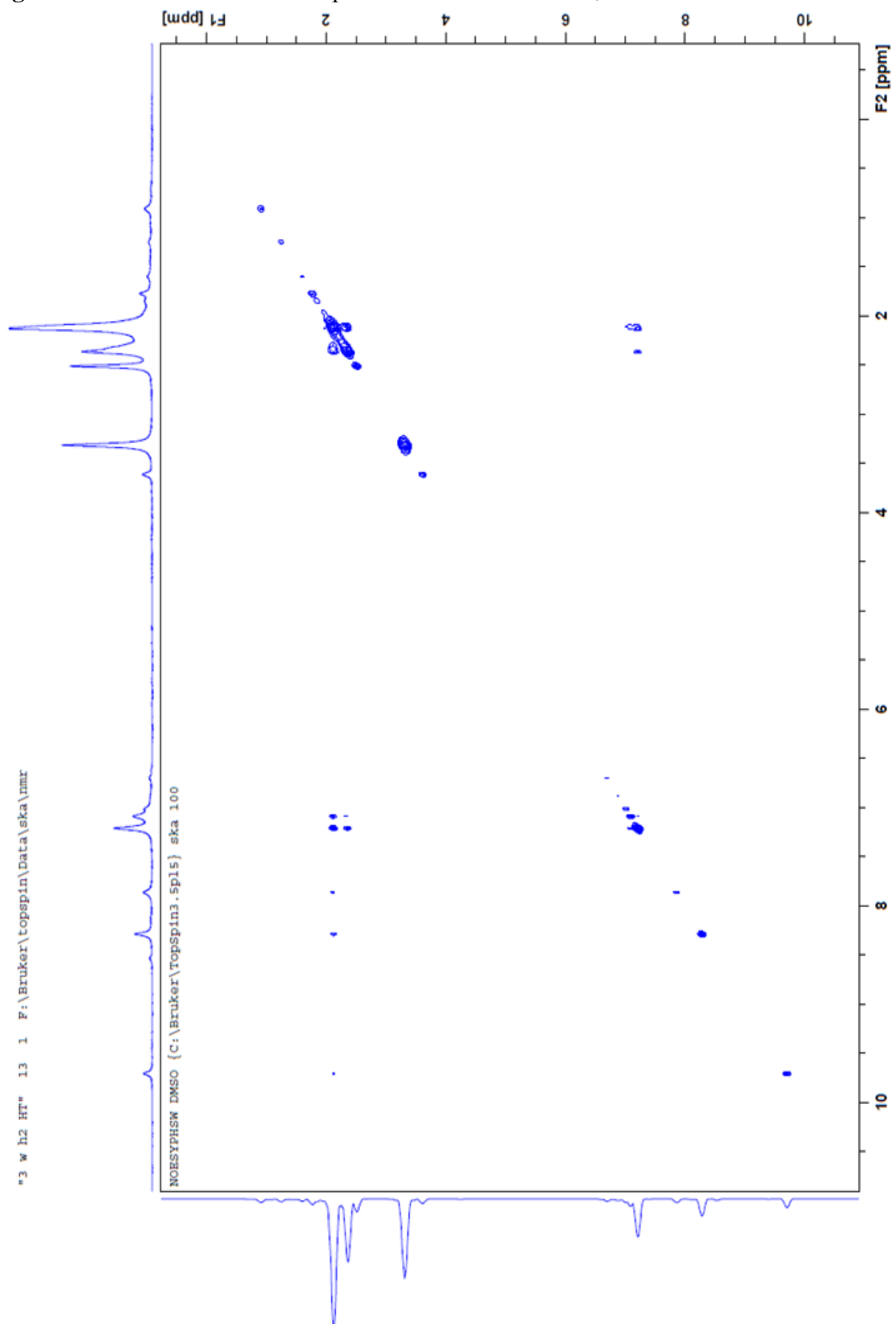**Figure A27**: 2D NOESY NMR Spectrum of **6** in DMSO–d_6

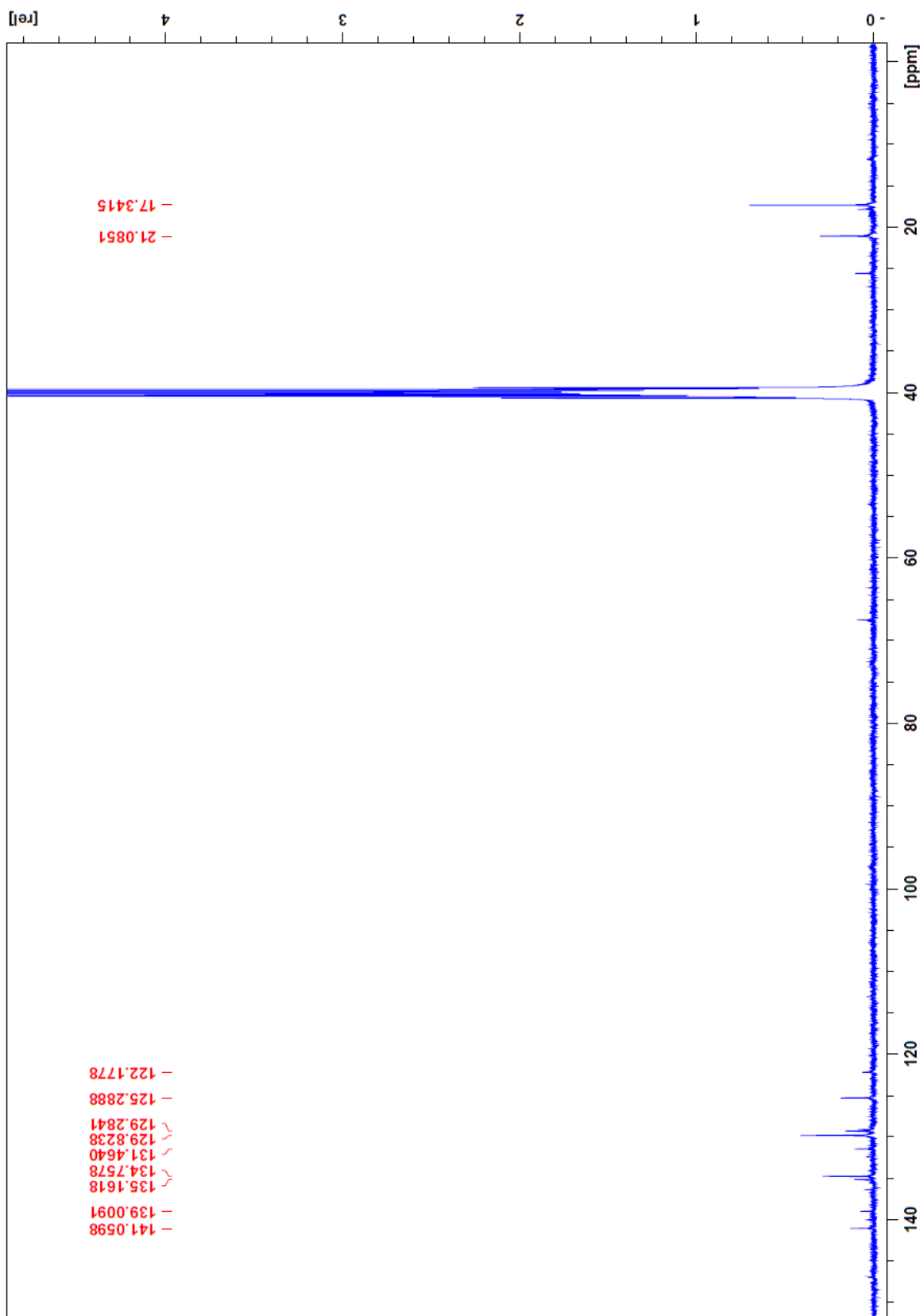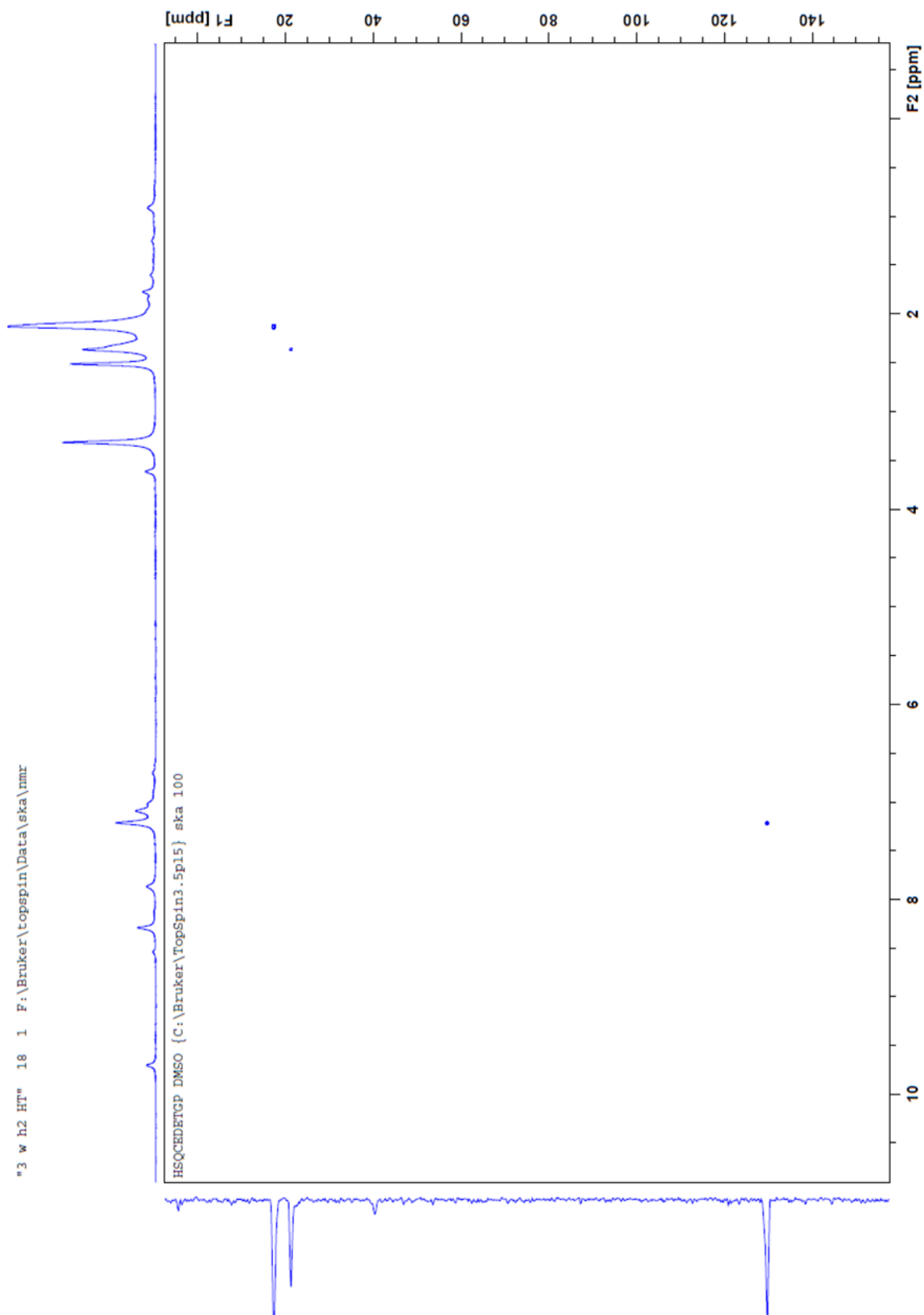**Figure A28**: ^{13}C NMR Spectrum of **6** in DMSO–d_6

Figure A29: 2D HSQC NMR Spectrum of **6** in DMSO − d_6
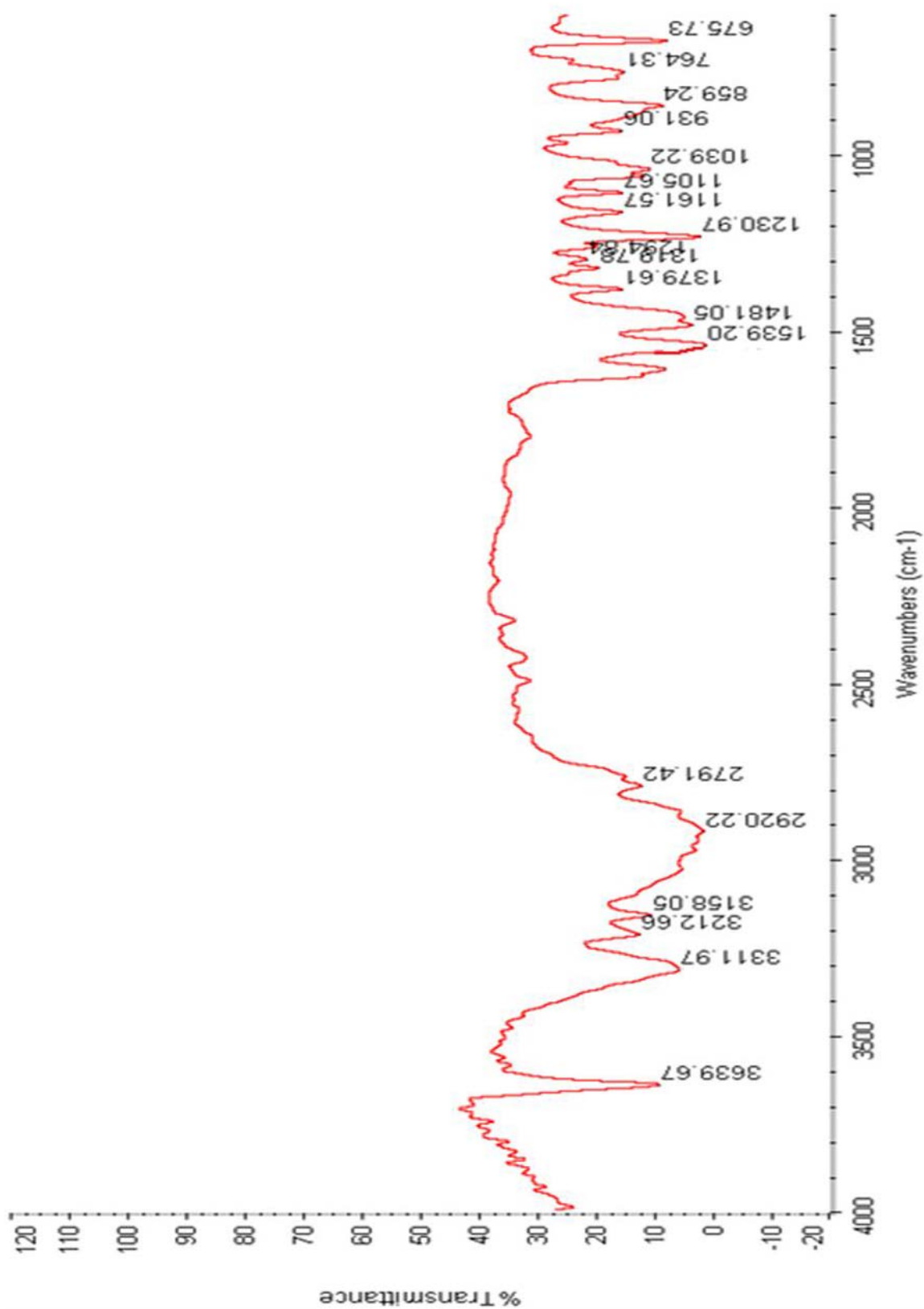
APPENDIX B: IR DATA

Figure B1: IR Spectrum of **2**

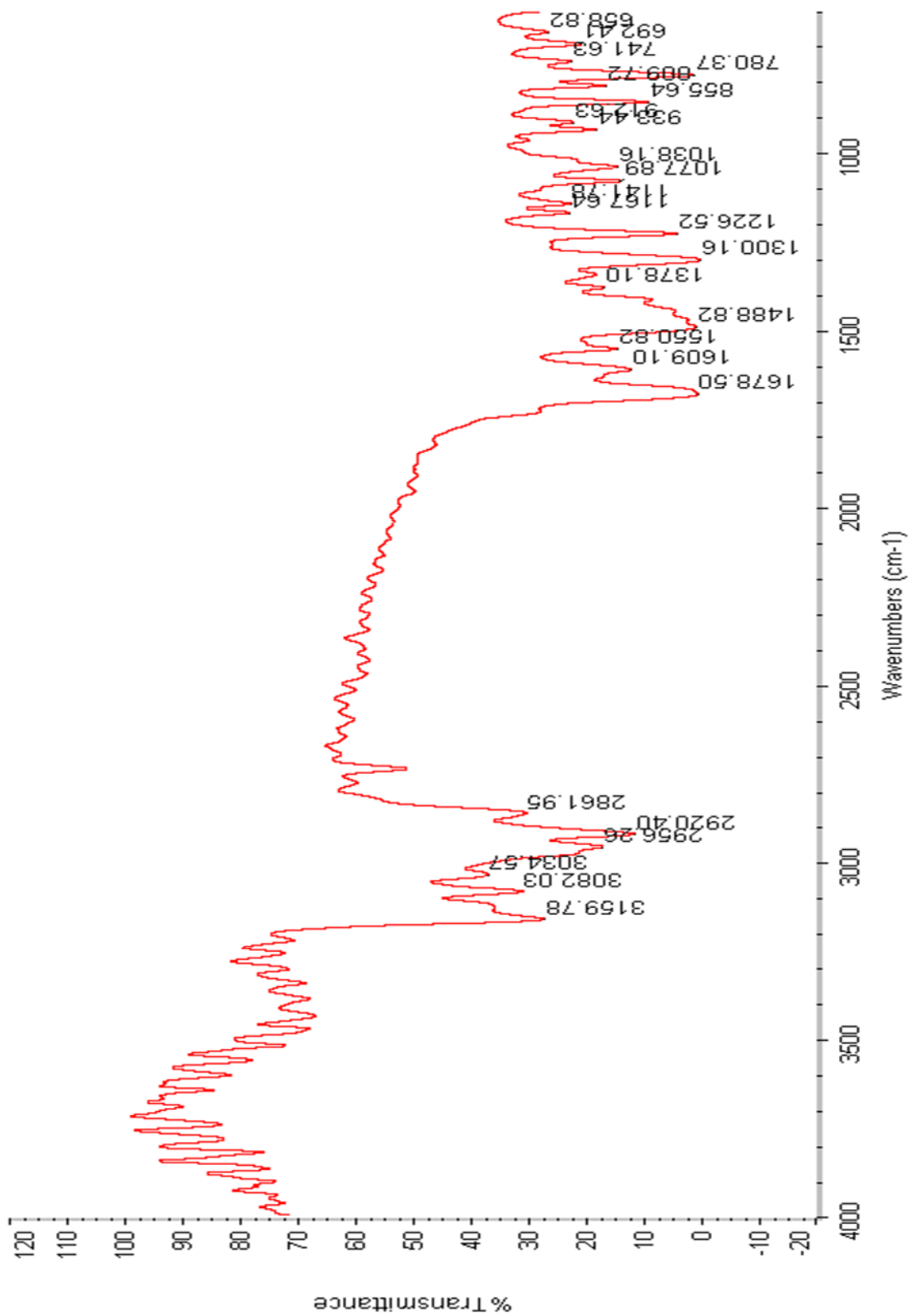**Figure B2**: IR Spectrum of **3a**

Figure B3: IR Spectrum of **3b**
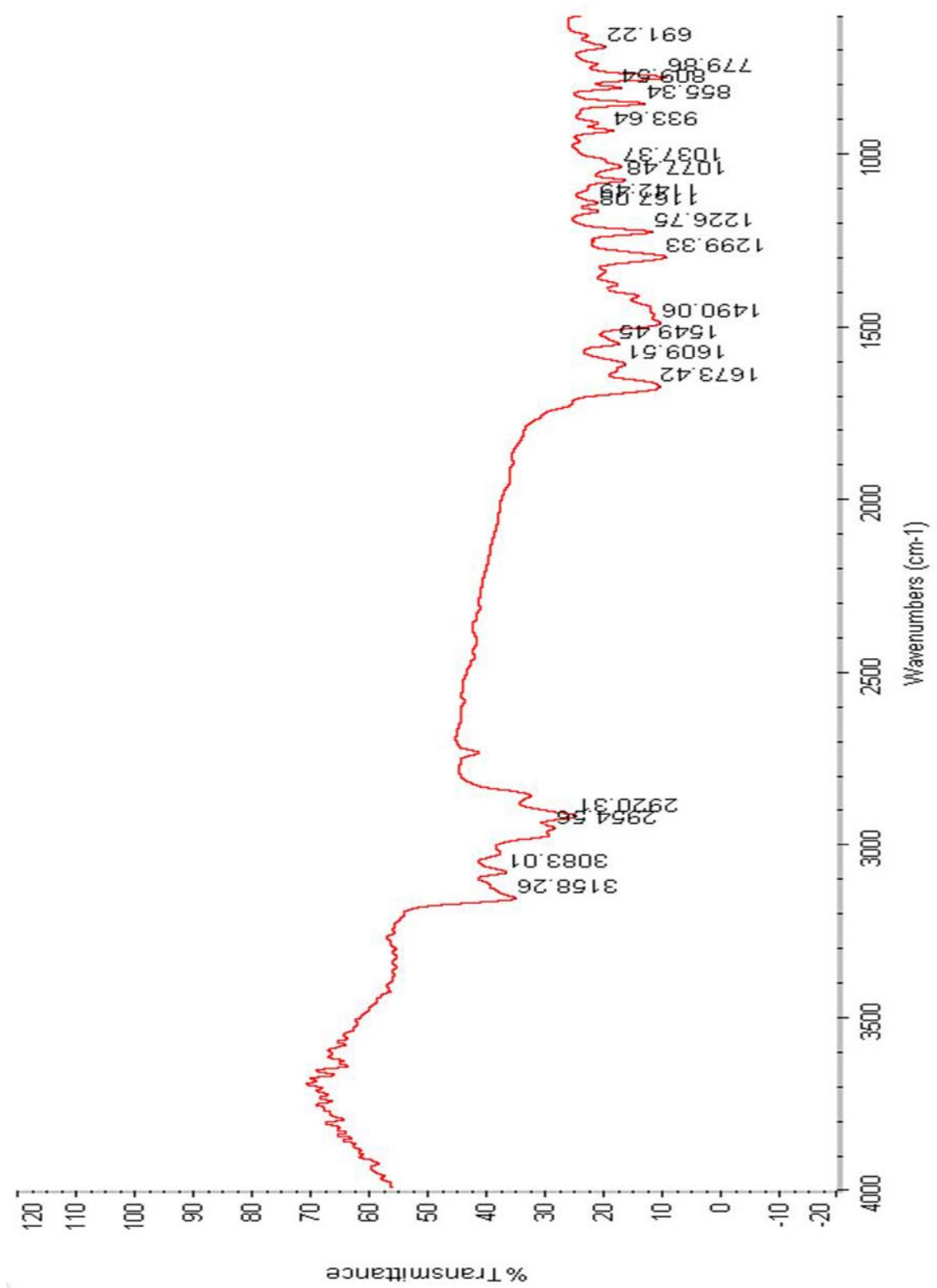
APPENDIX C: TGA DATA

Figure C1: TGA Profile of **3a**

419.9µg CO2
(13.51%)
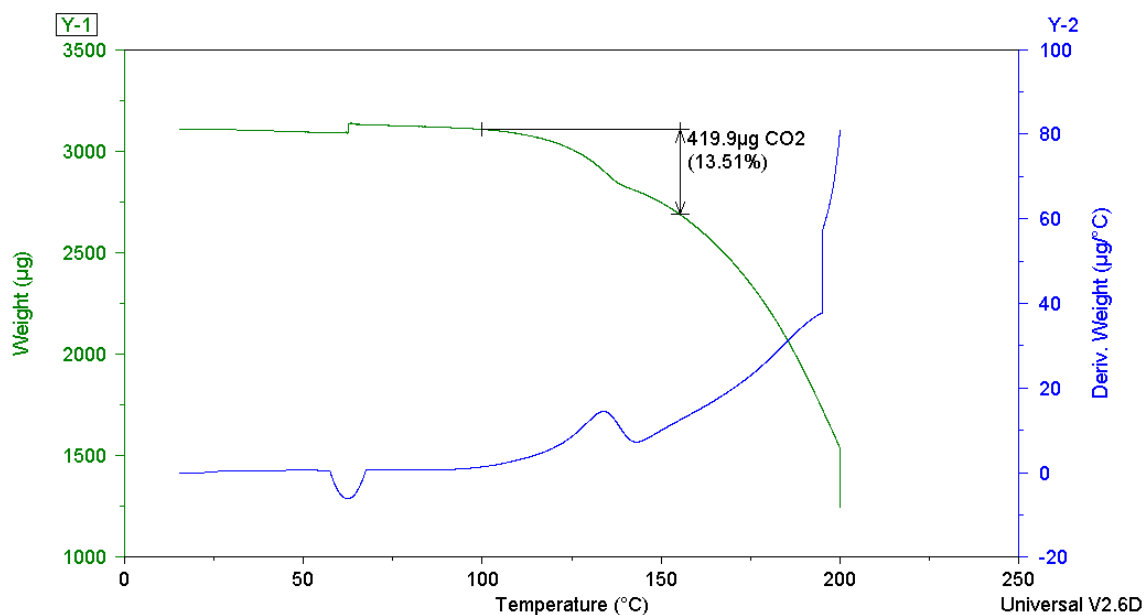
Figure C2: TGA Profile of **3b**

269.8µg CO2
(12.20%)
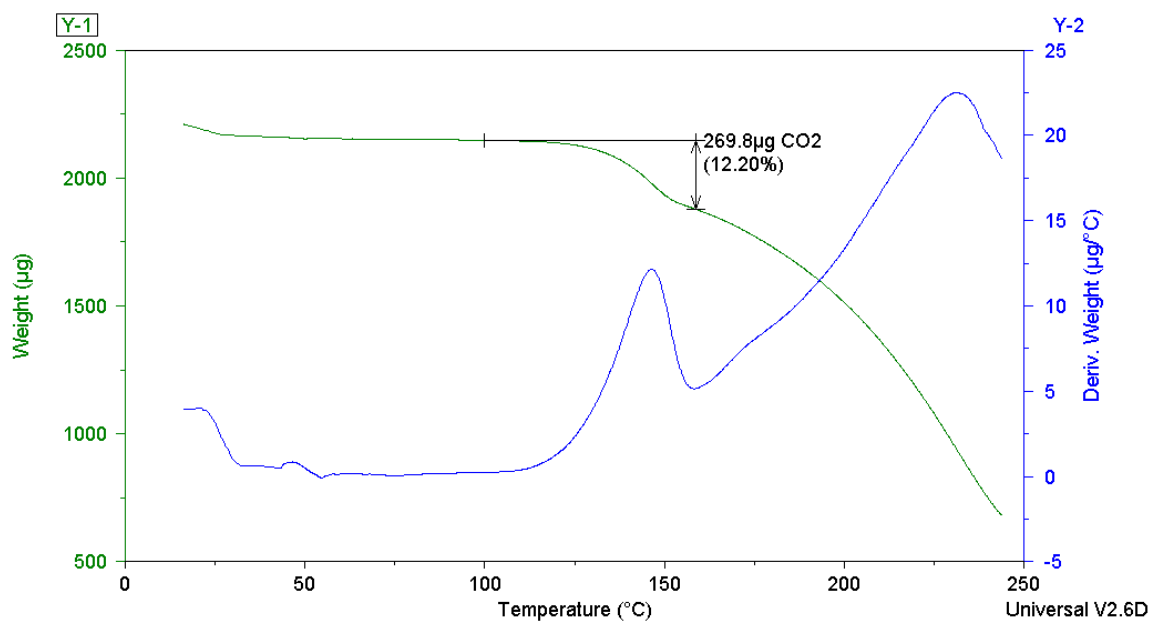
Figure C3: TGA Profile of **3b** Using 10.5220 mg
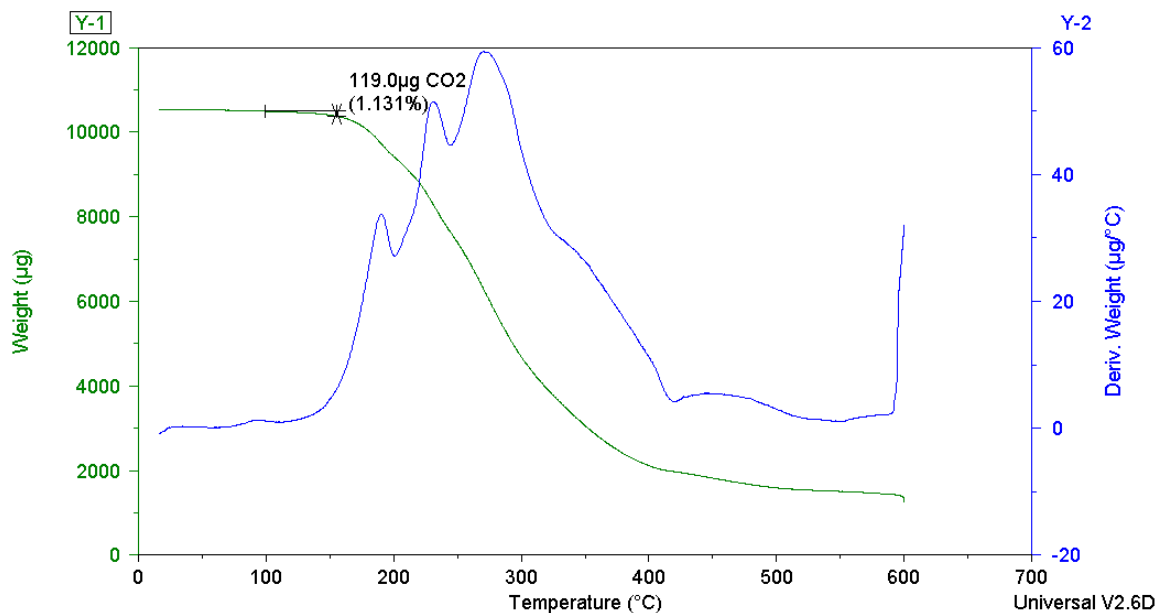
Figure C4: TGA Profile of **3b** Using 1.4750 mg
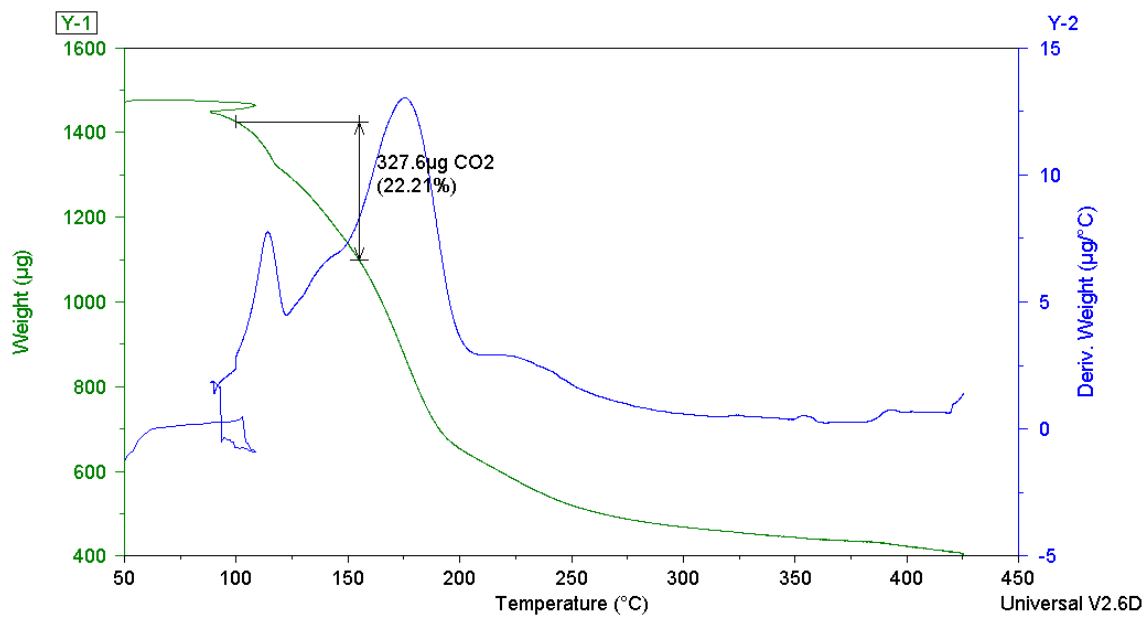
APPENDIX D: GC DATA

Table D1: Retention Time and Response of CO_2 Standard Collected for **3a**

Std. CO_2 Amount [uL]	Reten. Time [min]	Area [mV•s]
200.00	0.876	5.476
400.00	1.911	9.986
600.00	2.871	15.584
800.00	3.818	19.826
1000.00	4.742	22.600

Figure D1: Standards Graph of CO_2 Gas for **3a**

Table D2: Decarboxylation Test of Freshly Made **3a** Using H_2O and Acetonitrile Mix

Decarboxylation Test	Reten. Time (min)	Area (mV•s)	Amount [uL]
Peak 1	0.524	19.276	2000.000
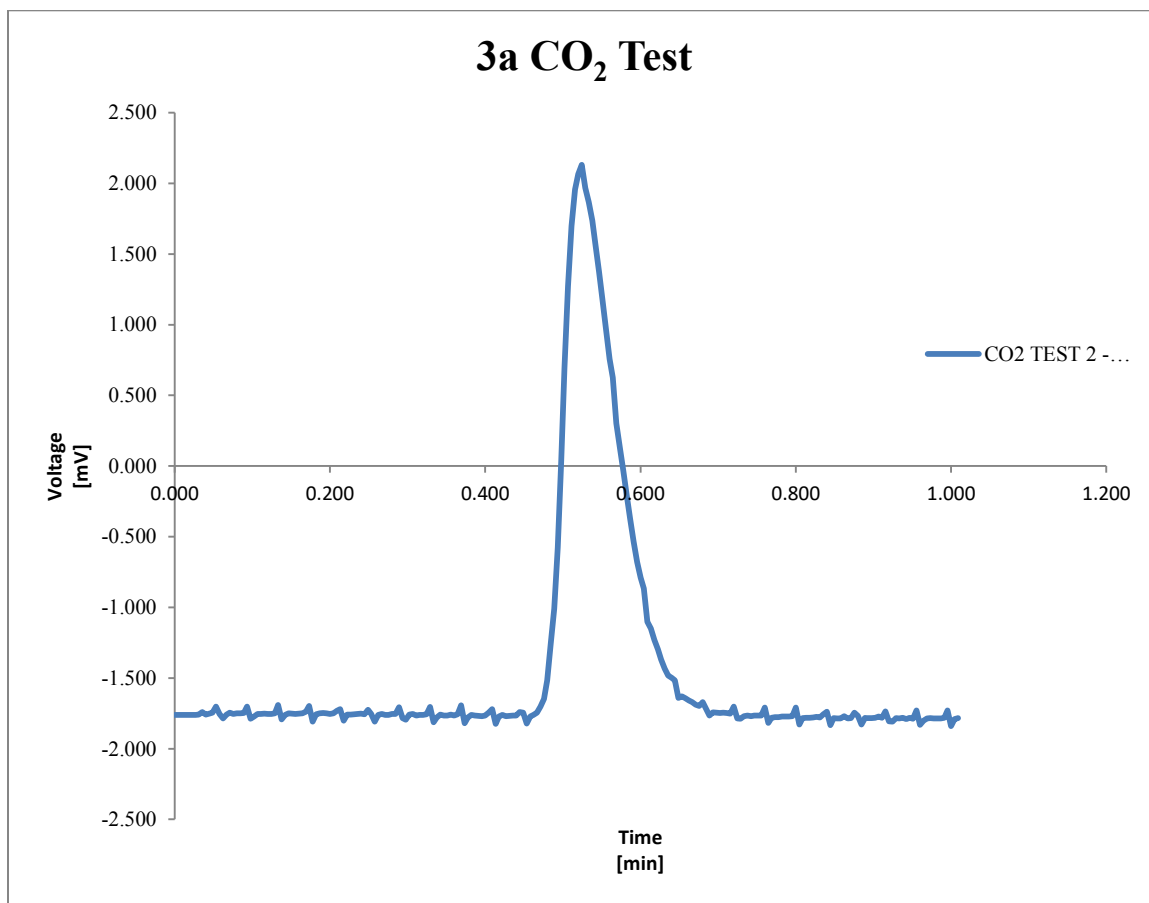
Figure D2: Decarboxylation of **3a** Using H_2O and Acetonitrile Mix

Table D3: Retention Time and Response of CO_2 Standard for **3b**

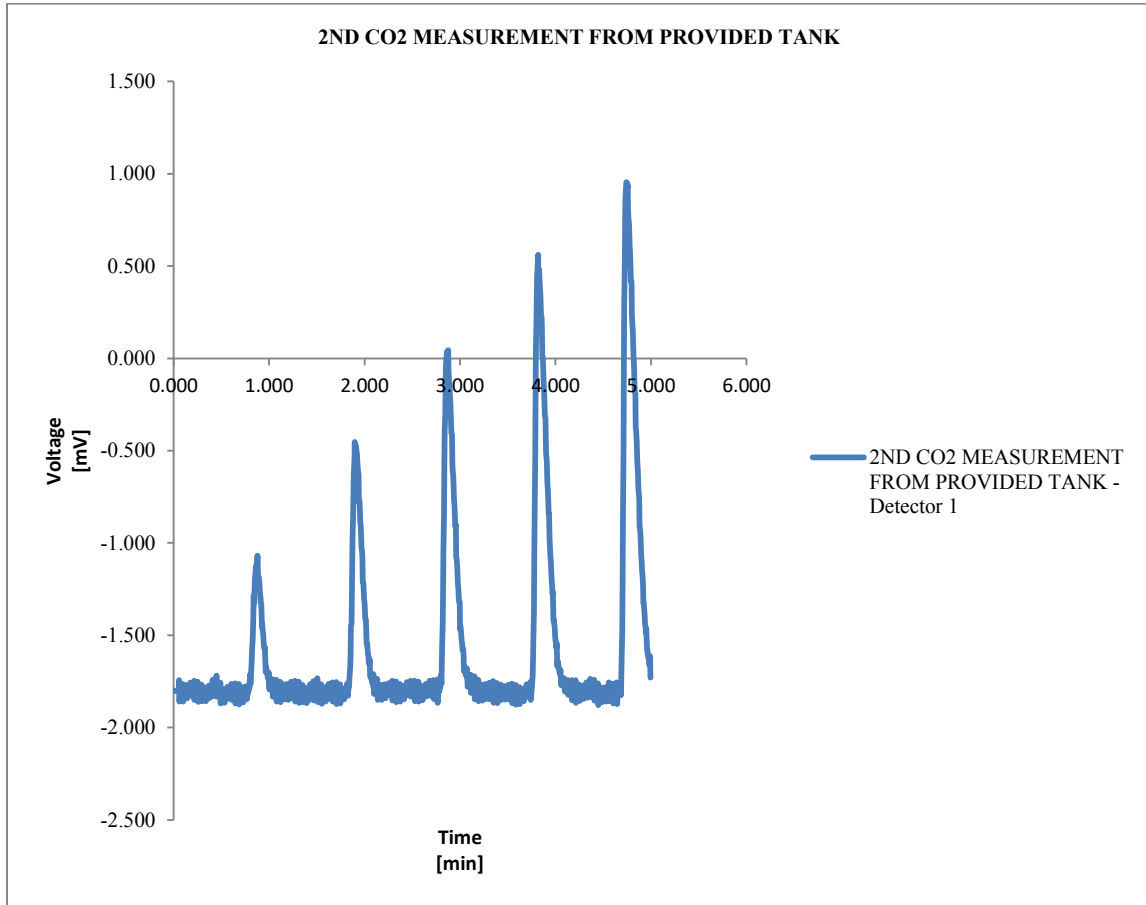| Amount of standard CO_2	Retention Time (min)	Response (mV•s)
200 µL	0.560	2.432
400 µL	0.556	5.630
600 µL	0.542	9.265
800 µL	0.520	12.478
1000 µL	0.502	13.704

Table D4: Retention Time and Response of N_2 Standard for **3b**

Amount of standard N_2	Retention Time (min)	Response (mV•s)
200 µL	0.213	2.033
400 µL	0.200	4.589
600 µL	0.200	6.983
800 µL	0.200	7.302
1000 µL	0.204	11.199
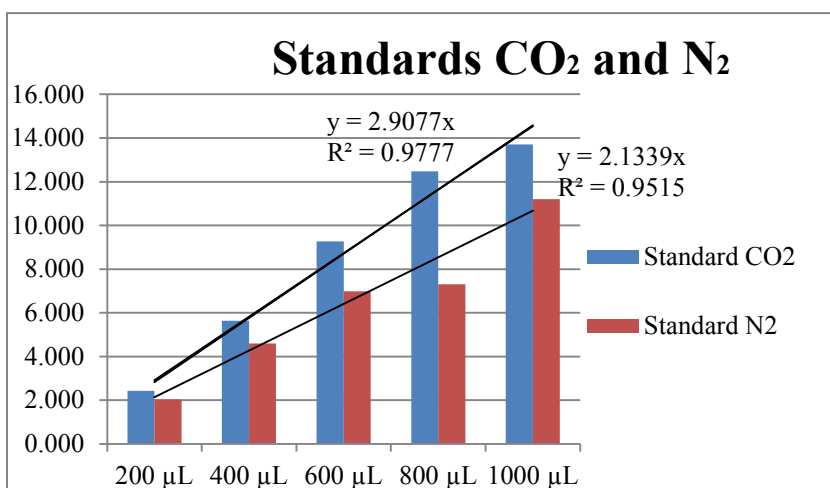
Figure D3: Combined Standards Graphs of CO_2 Gas and N_2 Gas for **3b**

Table D5: First Decarboxylation Result for **3b** Stability Test Using H_2O and Acetonitrile Mix

Decarboxylation test	Reten. Time (min)	Response (mV•s)	Amount [uL]
Peak 1	0.204	7.658	1000.00
Peak 2	0.569	4.050	
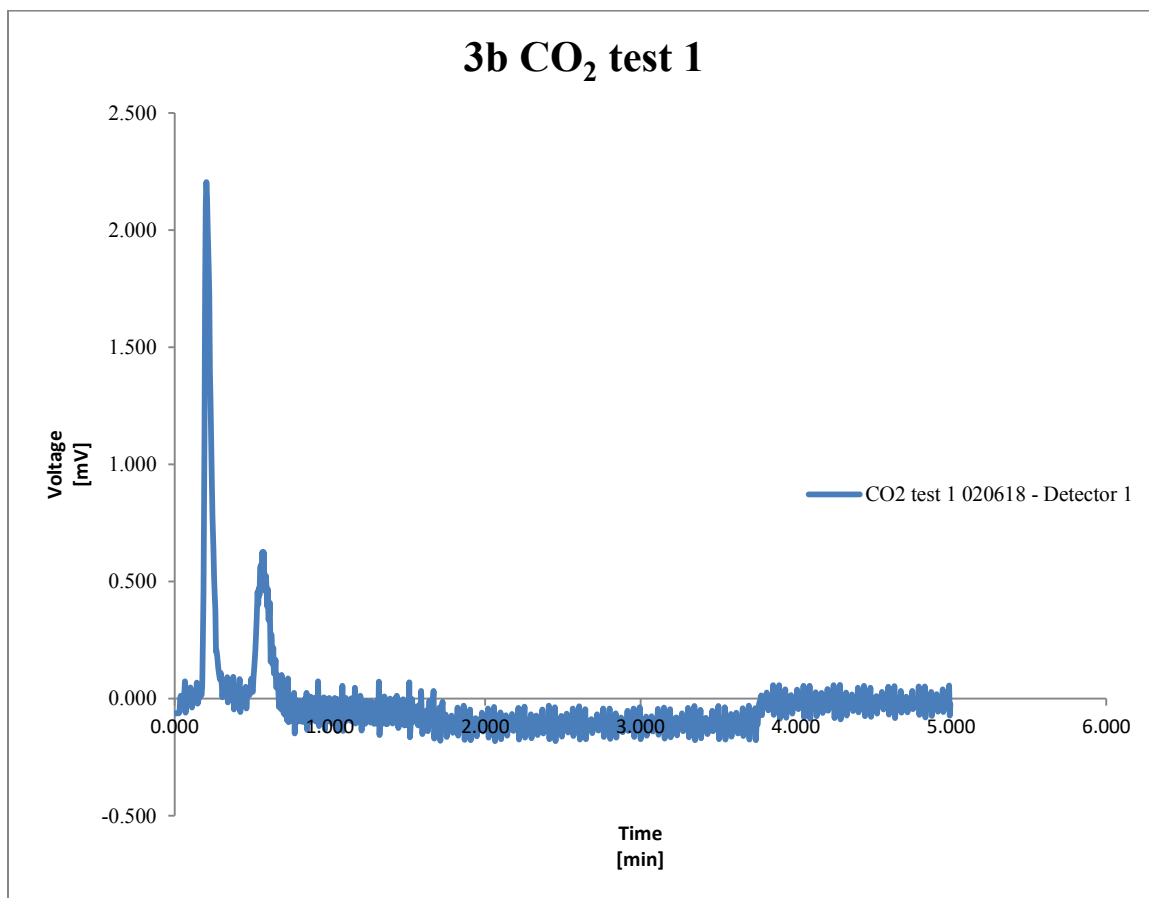
Figure D4: First Decarboxylation Result for **3b** Stability Test Using H_2O and Acetonitrile Mix

Table D6: Second Decarboxylation Result for **3b** Stability Test Using H_2O and Acetonitrile Mix

Decarboxylation test	Reten. Time (min)	Response (mV•s)	Amount [uL]
Peak 1	0.178	7.447	1000.00
Peak 2	0.533	4.814	
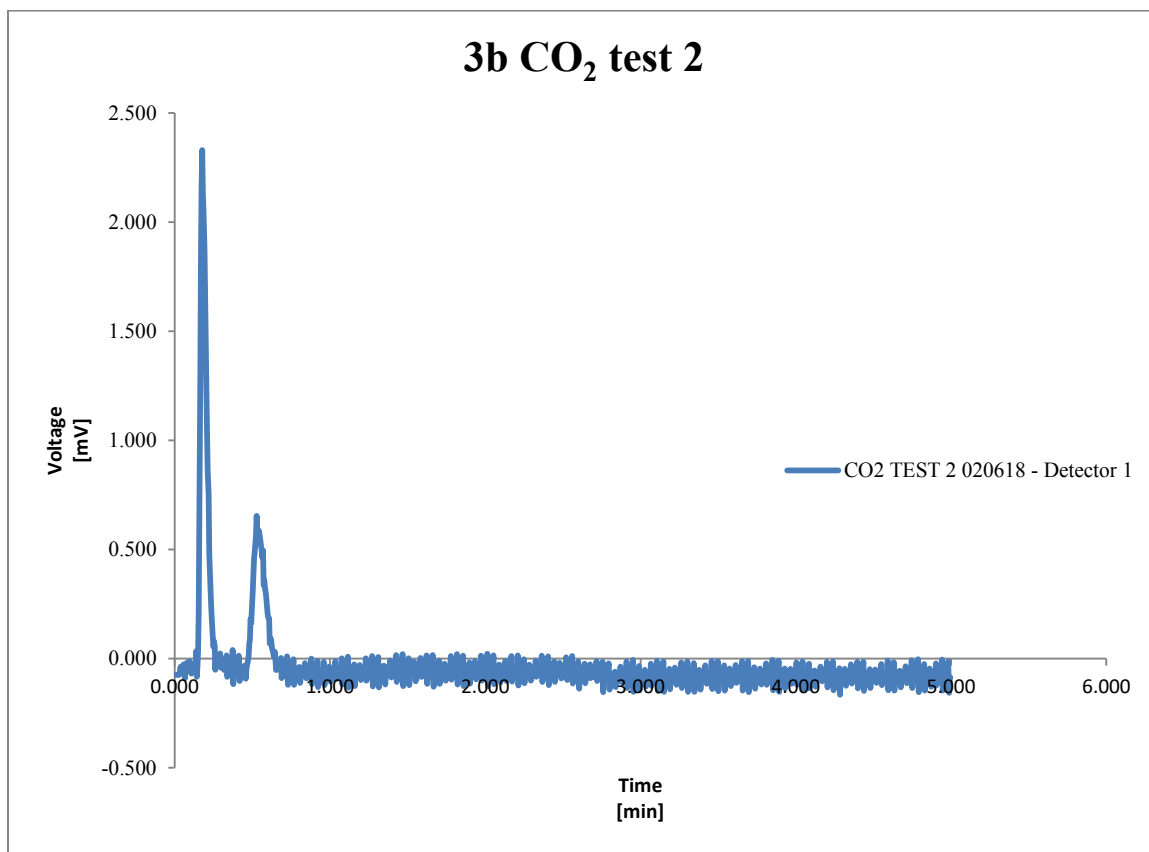
Figure D5: Second Decarboxylation Result for **3b** Stability Test Using H_2O and Acetonitrile Mix

Table D7: Third Decarboxylation Result for **3b** Stability Test Using H_2O and
Acetonitrile Mix

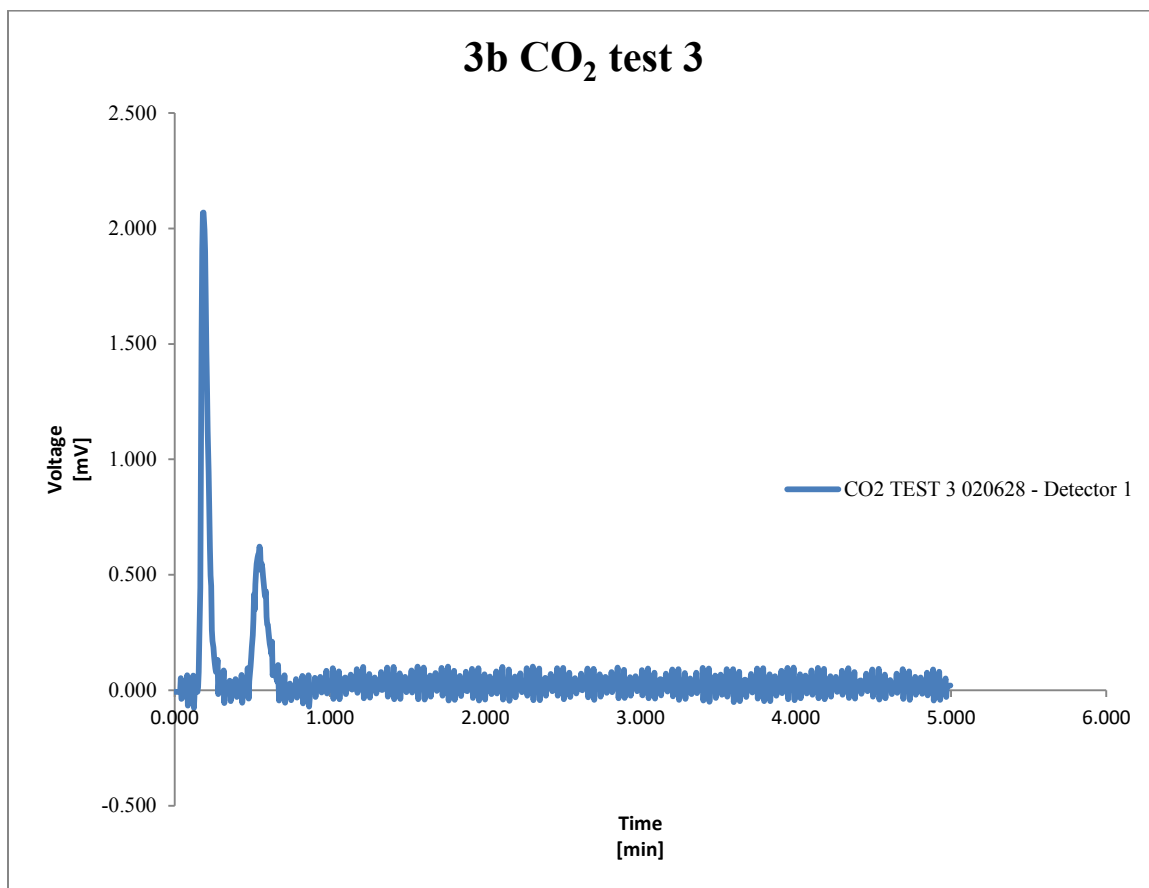| Decarboxylation test	Reten. Time (min)	Response (mV•s)	Amount [uL]
Peak 1	0.187	7.541	1000.00
Peak 2	0.547	4.097	

Figure D6: Third Decarboxylation Result for **3b** Stability Test Using H_2O and
Acetonitrile Mix

APPENDIX F: XRD PATTERNS

Table F1: Measurement Conditions of **3a**

Dataset Name	IMesCO2_1
File name	E:\Thesis\XRD\IMesCO2_1.raw
Measurement Date / Time	11/30/2015 12:26
Operator	Administrator
Raw Data Origin	BRUKER-binary V3 (.RAW)
Scan Axis	Gonio
Start Position [°2Th.]	5
End Position [°2Th.]	90
Step Size [°2Th.]	0.02
Scan Step Time [s]	2
Scan Type	Continuous
Offset [°2Th.]	0
Divergence Slit Type	Fixed
Divergence Slit Size [°]	1
Specimen Length [mm]	10
Receiving Slit Size [mm]	0.1
Measurement Temperature [°C]	25
Anode Material	Cu
K-Alpha1 [Å]	1.5406
K-Alpha2 [Å]	1.54443
K-Beta [Å]	1.39225
K-A2 / K-A1 Ratio	0.5
Generator Settings	36 mA, 36 kV
Diffractometer Type	Theta/Theta D5000
Diffractometer Number	0
Goniometer Radius [mm]	217.5
Dist. Focus-Diverg. Slit [mm]	91
Incident Beam Monochromator	No
Spinning	No

Table F2: Peak List of **3a**

Pos. [°2Th.]	Height [cts]
5.1388	16.6
10.6304	8883.23
10.8972	9440.42
12.2833	199.35
13.2856	989.2
14.3417	2542.96
15.4708	1247.94
16.5174	4100.8
17.2024	7348.19
17.6815	865.67

18.6166	121.51
19.6911	865.18
21.3971	1300.28
21.9465	2072.44
22.4287	1143.06
23.2107	842.5
24.3376	3954.73
24.989	2002.89
25.6776	1113.8
26.8459	2740.12
27.5962	518.34

Figure F1: XRD Pattern of **3a**
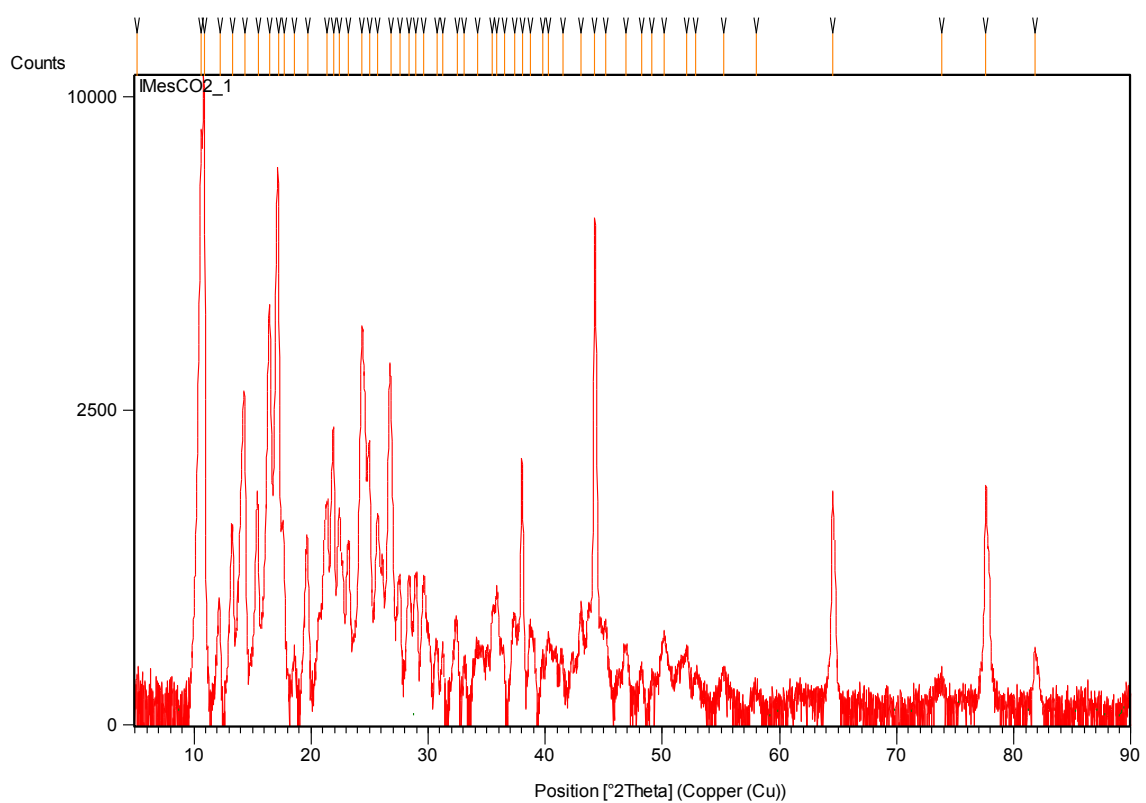
Table F3: Measurement Conditions of 6

Dataset Name	3wh2ht
File name	E:\Thesis\XRD\3wh2ht.raw
Raw Data Origin	Rigaku-binary (.RAW)
Scan Axis	Gonio
Start Position [°2Th.]	5
End Position [°2Th.]	90
Step Size [°2Th.]	0.02
Scan Step Time [s]	1
Offset [°2Th.]	0
Divergence Slit Type	Fixed
Divergence Slit Size [°]	1
Specimen Length [mm]	10
Receiving Slit Size [mm]	0.1
Measurement Temperature [°C]	25
Anode Material	Cu
K-Alpha1 [Å]	1.5406
Generator Settings	0 mA, 0 kV
Diffractometer Number	0
Goniometer Radius [mm]	240
Dist. Focus-Diverg. Slit [mm]	91
Incident Beam Monochromator	Yes
Spinning	No

Table F4: Peak List of 6

Pos. [°2Th.]	Height [cts]	FWHM [°2Th.]	d-spacing [Å]	Rel. Int. [%]
5.1822	70.88	0.384	17.03907	0.41
7.281	74.42	0.096	12.13151	0.43
8.1777	19.98	0.768	10.80309	0.12
10.8158	15376.94	0.36	8.17332	88.63
12.1812	1440.43	0.12	7.26008	8.3
13.1583	625.55	0.288	6.72304	3.61
14.239	8342.12	0.336	6.21512	48.08
15.376	2997.78	0.336	5.758	17.28
16.3857	2046.88	0.288	5.40541	11.8
17.1049	17349.27	0.36	5.17972	100
19.6158	1730.98	0.216	4.52198	9.98
21.1066	1138.7	0.336	4.20583	6.56
21.8351	2074.16	0.264	4.06712	11.96
22.679	1399.7	0.288	3.91765	8.07
24.249	5607.12	0.24	3.66746	32.32
24.8695	3717.43	0.264	3.57733	21.43
25.6129	1502.93	0.336	3.47516	8.66

26.7418	5776.45	0.36	3.33097	33.3
27.5158	1184.24	0.24	3.23901	6.83
28.8624	1165.89	0.264	3.09087	6.72
29.5273	765.11	0.288	3.02277	4.41
30.0467	448.88	0.24	2.97168	2.59
30.7429	213.96	0.336	2.90596	1.23
31.5073	1812.73	0.312	2.83718	10.45
32.1846	90.53	0.384	2.779	0.52
33.0655	84.94	0.288	2.70695	0.49
33.7573	135.03	0.336	2.65304	0.78
34.5504	206.96	0.24	2.59393	1.19
35.3992	474.38	0.288	2.53366	2.73
36.3647	301.12	0.192	2.46857	1.74
37.2578	654.53	0.288	2.41142	3.77
37.9826	11135.18	0.264	2.36706	64.18
38.9103	416.02	0.288	2.31273	2.4
40.2147	391.03	0.336	2.24067	2.25
41.4162	151.07	0.336	2.1784	0.87
42.2708	641.52	0.144	2.13632	3.7
44.223	17311.05	0.288	2.04643	99.78
45.2448	1077.58	0.384	2.00257	6.21
47.0688	81.62	0.576	1.92913	0.47
48.1182	112.67	0.24	1.88948	0.65
50.1689	197.52	0.672	1.81694	1.14
52.1267	175.03	0.48	1.75321	1.01
52.9661	75.77	0.384	1.72739	0.44
55.1327	104.37	0.576	1.66452	0.6
56.1933	153.67	0.384	1.63559	0.89
57.8405	49.33	0.96	1.59287	0.28
58.6275	37.71	0.144	1.57335	0.22
61.5391	135.79	0.192	1.50571	0.78
64.5298	4058.82	0.168	1.44296	23.39
66.0438	85.9	0.384	1.4135	0.5
69.1827	16.39	0.768	1.35683	0.09
71.5776	16.31	0.576	1.3172	0.09
73.7941	143.07	0.192	1.28302	0.82
75.1181	152.75	0.48	1.26366	0.88
77.6103	4441.19	0.216	1.22919	25.6
77.8818	1942.13	0.144	1.22558	11.19
81.7918	590.74	0.24	1.17659	3.4
83.7248	69.69	0.24	1.15428	0.4

Figure F2: PXRD Pattern of **6**